# The *Saccharomyces cerevisiae* Srs2 Helicase Regulates Homologous Recombination through the Disassembly of Recombination Intermediates

Kyle S. Kaniecki

Submitted in partial fulfillment of the

requirements for the degree of

Doctor of Philosophy

in the Graduate School of Arts and Sciences

COLUMBIA UNIVERSITY

2018

## ABSTRACT

The *Saccharomyces cerevisiae* Srs2 Helicase Regulates Homologous Recombination Through the Disassembly of Recombination Intermediates

Kyle S. Kaniecki

Life on Earth relies on a set of instructions encoded within an organism's genome that is passed along from one generation to the next. Inherent to this mechanism of propagation is the need to copy the genetic material before passing it along to the progeny. Errors in this process coupled with stochastic damage will inevitably lead to changes in these instructions and may result in a reduction of fitness or even death of an individual. Yet, these same changes are also responsible for the adaptation mandated by our dynamic environment. Thus, there exists a delicate balance between maintenance and alteration of genetic material that is embodied to a large part at the various intersections of DNA replication, recombination and repair. Homologous recombination (HR) has been well studied and found to play vital roles in many cellular processes from the repair of the harrowing double-stranded break, the restart of a stalled or collapsed replication fork, as well as proper chromosome segregation during meiosis, all with the goal of striking this delicate balance. And yet, while HR is incumbent for the fitness of an organism, if left unchecked this same process can become detrimental by preventing better suited DNA repair pathways, permanently arresting cell cycle progression and creating some of the very problems it was meant to address such as aneuploidy or cancer. Despite a wealth of knowledge, the precise regulatory mechanisms remain an active area of research as they provide likely targets to combat these persistent diseases. Motor proteins that translocate along DNA have been particularly compelling and elusive due to their transitory nature, as well as the inevitability of collisions with bound protein(s) or nucleic acid structures that are likely regulated intermediates in the process. The yeast Srs2 helicase/translocase has long been regarded as the prototypical "anti-recombinase" as it has been shown to dismantle the Rad51 presynaptic filament, but also displays contradictory pro-recombinase functions. *In vivo* studies of Srs2 have been hampered by its involvement in multiple bioprocesses beyond recombination, while bulk *in*

*vitro* approaches often produce conflicting results. Recent single molecule imaging of these players has shed light onto their involvement in the regulation of the various stages of the canonical pathway of HR. The Greene laboratory has developed ssDNA curtains to study the pre-synaptic filament and shown that Rad51-ssDNA filaments can create bonafide D-loop intermediates that would be incapable of repair and thus represent a toxic intermediate. These structures persist far longer than the entire process of DSBR *in vivo* and led us to hypothesize that motor proteins would be a key regulatory element to dismantle improperly paired intermediates for redistribution of the bound proteins and reengagement of the homology search process. Here I extend the use of ssDNA curtains to study Srs2 as it assembles into multimeric complexes to perform long-range disruption of various pre- and post-synaptic filament assemblies that include replication protein A (RPA), Rad51, Rad52, and D-loops. For the first time, direct observation of Srs2 translocating over RPA filaments is provided and shows these proteins are efficiently removed by Srs2. By including Rad52 on the RPA filament, I offer a refined model of the contradictory pro- and anti-recombinase activities of Srs2 through its antagonism of the single-strand annealing pathway in favor of HR. Additionally, Srs2 was found to initiate Rad51 disruption at breaks in the continuity of the filament marked by the persistence of replication protein A (RPA), Rad52, or the presence of an improper D-loop intermediate, the latter of which is efficiently disrupted before continuing translocation. In contrast to the prevailing model, we demonstrate that direct interaction between Srs2 and Rad51 is not necessary for long-range Rad51 clearance. These findings offer insights into the dynamic regulation of crucial HR intermediates by Srs2 and demonstrate that sub-nuclear concentrations of these proteins may be a likely driver for their activities.

**TABLE OF CONTENTS**

## LIST OF FIGURES

## LIST OF TABLES

## LIST OF ABBREVIATIONS

HR, homologous recombination

DSB, Double-strand break

CPT, camptothecin

MMS, methylmethane sulfonate

HU, hydroxyurea

NHEJ, non-homologous end joining

MMEJ, micro-homology mediated end joining

nt, nucleotide

knt, kilo-nucleotide

bp, base-pair

kb, kilobase

SSA, single strand annealing

SDSA, synthesis dependent strand annealing

BIR, break induced repair

CO, crossover

NCO, non-crossover

LOH, loss of heterozygocity

ATP, adenosine triphosphate

ADP, adenosine diphosphate

EM, electron microscopy

NGS, next generation sequencing

CFP, cyan fluorescent protein

GFP, green fluorescent protein

RFP, red fluorescent protein

RPA, replication protein A

TIRFM, Total internal reflection fluorescent microscopy

## ACKNOWLEDGEMENTS

This work would not have been possible without the contribution, collaboration, and support of numerous individuals. I would first like to thank current and former members of the Greene lab: Dr. Bryan Gibb for teaching me the ssDNA curtain technique; Justin Steinfeld and Chu “Frank” Ma for their help with proteins and regents; Tsuyoshi Terakawa for his significant contribution to statistical analyses and coding; John Brooks Crickard, Upasana Roy, and Chaoyou Xue for taking up the mantle of experiments regarding Dmc1 recombinase specificity, SHU complex and recombinase mediators, and human RECQ5 helicase anti-recombinase activity, respectively; and mostly Luisina de Tullio for shouldering much of the experimental data generation and analyses with me.

I’d like to thank the members of my committee for their invaluable advice and input over the years: Rodney Rothstein has been a phenomenal teacher and mentor since I did my first tetrad analysis in his class; Lorraine Symington for her exhaustive knowledge regarding DNA repair and her patience and effort in reviewing this document; Rubin Gonzalez for his experimental suggestions during lab meetings; and most recently Alberto Ciccia for his commitment to the genetics program and thought-provoking questions regarding helicases, DNA replication and recombination.

I’d like to thank my mother for being the saint she is and teaching me about hard work and perseverance, two qualities instrumental to complete a PhD. I’d like to thank my father for fostering my insatiable sense of curiosity and stepmom for being an ever-present voice of reason. Marina, Annette, Stephen, Leah, Jason, Jamie, Jessica, and Andrew, you have each left your individual fingerprint on this document.

Finally, I’d like to thank my mentor, Eric Greene. I am inspired by your continual commitment to scientific training and discovery, along with your near superhuman presentation abilities. The greatest science in the world can be lost with ineffective presentation and I doubt I could have found a better teacher than you. Additionally, thank you for being an endless source of patience and advice. Your ability to balance allowing my independent ambitions with your advice when it became necessary is an important reason I have found success in this program. Some of my most cherished memories over the past years were of our “passionate discussions” when we did not agree, and I greatly look forward to years of future discussions.

"…this thing that we call 'failure' is not the falling down,

but the staying down."

-Mary Pickford

# CHAPTER 1: INTRODUCTION

Homologous Recombination (HR), the exchange of nucleic acid information between two identical or closely related sequences, is a highly-conserved pathway from viruses to humans. The earliest experiments probing recombination in eukaryotes employed segregation analysis of individual meiotic products in yeast to dissect the most basic concepts and actors taking part in these processes. These experiments led to major theoretical advances exemplified in the Holliday model of recombination, followed by the Meselson-Radding model, and later the DSBR model of recombination[1,2,3]. Each of these pivotal papers was aimed at explaining recombination outcomes that the predecessor could not account for. Decades of research have now helped define the molecular players (Table 1-1) and pathways involved in recombination (Figure 1-1 & Figure 1-2).

This chapter will introduce three key cellular processes that utilize genetic recombination including (i) the repair of damaged DNA such as inter-strand crosslinks and a double strand break, (ii) the restart of stalled or collapsed replication forks, and (iii) during programmed events such as the accurate segregation of chromosomes during meiosis I. I will then go into more detail to explore some of the pivotal proteins that carry out recombination, followed by how SF1 & SF2 helicases operate with an emphasis on their perceived regulatory roles in genetic recombination. Throughout this chapter, I will stress how recombination is essentially regulated by the dynamic assembly and disassembly of recombination intermediates.

## 1.1 DNA DAMAGE AND REPAIR

Insults to the genetic code of an organism can be the result of either exogenous or endogenous sources. Endogenous sources may include reactive oxygen species (ROS) that are the result of various metabolic processes, collisions between genomic machineries, protein-DNA adducts, as well as programmed changes that vary widely by organism such as meiotic recombination, lymphocyte development,

horizontal gene transfer, and mating type switching in yeast. Exogenous sources of DNA damage include genotoxins such as camptothecin (CPT), methyl methanesulfonate (MMS), or hydroxyurea (HU) which have historically been used as tools to induce DNA damage with the goal of elucidating various repair mechanisms. High-energy particles such as UV- and gamma-irradiation will commonly cause ssDNA gaps and double strand breaks, respectively[4]. The double-stranded break (DSB) is often thought to be the most perilous of any type of damage as these lesions can result in chromosomal rearrangements, loss of large amounts of genetic information, and cell death[5]. The importance in combating these affronts to genomic integrity is emphasized by the fact that mutations in the genes necessary for their repair may result in inviability, neurological, immunologic, or developmental disease and are primary drivers of cancer[6-8].

### *1.1.1 Pathways to repair the double-strand break*

The two key pathways to repair a DSB are non-homologous end joining (NHEJ) and homologous recombination (HR), with the choice of which pathway to use largely depending upon the state of the DNA ends flanking a DSB (Figure 1-1). If the break has <4nt of ssDNA overhang and is absent protein-DNA adducts or hairpin caps, NHEJ is often considered the pathway of choice, particularly in mammalian cells[9]. In brief, the canonical pathway for NHEJ uses the Ku70-Ku80 heterodimer (Ku) to bind both ends of the DSB, while DNA ligase-IV (LigIV) catalyzes the ATP-dependent transfer of phosphate bonds to directly ligate the phosphodiester backbone[10]. Alternative mechanisms of direct ligation, called alt-NHEJ, include micro-homology end joining (MMEJ) and single-strand annealing (SSA)[9].

In contrast to NHEJ, both alt-NHEJ and HR require 3′-ssDNA ends and do not rely on Ku and LigIV. Clean breaks such as those generated by restriction enzymes can still employ alt-NHEJ or HR for their repair, while the decision to forego NHEJ is made by the Mre11-Rad50-Xrs2 (MRX) complex along with Sae2, which can displace Ku from the ends flanking a DSB (Figure 1-2). Mre11 and potentially Sae2 possess endonucleolytic function to nick DNA and remove any protein-DNA adducts or hairpin structures from the end of the break [11,12]. In the error-prone MMEJ, 1-16nt regions of microhomology that are revealed during initial resection may be annealed and directly ligated resulting in deletions flanking the

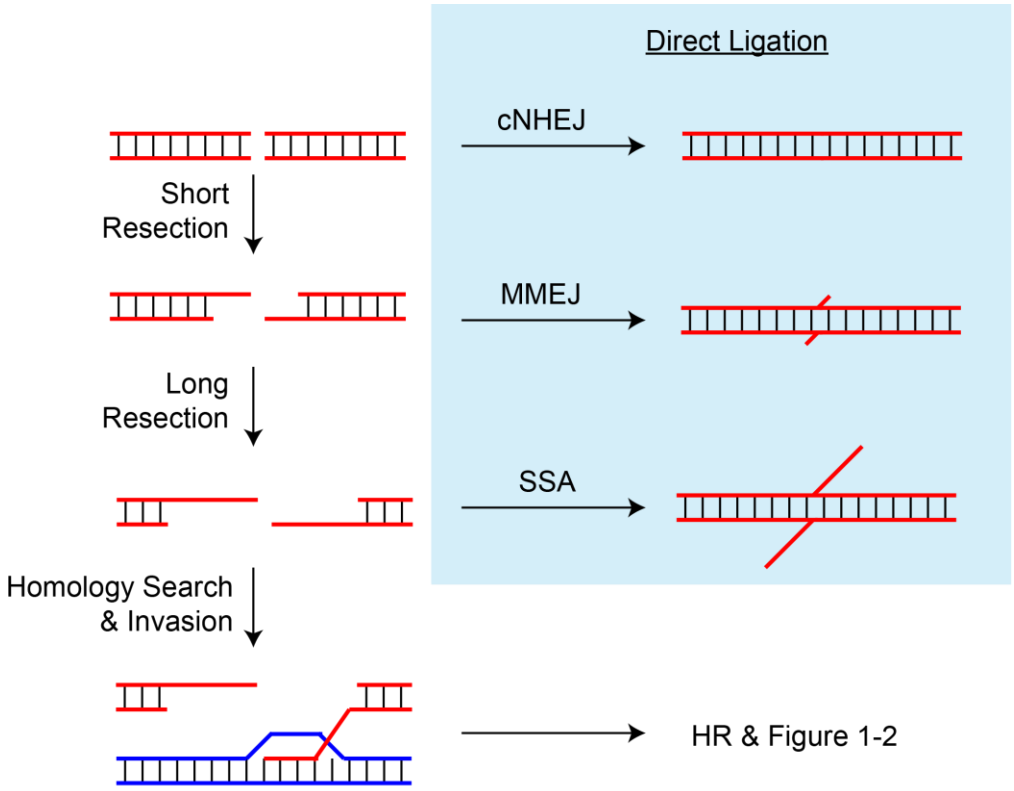


**Figure 1-1. Repair of a double-stranded break.** After sensing a double stranded break, the DNA can be directly ligated with Ku70-Ku80 in cNHEJ. Resected ends can reveal microhomologies that may pair and ligate, typically deleting short segments around the break. Longer resection can reveal larger regions of homology (>14bp) that may be paired by Rad52 and typically can result in larger regions of deleted sequence. The resected end may also undergo homology search and strand invasion to carry out HR.

DSB[9]. The Mre11-generated nick serves as an entry site for Exo1 5′→3′ exonuclease to reveal long 3′ ssDNA overhangs at a rate of about 4kb ($hr^{-1}$)[13]. The Sgs1-Top3-Rmi1 (STR complex) together with Dna2 flap endonuclease operate in parallel with, and may also substitute for, Exo1 to reveal long ssDNA tracks that vary in length depending on the availability and proximity of a template, with 2-4 kilo-nucleotides (knt) being revealed during the repair of DSBs in mitotic yeast cells[14].

The ssDNA that is revealed during resection is rapidly bound by the heterotrimeric replication protein A (RPA) in eukaryotes, or single-stranded binding protein (SSB) in *E. coli*. RPA-ssDNA will recruit Ddc2-Mec1 to the DSB[15-17] to phosphorylate Rad9 and activate the Rad53 and Chk1 checkpoint effector kinases (mammalian ATR pathway) to halt cell cycle progression until DSB repair completion[18]. In SSA, the Rad52 protein binds to RPA-ssDNA to promote the direct annealing of homologous sequences (>14bp of homology) flanking a DSB[19]. While Rad52 has strand annealing activities, its primary purpose

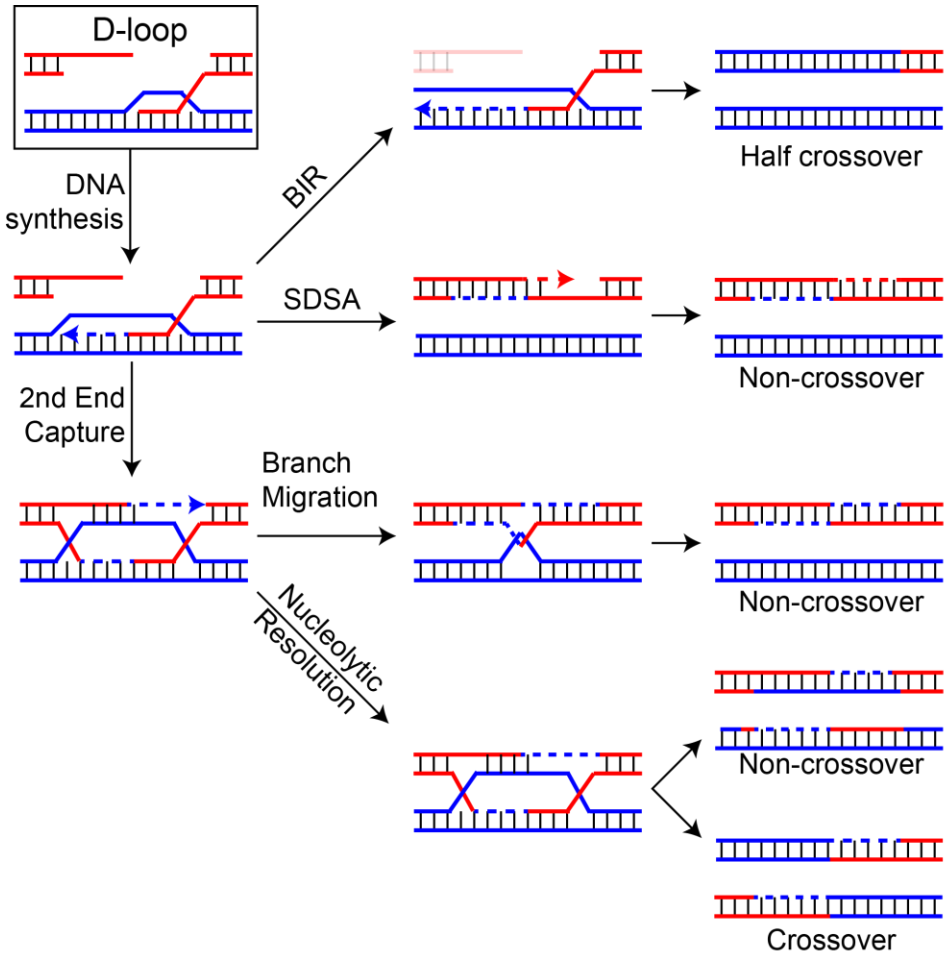


**Figure 1-2. Resolution of HR Subpathways.** Once a D-loop has formed (see Figure 1-1), DNA sythesis by specialized DNA polymerases copies the lost information around a break. If the second end is unavailable, replication can occur to the end of a chromasome resulting in a half-crossover. Dissolution of the D-loop before second-end capture results in sythesis dependent strand annealing and a non-crossover. Capturing the second end for directed sysnthesis can resolve by branch migration and result in a non-crossover. While nucleolytic resolution can result in either a crossover or non-crossover product.

is largely thought of as the Rad51 mediator to help displace RPA from the ssDNA and build the Rad51-ssDNA "pre-synaptic filament". The Rad51 filament requires the action of other HR mediators such as the heterodimer Rad55-Rad57 and the Shu complex (Shu1-Shu2-Csm2-Psy3) to remain stable. With the aid of Rad54, Rad51 promotes homology search for a correct template and strand invasion to create a D-loop and the "post-synaptic filament". Once the invading strand pairs with a template, Rad54 switches modes and dismantles the Rad51 filament to allow access to the primed substrate by the specialized DNA polymerases Pol η, Pol κ, Pol ζ, and in particular Pol δ[20,21]. This commonly occurs with the association of the clamp loader replication factor C (RFC), which in turn loads the proliferating cell nuclear antigen (PCNA) processivity clamp[22]. PCNA is a homotrimeric protein that encircles the DNA and is

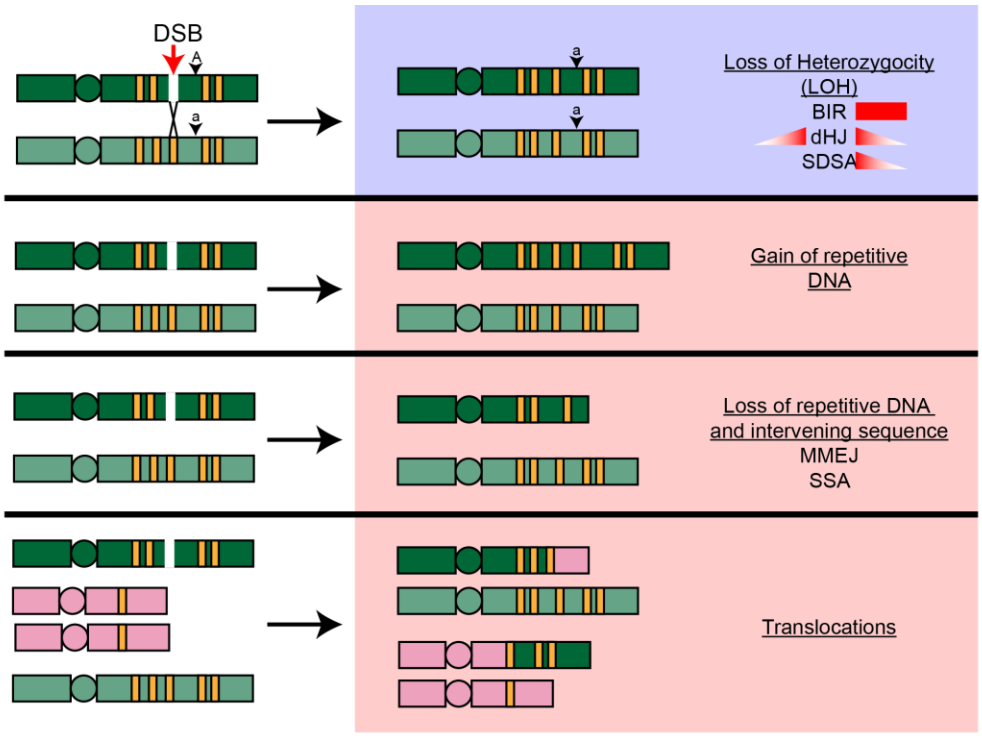


**Figure 1-3. Consequences of correct and aberrant DSBR.** When a double stranded break is repaired through one of the NHEJ or HR supbathways, the result can be deleterious, particularily when the DSB occurs in a region with a similar sequences or direct repeats present in the genome (orange boxes). Even when HR targets a correct donor sequence (blue box), the result can be a loss of heterozygocity on a single end (BIR & SDSA) or on both sides of a DSB (dHJ). BIR results in LOH from the break to the end of a chromasome, while a dHJ or SDSA produce LOH at a decreasing gradient farther from the DBS. When HR targets an incorrect locus (red box), the result can be a gain or loss of DNA sequence, especially when there are flanking repeat regions on the same chromasomes. MMEJ and SSA commonly result in a loss of repeats. Repeats on a seperate chromasome can result in translocations.

essential for replication by DNA Pol δ, while further stimulating the processivity of other polymerases[20]. Association of different polymerases with PCNA can impact their processivity and may influence the downstream pathway for HR resolution, a feature that is discussed further in sections 1.1.2 and 1.3.3[22].

If HR results in the exchange of the arms of a sister chromatid (or homolog for meiotic cells), the product is called a crossover (CO), while maintaining the original organization is a non-crossover (NCO) product. Because a template dsDNA is used to copy missing information, either CO or NCO events may lead to a gene conversion event where copying the information on the dsDNA template leads to loss of heterozygocity (LOH) where two distinct allelic sequences become identical (Figure 1-3). Additionally, depending on how chromatids segregate, a CO in G2 cells can result in LOH from the site of exchange to the telomere. LOH is an important driver of genetic disease and cancer, where a recessive mutation may be uncovered through the conversion of the wildtype dominant allele[23].

After limited extension, the D-loop may be dismantled to directly pair with the unextended second end of the DSB and complete repair through the synthesis-dependent strand annealing (SDSA) pathway to result in NCO products. In break-induced replication (BIR), DNA synthesis can also replicate through to the end of the template chromosome creating half-crossover products[24]. This feature is useful to maintain telomere length under conditions of high proliferation[25,26], but as the distance replicated increases, so do the chances for LOH. Engagement of the second end of a DSB with the displaced strand of the D-loop creates the double Holliday junction (dHJ) structure which can result in both CO and NCO products by nucleolytic resolution, while enzymatic dissolution through branch migration results only in NCO. Importantly, NCO products are the preferred outcome of mitotic DSBR as they avoid chromosome rearrangement events making the extended D-loop a critical intermediate in controlling CO/NCO outcome[27].

### *1.1.2 Restart of collapsed or stalled replication forks*

Replication fork stalling leads to gaps that may be recovered by different pathways, including translesion synthesis (TLS), template switching by fork regression, or HR[28]. Genetic evidence points to TLS and template switching as the preferred pathway to restarting a stalled replication fork. However, mutations to the HR machinery confer sensitivity to fork stalling agents, suggesting that HR does play some role in the restart of a fork. In mammalian cells, BRCA2 has been found to be critical for preventing MRE11-mediated degradation of stalled replication forks by stabilizing RAD51 filaments, indicating the HR machinery is useful in protecting these structures rather than promoting homology directed repair (HDR).

The proliferating cell nuclear antigen (PCNA) clamp is a pivotal hub for signaling which repair pathway a fork should choose. Mono-ubiquitination on lysine 164 by the Rad6-Rad18 E2-E3 complex recruits TLS polymerases through their ubiquitin binding motifs[29]. Subsequent poly-ubiquitination of PCNA by Ubc13-Mms2 (E2) and Rad5 (E3) induce fork regression, an activity that was recently also identified in mammalian cells and dependent upon the DNA translocase ZRANB3[30]. The Mph1 helicase has also been shown to induce fork regression in vitro, although this activity has not been shown to

depend on PCNA modification[31]. As opposed to ubiquitination, K164 and K127 may be SUMOylated by Ubc9 to prevent HR at the stalled fork through a direct interaction with the helicase Srs2 that utilizes a mechanism discussed below.

### *1.1.3 Programmed genetic recombination*

Beyond its use in resolving stochastic genomic insults, recombination can also be programmed to occur in response to various conditions. For example, yeast can undergo mating-type switching through HDR of a DSB at the *MATa* or *MAT*$\alpha$ locus template by transcriptionally silent donor cassettes and provided one of the earliest models of genetic recombination. Sexually reproducing organisms utilize genetic recombination to randomly allot half of a parental genome to their progeny. Additionally, in 1964 Hermann Muller introduced the idea of “Muller’s Ratchet” where asexually reproducing organisms will accumulate deleterious mutations at each generation, which gave a purpose for recombination in sexual reproduction[32]. As opposed to vertical transfer of genetic information from parents to offspring in sexually reproducing organisms, asexually reproducing prokaryotes can avoid Muller’s Ratchet through a process called horizontal gene transfer (HGT) where genetic material can be transferred from one organism to another in a process requiring genetic recombination. HGT is a primary driver for the spread of antibiotic resistance and pathogenicity, as well as providing a key tool for genetic engineering, thus mandating a thorough understanding[33].

To ensure accurate chromosome segregation during the first meiotic division in eukaryotes, each homolog must create at least one crossover product to create the tension feedback on the microtubule-organizing center necessary for proper segregation of DNA with the added benefit of allelic diversity[34]. This contrasts with mitotic HR for DSBR that would prefer non-crossover products to avoid potential translocations and loss of heterozygocity (LOH). Two discoveries by the Szostak group drew a connection between meiotic recombination and mitotic HR for DNA repair; that meiotic repair is initiated from DSBs[35], and that there was a decrease in gene conversion events further from these DSBs[36]. The conserved gene *SPO11* encodes an endonuclease that was soon found to be the initiator of these DSBs[37,38].

While mitotic DSBR relies purely on Rad51, meiotic HR employs two recombinases, Rad51 and Dmc1[39]. Rad51 is believed to nucleate a mixed filament and it is Dmc1 that is thought to be primarily responsible for the strand exchange during meiosis, with Hed1 inactivating the Rad51 strand exchange activity[40]. Dmc1 is structurally and functionally similar to Rad51, while cells lacking Dmc1 fail to repair Spo11-induced DSBs and arrest at the pachytene stage during the first meiotic division[41]. In contrast to Rad51 which is biased toward sister chromatid exchange, Dmc1 is biased toward inter-homolog exchange[42], a feature that may be mediated by the translocase Rdh54 along with other axis proteins such as Hop1, Mek1, and Red1.

## 1.2 THE MOLECULAR PLAYERS OF HOMOLOGOUS RECOMBINATION

Early geneticists broadly classified DNA repair from radiation damage into epistasis groups comprising three primary pathways; the *RAD3* epistasis group including *RAD1*, *RAD3*, and *RAD4* which are involved in excision repair; the *RAD6* epistasis group which includes *RAD6* and *RAD18* are involved in the error-prone post-replicative repair (PRR); and the *RAD52* epistasis group that includes members such as *RAD51*, *RAD52*, *RAD55*, *RAD57*, *RAD54*, *MRE11*, and *XRS2* which are involved in the recombinational repair. The temporal organization of repair factors has been of considerable interest and must take place in a concerted fashion to properly function (Figure 1-4). For example, regulating the timing of resection is critical as it commits the cell away from the cNHEJ pathway, while DNA synthesis must only recruit polymerases after a donor dsDNA template has been identified. Single cell (SC) optical studies, analogous to single-molecule (SM) studies that are discussed below, have been integral to deciphering this coordinated activity of recombination proteins to address their order of arrival, approximate concentration and diffusion characteristics within the environment of a living cell[43].

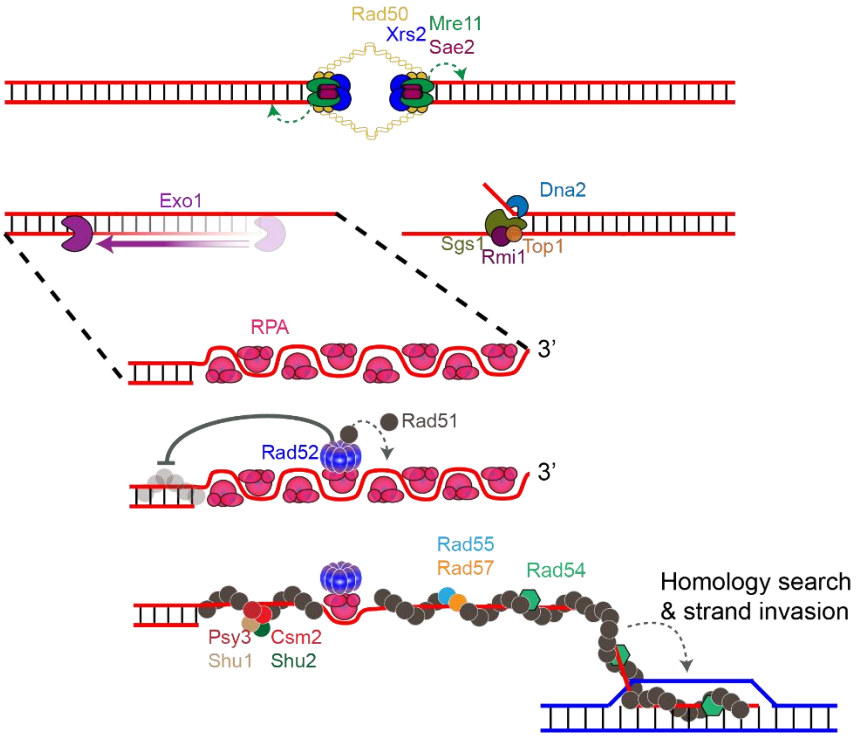


**Figure 1-4. Molecular Players of DSBR.** Once a double-stranded break is detected by the cell, the Mre11-Rad50-Xrs2 (MRX) complex along with Sae2 will nick the DNA to create entry points for processive resection. The Exo1 nuclease or Sgs1-Top3-Rmi1 together with Dna2 will perform long-range resection to reavel 3' ssDNA over-hangs that is rapidly bound by RPA. Rad52 binds both RPA and Rad51 and facilitates the formation of the Rad51 filament on ssDNA, while preventing its accumulation on dsDNA. The mediator proteins Rad55-Rad57, Psy3-Csm2-Shu1-Shu2 (Shu complex), and Rad54 stabilize the Rad51 filament. With the aid of Rad54, the Rad51 presynaptic filament will undergo homology search and strand invasion of a donor dsDNA template.

### *1.2.1 Single-strand binding proteins and RPA*

RPA is an essential and modular ssDNA binding protein made up of three subunits, Rfa1, Rfa2, and Rfa3 (Figure 1-5). The variety of conformations and interaction partners highlights the diverse utility of the protein. RPA participates in all cellular transactions involving a ssDNA intermediate and serves several purposes including resisting base-pairing, acting as a hub to coordinate other DNA processes, and protection of the ssDNA from nucleolytic degradation[44]. Paradoxically, while RPA is required for HR to occur, it also follows a model of competitive inhibition in the formation of the Rad51-ssDNA filament and must thus be efficiently displaced under the correct circumstances.

RPA has four core ssDNA binding domains (DBD); three of which reside within the large Rfa1 subunit (binding domains A, B, and C), with a fourth in the intermediate Rfa2 subunit (binding domain D)

providing a tight interaction on the order of $10^{-9}$–$10^{-10}$ M with ssDNA[45]. Although RPA binding is not sequence specific, it will bind polypyrimidines over polypurines. The multi-domain nature of RPA allows it to bind in at least 3 modes that contact between 8-30nt of ssDNA depending on how many of the DNA-binding domains are engaged. To achieve the full 30nt binding mode, a sequential engagement from 5′→3′ on ssDNA occurs first through domains A & B to bind 8nt, followed by C to expand the contact to 12-23 nucleotides, and finally D with all 30nt in contact with the complex[46]. The C-terminus of Rfa2 contains a winged-helix domain that is critical for protein-protein interactions, including Rad52, while the N-terminus is a target for phosphorylation by CDK and in response to DNA damage by Mec1/Tel1[47]. The purpose of these modifications is unclear, and phospho-mutants have a mild phenotype. The ATR/Mec1/Rad3 DNA damage checkpoint is activated by RPA bound to ssDNA and thus becomes a critical substrate for the regulation of DSBR repair[17].

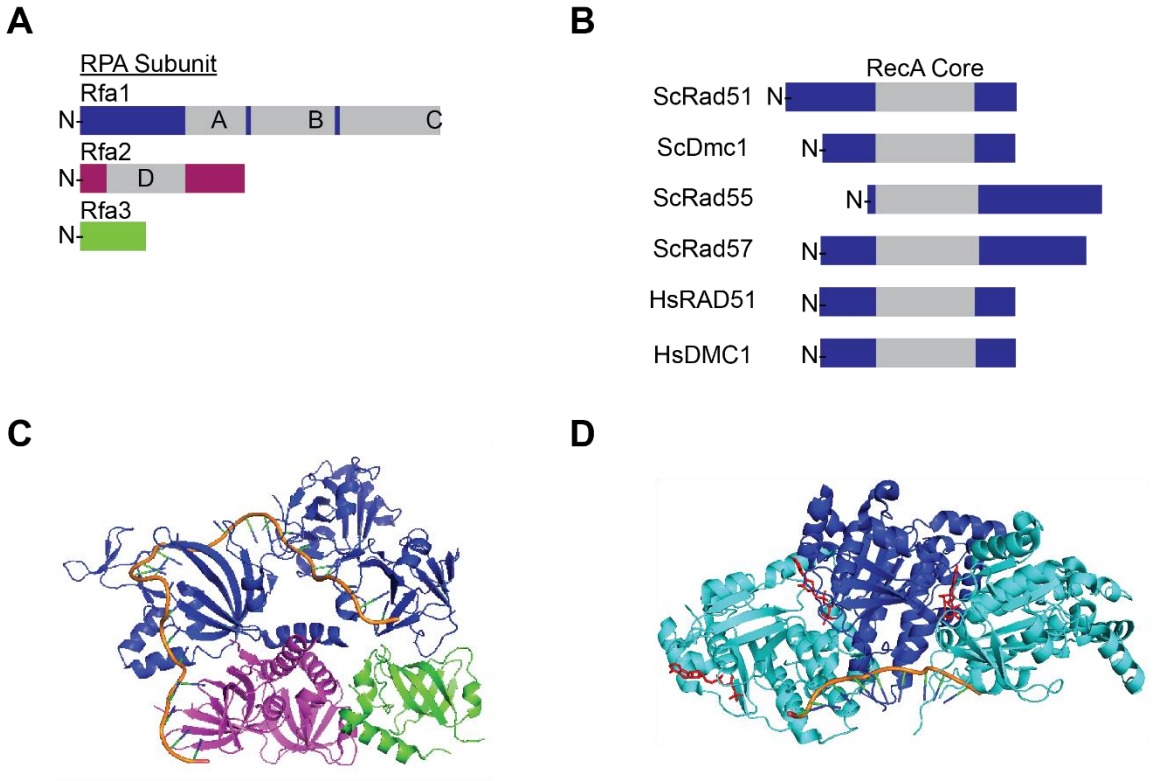


**Figure 1-5. Structures of RPA and Rad51.** (A) and (B) are the primary organizations of the heterotrimeric RPA, and Rad51 and its paralogues and human homologues, respectively. In (A), the four DNA binding domains are highlighted in grey. In (B), the grey highlighted area represents the location of the conserved RecA core ATPase motif, and illustrates the protein- and species-specific N- and C-terminal areas. (C) is the crystal structure of RPA encircling ssDNA with the blue, red and green regions representing the Rfa1, Rfa2, and Rfa3 subunits, respectively. (D) is the cryo-EM structure of the human RAD51 presynaptic filament with three monomers of Rad51 bound to ssDNA (orange). The ATP molecule (red) is placed at the interface between each monomer.

*1.2.2 The RecA/Rad51 family of recombinases*

The core recombinase responsible for the pairing and strand invasion steps of HR is Rad51 (RAD51 in humans, RadA in archaea, and RecA in *E. coli*). While Rad51 is not essential in yeast, mutants show extreme sensitivity to ionizing radiation[48]. RAD51 is essential in higher eukaryotes[49,50] where its absence results in the accumulation of DSBs[51] and cell cycle arrest. Members of the RecA/Rad51 family of recombinases form right-handed helical filaments on both ssDNA and dsDNA (Figure 1-5)[52,53,54,55,56,57]. Using fluorescence spectroscopy, a two-step model of filament formation starting with a rate-limiting nucleation phase followed by elongation was first proposed for bacterial RecA[58] and later extended and confirmed in yeast and human Rad51[59,60]. Stable nucleation events require 6 monomers of Rad51, which is also roughly the number per turn of the nucleo-protein filament (NPF)[61]. The ssDNA within the NPF adopts a B-form-like conformation over 3nt stretches and thus restricts homology search to Watson-Crick type base pairing[62]. Between these triplets, the sugar-phosphate backbone is stretched lending an increase in length and under-wound character to the larger filament that is proposed to facilitate dsDNA invasion[62].

Early biochemical work[63], in combination with genetic analysis demonstrated these proteins were DNA-dependent ATPases[64]. Basal ATP hydrolysis by Rad51 is slow at ~0.004 ($s^{-1}$)[65] and believed to occur randomly throughout a filament while ADP is continually replaced by ATP. Crystal structure of a Rad51 pre-synaptic filament show that an ATP molecule binds between two monomers of a Rad51 filament. The Walker-A motif from one monomer is the catalytic core, while a neighboring Rad51 monomer uses an ATP cap structure to keep the nucleotide cofactor in place. ATP binding is associated with an increase in ssDNA affinity and the active presynaptic filament. Hydrolysis of ATP by Rad51 reduces the affinity for ssDNA leading to spontaneous filament disassembly and is a key regulator of recombinase activity that may be modulated through protein-protein interactions or salt. Intriguingly, our SM experiments along with other ensemble approaches demonstrate that when calcium is used as the coordinating divalent cation, Dmc1, RAD51, and DMC1, all show marked reduction in ATP hydrolysis activity, while Rad51 is largely unperturbed[66]. The mutation of the lysine residue in the Walker A box of yeast Rad51 ($Rad51^{K191R}$) ablates DNA-dependent ATP hydrolysis activity and engenders sensitivity to

certain DNA damaging agents[63,67-69]. However, the Rad51$^{K191R}$ mutant protein still binds to ssDNA and promotes DNA strand exchange[67-69].

Rad51 dissociation from ssDNA has been shown to occur in bursts[70] arguing for a model where a Rad51-ssDNA filament is stable regardless of the nucleotide identity bound by internal Rad51 monomers, only so long as the terminal Rad51 has ATP bound. If the last Rad51 monomer within the filament hydrolyzes its bound ATP, the number of Rad51 monomers that will dissociate will depend on how many Rad51-ADP monomers are directly adjacent to the filament end. Residues 374-381 from a 3′ Rad51 monomer form the ATP cap that orients the ATP molecule that would be hydrolyzed by the 5′ neighboring Rad51 monomer through a salt bridge between the γ-phosphate of ATP[71]. This ATP cap is absent from Rad51 paralogues such as Rad55-Rad57 and the Shu complex that are known to stabilize the Rad51 filament. A HsRAD51$^{D316K}$ mutant displayed reduced ATP hydrolysis enhanced discrimination of ssDNA versus dsDNA and significantly enhanced recombinase function arguing the ATP cap plays a prominent role in ATP hydrolysis rates and regulation of the recombinase[71].

*In vitro* studies have shown that salt can have major impacts on the formation and stability of Rad51 filaments. Low concentrations of the monovalent potassium ion are better for filament formation[72]. ScRad51 filaments form efficiently in magnesium containing buffers, while ScDmc1, HsRAD51, and HsDMC1 all require calcium in the buffer for filament assembly[66,73]. Calcium in these systems is proposed to slow the ATPase activity and leads to more efficient filament assembly[74].

Rad51/RecA recombinases contain a primary DNA binding domain that is necessary for ssDNA filament formation, while a secondary DNA binding domain interacts with the incoming dsDNA template to align the two molecules for strand invasion[39,52]. *rad51$^{I345T}$* was isolated as a suppressor mutation that partially bypasses the requirement for Rad55-Rad57 and is proposed to increase the affinity for ssDNA over wtRad51[75]. This mutation resides in the second of two loops known to interact with ssDNA and the presynaptic filament. Alternate protein-protein interfaces show slight differences and have suggested a Rad51-dimer is the functional unit within the filament[57]. These interfaces are species specific and been shown to be important for filament formation, stability, ATPase and recombinase activities.

Dmc1 is the meiosis specific recombinase in eukaryotes and shows 150/334 identical amino acids to Rad51. The largest difference between the two is an additional 64 amino acids at the N-terminus of Rad51 that is absent from Dmc1.

### *1.2.3 Recombination mediators*

The Rad51 mediators, Rad52, Rad55-Rad57, Rad54, and members of the Shu complex (Shu1-Shu2-Psy3-Csm2) work synergistically through various modes to promote the formation and/or stability of the Rad51 presynaptic filament[76]. By promoting the key intermediate for HDR, these proteins represent a key regulatory role in DNA repair and have been of considerable interest. This notion is highlighted by the increased incidence of cancer in humans that harbor various mutants.

The seminal paper that first described the Rad51 protein as functionally similar to RecA also provided the crucial insight that Rad51 directly interacts with Rad52[63] that was later mapped to the C-terminus of Rad52. Yeast two-hybrid screening identified three Rad51 point mutants, Rad51$^{A320V}$, Rad51$^{Y388H}$, and Rad51$^{G393D}$, that all display reduced Rad52 interaction[77]. Rad52 forms heptameric ring structures[78] and helps to overcome the inhibition of RPA-ssDNA for Rad51 filament formation[79]. Rad52 and RPA also directly interact and cooperate to promote ssDNA annealing, an activity that is critical for Rad52-mediated promotion of SSA between direct repeats[80,81]. Additionally, Rad52 can directly interact with Rad55-Rad57[76].

In contrast to yeast cells where *rad52* null mutants display a severe phenotype, mammalian *RAD52* is largely dispensable due to overlapping function with the tumor suppressor gene *BRCA2*. However, human *RAD52* is clearly important for DSBR as it is synthetically lethal with several other DSBR proteins including *XRCC3*[82], *BRCA2*[83], *BRCA1* and *PALB2*[84]. Additionally, lifetime risks of 50-70% for breast and 15-55% for ovarian cancers are found to be due to inherited mutations in BRCA1/2, demonstrating the high penetrance of these mutations[85]. The redundancy between human *BRCA2* and *RAD52* indicate HsRAD52p may be a valuable target for cancer therapies to compensate for mutations in BRCA2 and thus requires a thorough understanding.

Rad55, Rad57, Shu1 and Psy3 are proposed Rad51 paralogues, although they cannot independently perform homology search or strand invasion without the core Rad51 recombinase[86,87]. Humans contain 5 RAD51 paralogues RAD51B, RAD51C, RAD51D, XRCC2, and XRCC3[88,89] and these proteins can also be viewed as mediators as they have been shown to stabilize the RAD51 filament[90].

Mutant *rad55* or *rad57* cells are sensitive to IR and MMS DNA damage, while overexpression of Rad51 protein can partially suppress the phenotype. While both members contain the core ATPase domain, it appears only ATP binding and hydrolysis is required by Rad55, not Rad57[91]. Cytological studies showed that Rad51 focus formation was independent of Rad55-Rad57, while Rad55-foci required Rad51, indicating Rad51 is first to arrive at a DSB[43]. Biochemical analysis suggested the Rad55-Rad57 heterodimer exist embedded within the Rad51 filament to potentially "cap" a Rad51 filament and limit the ATP hydrolysis at a filament end[92].

The Shu complex was identified in a genetic screen for mutants that suppressed the slow growth phenotype of *top3Δ* mutants[93]. Structural information revealed that Psy3 and Csm2 adopt a similar $\alpha$-$\beta$ fold reminiscent of the RecA core of the Rad51 recombinase, while Shu1 and Shu2 were dispensable for DNA binding[94]. Fluorescence anisotropy measures implied purified Psy3-Csm2 heterodimers prefer to bind forked and flapped ss/dsDNA structures[95]. A recent crystal structure for the entire Shu complex demonstrated Csm2-Psy3 and Shu1-Shu2 form two sets of heterodimers that are structurally similar, while residues in Psy3 and Shu1 bridge the two pairs of heterodimers into a V-shaped structure[96]. This study also proposed that the Shu complex contains two separate DNA-binding regions; the first is made up of residues within Psy3-Csm2 and primarily binds to ssDNA, while the second resides within the Shu1-Shu2 heterodimer and primarily binds dsDNA, further implying the Shu complex would prefer to bind ss/dsDNA junction structures. Deleting either Psy3 or Csm2 showed reduced Rad55 foci formation, suggesting the Shu complex is important for recruiting Rad55-Rad57 dimers to IR-induced DSBs[95].

Rad54 is a member of the Snf2-family of SF2 helicases which translocate on dsDNA without strand separation[97]. Rad54 is also classified as a recombination mediator as it has been shown to stabilize the Rad51-ssDNA filament in an ATP-independent manner and is required for efficient strand invasion by Rad51, while *rad54* mutant yeast display a similar reduction in recombination as *rad51* or *rad52* mutants for spontaneous DSBR. Rad54 does not appear absolutely necessary for meiotic HR as

25-65% of meiotic cells remain viable and may be due in part to the redundancy in function of the Rdh54/Tid1 protein[21]. The ATPase activity of Rad54 has been proposed to enhance HR through several means including the removal of bound proteins on the dsDNA template, induction of negative supercoiling on the template to enhance pairing by Rad51, and simply translocating along the dsDNA to aid in a 1-dimensional homology search process. Once a Rad51 filament has paired with a donor dsDNA, Rad54 is proposed to switch gears to dissociate Rad51 from the filament to give access of the primed substrate to DNA polymerase delta[98]. Species-specific contacts between Rad54 and Rad51 were required to observe a six-fold increase in ATPase activity of Rad54 by Rad51-bound to dsDNA[99], while Rad54 foci formation at DNA damage sites required both Rad55-Rad57 and Rad51 indicating it arrives after the pre-synaptic filament has formed[43].

### 1.3 HELICASES IN THE REGULATION OF HR

All organisms express multiple helicase enzymes owing to their utility in unlocking information sheltered within dsDNA and also indicates the specialization of function these proteins can obtain[100]. These motor proteins typically hydrolyze ATP to translocate over nucleic acids and under certain circumstances separate the two strands of base-paired nucleic acids. Helicases can play both facilitating and antagonizing roles in nearly every DNA metabolic event, including HR and replication fork restart[100-102]. For example, helicases can promote resection around a DSB, remove recombinases from a pre-synaptic filament, process the post-synaptic filament to enable DNA polymerase binding, and migrate recombination intermediates to affect the CO/NCO ratio of DSBR.

There are 3 helicases in yeast that have been shown to be key regulators of HR; Srs2, Mph1, and Sgs1. Mutation analysis has shown that each of these enzymes carry out multiple specific functions that may sometimes overlap[103,104]. For example, the helicase activity of Sgs1 (human BLM), mediates the resection of ssDNA, joint reversal, dHJ dissolution, and DDR signaling[105]. Both *srs2* and *sgs1* single mutants display mitotic hyper-recombination and elevated levels of chromosome missegregation[106] indicating the proteins are involved in suppressing inappropriate recombination. Mph1 (human FANCM) is a member of the SF2 DEAD/H superfamily of helicases and promotes Rad51-dependent restart of stalled

replication forks[104] as well as robust D-loop dismantling activity *in vitro*[107]. Mutation in the genes encoding the helicases involved in HR regulation result in human disease such as Fanconi Anemia (FA), Bloom syndrome, Warner syndrome, and an increased incidence of cancer, and all highlight the importance of these understanding how these enzymes function (Table 1-1).

### *1.3.1 SF1 helicase mechanisms*

DNA helicases and translocases can be broadly categorized into six superfamilies based on the number and sequence of amino acids residing in shared motifs. The two largest superfamilies (SF1 & SF2) are highly related, but diverge in the sequence and arrangement of seven core motifs; I, Ia, II, III, IV, V, and VI[108]. Both SF1 and SF2 contain members that may translocate on DNA and/or RNA in a 3′→5′ or 5′→3′ direction and have activities in DNA replication, recombination, and translation[100].

UvrD is a bacterial SF1 helicase/translocase that is highly similar to PcrA, Rep, and Srs2 helicases (Figure 1-6A). These proteins contain the SF1 core helicase domain made up of sub-domains 1A, 1B, 2A, and 2B with crystallization studies of UvrD, PcrA and Rep showing that sub-domains 1A and 2A form the ATP binding cleft with structural and sequence similarities to the core of the RecA protein. Ensemble studies have suggested these four related proteins exist in a monomeric form in solution which are sufficient for ssDNA translocation, while dimers are required for helicase activity. The precise orientation and mechanism of this dimerization is not understood and no clear dimer interface has been identified to date. Alignment between these relatives shows reduced similarity at domain interfaces[109], indicating that the interaction between these sub-domains may be involved in regulating protein activity.

These helicases may differ in their preferred DNA substrate; Studies of UvrD showed that it could initiate ssDNA translocase activity at the ss/dsDNA junction of a 5′ ssDNA tail and the specificity of starting translocation from this area is dependent upon residues within the 2B domain. UvrD$^{D420P}$ point mutants showed a six-fold increase for initiating translocation from these junctions[110], and this residue is already a proline in Rep and Srs2 indicating each of these may have evolved specialized functions.

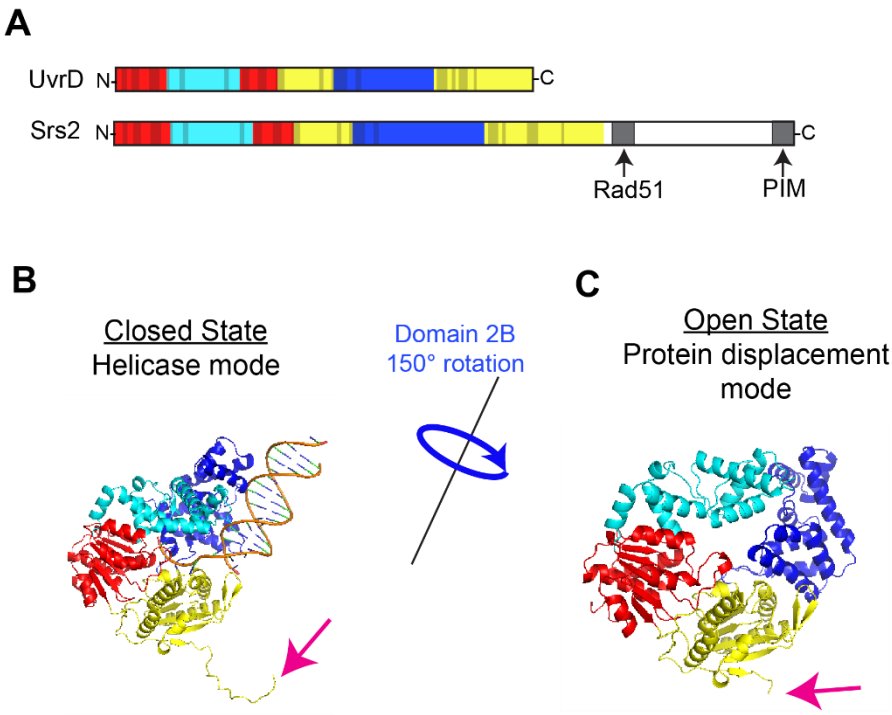


**Figure 1-6. Organization of SFI domains and consensus motifs.** (A) primary organization of bacterial UvrD and yeast homologue Srs2. Domains 1A, 1B, 2A, and 2B are in red, cyan, yellow and blue, respectively. Shaded regions within the helicase domain are the conserved helicase motifs. At the C-terminus of Srs2 lies the Rad51interaction domain and PCNA interaction motif (PIM). The open (B; PDB: 3LFU) and closed (C; PDB: 2IS6) crystal structures of EcUvrD. The 2B subdomain undergoes a 150-degree rotation and is believed to switch the protein from helicase to protein displacement activities. The pink arrow points to the C-terminus where Srs2 contains an additional ~400 amino acids.

The combination of bulk biochemical, FRET, and structural studies have revealed that these helicases may occupy an open or closed conformation[109,111,112]. In the closed conformation, subdomain 1B restricts the mobility of domain 2B and prevents it from interacting with domain 2A. This in turn ensures that the GIG motif with 2B can interact with dsDNA duplex ahead of the helicase (Figure 1-6B). In this case, a ss-dsDNA junction forms a “L” shape with the ssDNA appearing orthogonal to the dsDNA. The 3′-ssDNA is threaded through a groove made up of domains 1A and 2A at their interface with 1B and 2B. This closed conformation uses a wrench-and-inchworm model for helicase activity with a two-part power-stroke. The binding and hydrolysis of ATP is the first step and induces the separation of the first base pair at the ss/dsDNA junction. Release of ADP + Pi is accompanied by a 20° rotation between domains 1A and 2A where the nucleotide cofactor is released and the ssDNA is shifted +1nt to repeat the process.

In the open conformation 2B is rotated between 130-160° away from 1B to interact with 2A (Figure 1-6C). This "open" conformation is believed to mediate ssDNA translocase and protein displacement activities, while it can also carry out helicase activity using a strand displacement model, rather than wrench-and-inchworm. Using fluorescence resonance energy transfer (FRET), it was determined that UvrD adopts a more open conformation with increasing lengths of 3′ ssDNA tails or increasing NaCl concentration indicating both the DNA substrate as well as electrostatic interactions can modulate the open/closed state[112]. The authors also found that the swivel of the 2B sub-domain occupies intermediate states that correlate to nucleotide cofactor and ssDNA binding events. The Rep helicase will only rotate 2B 130° from 2A, creating an "intermediate" open state, and deleting the entire 2B in Rep creates a protein with twice the helicase activity indicating 2B is auto-inhibitory for Rep[113]. From these studies, it becomes evident that these SF1 members occupy several different primary, secondary, tertiary, and even quaternary organizations that impart specialized activities under various conditions, thus adding to the layers of complexity when studying these enzymes.

### *1.3.2 The helicase/translocase Srs2*

Genetic studies were the first to identify *SRS2* (Suppressor of *rad6*) as the second of two mutations that suppress trimethoprim-sensitivity in a *rad6-1 rad18-2* strain[114]. *SRS2* was unique from *SRS1* in that it also conferred resistance to UV sensitivity in the same background, but not gamma-radiation, suggesting it had broad and potentially separation of function effects upon DNA repair and did not solely function to suppress damage from trimethoprim. Screening for mutations that increased UV-radiation sensitivity uncovered the *RADH* gene, while analysis of the primary amino acid sequence showed it contained all the consensus domains of an SF1 helicase with a high degree of homology to bacterial helicases UvrD and Rep[115]. The Klein laboratory identified *HRP5* in a screen for hyper-recombination, and after cloning the gene demonstrated it was allelic to both *SRS2* and *RADH*[116]. The purification of a His-tagged Srs2 protein confirmed that the *SRS2* gene encoded a DNA-dependent ATPase with a 3′ to 5′ directional bias on ssDNA[117].

The finding that *srs2* suppression of *rad6* requires *RAD52* served as the first evidence that *SRS2* also functioned through recombinational repair[118]. One of the many hypotheses the authors concluded with was that *SRS2* may alter the "level, activity, or stability" of a *RAD52* group protein. It wasn't until 1992 when Frances Fabre's group published a paper that confirmed this hypothesis using a screen for suppressors of UV- and gamma-ray sensitivity of *srs2::LEU2* diploid mutant strains[4]. It was noted that *srs2* single mutants were more toxic in diploid strains than haploids, while out of the 11 identified semi-dominant suppressors, all were heterozygous *rad51* mutants. Furthermore, by examining the differences between the survival of these mutants when exposed to either UV- or gamma-radiation led to the profound proposal Srs2 removes recombinational proteins from ssDNA gaps. The increased sensitivity to *srs2* in diploids was later shown to be the result of increased inter-homolog recombination[119]. Two papers were simultaneously published in Nature with biochemical and electron microscopy evidence that the mechanism of recombination suppression by Srs2 was to dismantle the pre-synaptic Rad51 filament[120,121], a function that is commonly referred to as "strippase" activity.

While the Srs2 helicase has never been crystalized, the primary organization of Srs2 shows the conserved SF1 helicase domain resides in the N-terminus from residues 1-776, while the ~400aa Srs2-specific C-terminus is involved in protein-protein interactions and is the target of PTMs (Figure 1-6A). Mutating the Lysine at position 41 to an alanine or serine within the Walker A motif abolishes ATPase, helicase/translocase and Rad51 antagonism activities[120,122]. Interestingly, the ATPase dead *srs2$^{K41A}$* mutant displayed an enhanced hyper-recombination phenotype beyond that of *srs2* deletion strains, suggesting that the presence of Srs2$^{K41A}$ can prevent a redundant mechanism from rescuing the phenotype, or that the protein is toxic[123]. Srs2 hydrolyzes ATP at a rate of $\geq$ 50 sec$^{-1}$, and can unwind forks, flaps, blunt end dsDNA, and 5′ ssDNA overhangs while the preferred substrate to initiate helicase activity from is a 3′ ssDNA overhang of at least 10nt[124]. Stop flow experiments with monomeric Srs2 demonstrated a translocation velocity of 300nt (sec$^{-1}$) on naked ssDNA[65].

Using a yeast two-hybrid system, the Rad51 interaction domain of Srs2 was mapped to residues 783-914[125]. Subsequent sequence analysis of residues 833-864 revealed a variant of the BRC (BRCv) repeat present in BRCA2 that is known to interact with, and stabilize a Rad51-ssDNA filament. This BRCv is also present in other helicases known to partake in HR regulation including Sgs1 and HsRECQ5, while

the Srs2$^{L844A}$ point mutant protein was strongly deficient in both Rad51 interaction and inhibition of D-loop formation *in vitro*[126]. The Rad51 mutants, Rad51$^{Y388H}$ and Rad51$^{G393D}$, that were identified as impaired for their interaction with Rad52[77] also display a reduced interaction with Srs2, implicating the C-terminus of Rad51 as the location where Srs2 interacts[127]. Moreover, these lines of evidence imply that Srs2 and Rad52 may compete for the same binding location on a Rad51 filament to fulfill their anti- and pro-recombinase functions, respectively. This assertion was supported by an *in vitro* strand exchange assay that showed that Srs2 antagonism of Rad51-mediated D-loops could be partially overcome by the addition of Rad52, although higher concentrations of Srs2 was able to partially overcome this inhibition[128], suggesting the concentration of Srs2 at a repair center could impact whether Rad52-promoted HR, or by extension SSA, would be successful.

Important for this work, C-terminal truncation mutants of Srs2 that include a minimum of residues 1-860 demonstrate unperturbed ATPase/helicase activities on a 3′-tailed substrate[125,65] and ATPase activity on circular M13mp18 ssDNA. Furthermore, we and others have found these truncation mutants are less prone to aggregation and ease the production of large amounts of soluble protein that elutes from a gel filtration column as a single peak roughly corresponding to a monomer. Bulk biochemical approaches indicate the truncated Srs2$^{1-860}$ mutant that lacks a large portion of the Rad51 interaction domain is severely compromised for its Rad51 antagonistic activity[65,125,129]. The apparent binding between Srs2$^{1-898}$ and Rad51 was measured as $K_D$ = 15μM ± 5μM[65].

In stop flow measurements, the ATPase dead Srs2$^{1-898:K41A}$ could not antagonize Rad51 filaments, even at high concentrations (1.5μM Srs2:4μM Rad51) and is strong evidence that translocase activity is required for Rad51 filament antagonism. Analogously, a synthetic peptide corresponding to residues 861-898 failed to interact with Rad51, and high concentrations of this peptide failed to inhibit Rad51 filament clearing activity of Srs2$^{1-898}$, while an alternative explanation could be that the peptide failed to fold properly. Using the Rad51 mutant proteins Rad51$^{K191R}$ that hydrolyzes ATP 4-fold slower than wtRad51, and Rad51$^{E221D}$ that hydrolyzes ATP 10-fold faster than wtRad51, Srs2 was proposed to induce ATP hydrolysis within the Rad51 filament and catalyze its removal one monomer at a time[65]. In contrast, *in vivo* SC studies found that the *srs2$^{Δ875-902}$* mutant that lacks a large portion of the Rad51 interaction domain could still antagonize Rad51 foci accumulation[122].

Adding to this complexity, Srs2 also displays pro-recombination roles. In one study, deleting either *sgs2* or *srs2* increased the number of CO events 3-4 fold in an ectopic recombination assay (5% of HR events in WT cells are resolved as COs), and deleting *srs2* in a *RAD51* overexpression strain almost completely eliminated NCOs, while overexpression of *Srs2* nearly eliminated CO events[130]. These results promoted the idea that Srs2 is involved in shuttling recombination events into the SDSA pathway, a hypothesis that is supported when observing that GC events occur primarily on a single side of individual DSBs when Srs2 is properly functioning. possibly either by preventing second end capture, or by dismantling an extending D-loop. *In vitro*, Srs2 was capable of antagonizing paired D-loop structures, although Mph1 appears to be better suited for this task[107]. In fact, Rad54, Mph1, Sgs1, and Srs2 have all been proposed to remove Rad51 from paired D-loops to one degree or another, although Rad54 is generally considered the primary modality for these purposes, further adding speculation as to which substrate, the presynaptic or post-synaptic filament, Srs2 acts upon[99].

Finally, *srs2* deletion strains that had delayed repair kinetics sufficient to activate the Rad53 checkpoint showed that they were impaired in recovering from cell cycle arrest, even though these cells are capable of completing repair of the DSB[131]. These cells were later found to have persistent Ddc2 and RPA foci, and despite the completion of repair and removal of the 9-1-1 clamp, Dpb11 remained associated with chromatin[132].

### *1.3.3 Regulation of Srs2 activity*

Given the various and sometimes contradictory functions ascribed to Srs2, the regulation of activity would appear paramount for proper function. Four potential modalities of Srs2 regulation have been suggested and include regulation at the level of transcription, post-translational modifications (PTMs), recruitment, and protein-protein interactions.

Null *srs2* mutants are UV-sensitive only when treated in the G1 phase of the cell cycle[4], as these produce lethal recombination intermediates between homologous chromosomes rather than sister chromatids that are present in S and G2 phases. *SRS2* is expressed at low levels throughout the cell cycle, but is induced at the G1 to S phase boundary coincident with the expression of other DNA

synthesis genes in mitotic cells, as well as under DNA damage conditions, but only during G2[133]. Additionally, *SRS2* expression is induced in meiotic cells that have just begun replicating their DNA. Overexpression of *SRS2* in meiotic cells removes Rad51 foci from the chromosomes, but does not impact the level of fluorescent Dmc1 foci, indicating that Srs2 cannot disassemble Dmc1 filaments, although this feature had not been tested *in vitro*[122].

Cdk1 targets several residues in the C-terminal domain of Srs2 for phosphorylation including T604, S698, S833, S879, S890, S893, S933, T935, S938, S950, and S965. To decipher how PTMs may regulate Srs2, Soponaro and colleagues created a mutant $Srs2^{7AV}$ construct that could not be phosphorylated to compare with the constitutively phosphorylated $Srs2^{7DE}$ counterpart[134]. It appeared that while phosphorylation was not necessary for the removal of toxic Rad51 filaments, Cdk1-dependent phosphorylation targets Srs2 to bias recombination outcomes into the SDSA pathway.

The C-terminus of Srs2 was found to interact with PCNA that has been SUMOylated on K164 by Siz1 in response to stalled replication forks[135-137]. Later refinement of this Srs2 region showed a degenerate PCNA-interacting motif in residues 1149-1156 and a conserved SUMO-interaction motif (SIM) in the residues 1169-1174 and both are required to specifically recognize SUMO-PCNA[135]. These interactions tether Srs2 to the replication fork machinery to antagonize Rad51-mediated HR at a collapsed, but not stalled fork[128] and shuttle them into the PRR pathway over HR.

The impact of recombination mediators on Srs2 activity has also been an area of active research, and there are reports, sometimes conflicting, about the influence of these proteins on Srs2 activity. Using SC analysis in combination with *in vitro* strand exchange assay, it was proposed that while Srs2 removes Rad51 filaments indiscriminately, Rad52 can resist the Srs2-mediated clearance of Rad51 filaments and acts as a quality control mechanism to restrict HR to proper events[128]. Interestingly, $rad51^{Y388H}$ and $rad51^{G393D}$ are simultaneously impaired for Rad52 and Srs2 interaction suggesting a competitive binding model may play a role in Rad51 promotion versus antagonism[127]. Rad52 could indirectly resist Srs2-mediated antagonism of the Rad51 filament by promoting Rad51 filament formation kinetics, or by directly preventing Srs2 from clearing Rad51 by inhibiting Srs2 binding, translocation or interaction with Rad51.

Both members of the Rad55-57 heterodimer are paralogues to Rad51 and stabilize the presynaptic filament when challenged with high salt[92]. These proteins contain the RecA ATPase domain

but differ from Rad51 in that they lack the N-terminal ~40aa while also containing an additional C-terminus absent in Rad51. Pull down assays showed that Srs2 directly interacted with the Rad55-Rad57 heterodimer with a higher affinity than Rad51-Srs2. Mixed Rad51-Rad55-Rad57 filaments were shown *in vitro* to resist the filament clearance activity of Srs2 when viewed by EM. Bulk biochemical experiments showed that Rad51-Rad55-Rad57 on a 3′-tailed ss/dsDNA junction resisted Srs2 helicase activity, even when Srs2 was in 5-fold molar excess to Rad55-57 and suggested that the heterodimer prevents Srs2 translocation rather than binding in solution to sequester it away from Rad51 filaments. Further supporting this hypothesis is that Rad55-Rad57 heterodimers were able to pull down Rad51 and Srs2 in a 1:1:1 stoichiometry, implicating the binding location of Srs2 on Rad55 is separate from Rad55 binding to Rad51[92]. Surprisingly, Rad55-Rad57 did not alter Srs2 ATPase activity in bulk, arguing against a model where Srs2 cannot translocate past a Rad55-Rad57 heterodimer, or alternatively that Rad55-Rad57 decouples Srs2 ATPase activity from its translocase activity[92].

The Shu complex has also been suggested to attenuate Srs2 anti-recombinase activity. In comparison to Rad55-Rad57 which is proposed to function by halting Srs2 translocation, Srs2 foci at induced DSBs significantly increased in a *shu1* mutant cell line, indicating the Shu complex functions to limit the recruitment of Srs2 to DSBs[87].

### *1.3.4 The search for the human Srs2 homologue*

While a direct human homologue to Srs2 has yet to be identified, RTEL1 and RECQ5 are proposed to be functional homologues because they also dismantle presynaptic RAD51 filaments[138,139]. Reminiscent of the interaction between Srs2 and Rad51, RECQ5 has been shown to directly interact with RAD51 using a 70 amino acid region that lies outside the conserved helicase domain and also contains a BRCv motif that is found in Srs2[138]. Mutants that impair this interaction show equivalent ATPase activity, but have a moderate reduction in their displacement of RAD51 from ssDNA.

*S. pombe*, mice and humans all possess a SF1 helicase, FBH1, bearing an amino-terminal F-box domain known to ubiquitinate target proteins, while S. cerevisiae do not have this protein. HsFBH1 can directly interact with RAD51 to disrupt a RAD51-ssDNA filament *in vitro*, as well as RAD51 foci formation

*in vivo*, arguing it is a functional homologue to ScSrs2[140]. Interestingly, providing HsFBH1 in yeast *srs2Δ* cell lines can rescue the MMS-sensitivity but not a *rad6* synthetic lethality, supporting the idea that the helicase activity of Srs2 alone, without a clear Rad51 interaction, can function in certain steps of HR regulation. HsFBH1 is often mutated in melanoma cells, arguing these activities are relevant to human cancer[141]. Similarly, the human PARI UvrD-like helicase appears to antagonize RAD51-mediated HR. Like Srs2, PARI also interacts with PCNA and RAD51 to tether the helicase to a replisome and prevent HR at replication forks[142].

Taken together, while humans do not contain a direct Srs2 homologue, several helicases including RECQ5, FBH1, and PARI have evolved to perform specific functions of the multi-functional Srs2. Mutations in the human helicases BLM, WRN, and RECQ4 helicases give rise to Bloom's syndrome, Werner's syndrome, and Rothmund-Thomson syndrome, respectively, and demonstrate a need for clear understanding of helicase activity in regulating HR.

## 1.4 CONCLUSION

Although HR is critical for cell survival, it must be kept in check to keep it from blocking replication forks, creating toxic intermediates, and preventing better suited repair pathways. To this end, the dynamic formation and stability of the Rad51 pre-synaptic filament intermediate serves as a key control center to dictate the eventual success of HR. Recombination mediators enhance the forward reaction, while the Srs2 helicase has been shown to dismantle the Rad51 presynaptic filament to drive the reverse direction. The balance between Rad51 filament formation and disassembly may be partially mediated through post-translational modifications and/or relative concentrations of each protein at a repair center.

Srs2 has drawn the fascination and ire of researchers given that mutations exhibit pleiotropic effects from anti- to pro-recombination, as well as its redundant function with other yeast helicases. Furthermore, Srs2 is involved in DNA metabolic processes outside recombination including the maintenance of the replication fork, post-replication repair, checkpoint responses, DNA triplet repeat maintenance and NHEJ, complicating genetic approaches. The transient nature of motor proteins makes them elusive targets for ensemble approaches that rely on discrete snapshots of population averages that

may progress through several intermediates. Due to these factors, several critical questions surrounding Srs2 remain; How does Srs2 dismantle Rad51 filaments, and is this dependent upon the Rad51 interaction domain? What is the activity in dismantling mixed recombination filaments composed of RPA, Rad51, Rad52 and other mediator proteins? Does the oligomeric state impact helicase and/or strippase activities? Can Srs2 dissociate Rad51 D-loops, and under what context(s)? The purpose of this thesis was to develop new experimental methods to help address some of these questions, as well as poise future experiments for a deeper understanding of genetic recombination.

| Function | *Escherichia coli* | *Saccharomyces cerevisiae* | *Homo sapiens* | Disease |
|---|---|---|---|---|
| **Single Stranded Binding** | SSB | Rfa1–Rfa2–Rfa3 (RPA) | RPA1–RPA2 –RPA3 (RPA) | |
| **End Resection** | RecBCD<br><br>RecQ-RecJ | Mre11–Rad50–Xrs2 Sae2<br>Exo1<br>Dna2–Sgs1–Top3– Rmi1 | MRE11–RAD50 –NBS1, CtIP<br>EXO1<br>DNA2–BLM–TOP3 –RMI1–RMI2<br>DNA2-WRN | Nijmegen breakage syndrome; AT–like disorder<br>Colorectal cancer<br>Bloom syndrome |
| **Recombinases** | RecA | Rad51<br>Dmc1 | RAD51<br>DMC1 | Fanconi Anemia (group R) |
| **Mediators** | RecFOR | Rad52<br>Rad55–Rad57<br>Psy3–Csm2–Shu1 –Shu2 | BRCA2–PALB2<br>RAD51B–RAD51C –RAD51D–<br>XRCC2–XRCC3<br>RAD51D–XRCC2 | Breast cancer |
| **Helicase/ Translocase** | UvrD<br>Rep<br>PcrA | Srs2<br>Mph1<br>Sgs1<br>Rad54 | RECQ5, FBH1, PARI<br>WRN, FANCM<br>BLM<br>RAD54A/B<br>RTEL1 | Bloom Syndrome<br>Werner Syndrome<br>Hoyeraal– Hreidarsson Syndrome |
| **Dissolvases and Resolvases** | RecQ- TopoIII<br>RuvC | Sgs1-Top3-Rmi1<br>Mus81–Mms4<br>Slx1–Slx4<br>Yen1 | <br>MUS81–EME1<br>SLX1–SLX4<br>GEN1 | Bloom Syndrome<br><br>Fanconi Anemia |

**Table 1-1. Functional grouping of E. coli, S. cerevisiae, and human recombination proteins with associated human diseases.** This is not meant to be an exhaustive list, but more so to identify homologues that are discussed within the text.

## CHAPTER 2: VISUALIZING GENETIC RECOMBINATION BY SINGLE-MOLECULE OPTICAL MICROSCOPY

Portions of this chapter have been adapted from the following publications:

Pokhrel N, Origanti S, Davenport EP, Gandhi D, Kaniecki K, Mehl RA, Greene EC, Dockendorff C, Antony E. Monitoring Replication Protein A (RPA) dynamics in homologous recombination through site-specific incorporation of non-canonical amino acids. *Nucleic Acids Res*. 2017 Sep 19;45(16):9413-9426.

Kaniecki K, DeTullio L, Greene EC. A change of view: homologous recombination at single-molecule resolution. *Nat Rev Gen*. 2018 Apr;19(4):191-207.

Kaniecki K*, DeTullio L*, Greene EC. Single-stranded DNA curtains for studying the Srs2 helicase using total internal reflection fluorescence microscopy. *Methods Enzymol*. 2018;600:407-437.

### 2.1 OVERVIEW

Notwithstanding the impressive detail genetic and bulk biochemical approaches have offered into the mechanisms of HR, SM studies have the potential to further our understanding by providing even more detailed insights into reaction mechanisms, and these methods are particularly beneficial for reactions that involve heterogeneous populations, transient intermediates, or both, as is often the case with reactions involving helicases. Indeed, SM methods have proven deeply insightful for understanding helicases, and some examples include SM studies of the RecBCD complex[143,144], which is involved in DNA end-processing in *E. coli*, the bacterial Rep, UvrD, and PcrA helicases[145-147], the archaeal helicase XPD[148], and the eukaryotic helicases Srs2 and Pif1[149,150]. To help expand this tool box of methods

available for SM studies of helicases involved in HR, I applied the ssDNA curtain assay to study Srs2 activities at the single molecule level[151,152]. This chapter will detail the purification of Srs2 variants, the ssDNA curtain methodology, including data analysis, as well as the supporting bulk methodology I applied to generate the results described in chapters 3 and 4.

## 2.2 SSDNA CURTAINS FOR STUDYING PROTEIN-SSDNA INTERACTIONS

We have developed DNA curtains as a tool for real time visualization of protein-nucleic acid interactions at the single molecule level using total internal reflection fluorescence microscopy (TIRFM)[153-155]. In brief, DNA curtains are prepared by first depositing metal barriers and anchors on the surface of a fused silica microscope slide by electron beam lithography. The slide is then coated with a fluid lipid bilayer, which prevents nonspecific surface adsorption and provides a mobile platform for anchoring DNA molecules through a biotin-streptavidin linkage. Buffer flow is used to push the DNA molecules into the barriers where they all align with one another[153,155]. If desired, the second DNA end can be attached to a downstream anchor point[154]. This approach can be used with dsDNA or ssDNA and allows for the direct visualization of hundreds of individual DNA molecules by TIRFM, thus offering a flexible experimental platform that can be adapted to the study of many types of protein-DNA interactions[66,73,156-163]. We have recently provided detailed descriptions of the TIRFM instrumentation used for these assays, the nanofabrication methods for making patterned slide surfaces with electron beam lithography, and the procedures for preparing microfluidic flow cells[164-166]. Here, we describe methods for how ssDNA curtains can be used to study the *S. cerevisiae* helicase Srs2 as it acts upon ssDNA substrates bound by either Rad51 or RPA. Included in this information are details on fluorescent protein purification, ssDNA substrate preparation, and further details on bilayer deposition and ssDNA curtain preparation. We then provide a detailed overview on experiments using fluorescently-tagged or unlabeled Srs2, and analysis of the resulting data.

*2.2.1 Protein and ssDNA Preparation.*

A key aspect of using ssDNA curtains for studying the activities of Srs2 and other HR-related proteins, is the need to prepare and purify proteins. For much of our work on HR we rely upon proteins that are labeled with GFP or mCherry; when denoting a protein that may contain either GFP- or mCherry tag, I will use the XFP (X Fluorescent Protein) label. Although GFP and mCherry are perhaps not as bright and photo-stable as many organic fluorophores, they offer the advantage of providing a homogenous protein preparation where all of the proteins are labeled. Moreover, GFP-tagged versions of many HR proteins have already been evaluated through *in vivo* studies, including GFP-Srs2 and GFP-RPA, thus validating their biological functions[43,128,167]. For all GFP-labeled proteins, we employ the $GFP^{A206K}$ mutation to prevent dimerization by the label[168]. For XFP-labeled proteins that have not yet been tested, genetic assays are readily available to validate biological activities. Here, we will describe the procedures for producing unlabeled and XFP-tagged Srs2 and RPA. For ssDNA curtains using Rad51, we rely upon unlabeled version of the protein, as GFP-tagged Rad51 is not functional *in vivo*[43]; procedures for purifying unlabeled *S. cerevisiae* Rad51 have been described elsewhere[68].

*2.2.2 Purification of GFP-tagged Srs2.*

Several Srs2 variants were purified including N-9xHis-XFP-GGPGG-$Srs2^{898}$, N-9xHis-XFP-GGPGG-$Srs2^{1-898:K41A}$, N-9xHis-XFP-GGPGG-$Srs2^{1-860}$, unlabeled N-9xHis-$Srs2^{1-898}$, or N-9xHis-$Srs2^{1-860}$. The labeled variants retained biological activity *in vivo* when including the GGPGG linker between the fluorescent tag and Srs2.

1. XFP-Srs2 variants were expressed in *E. coli* from a pET15b vector, while unlabeled Srs2 was expressed from a pET11c vector.

2. Bacteria are grown at 37C to an OD600 of ~1.0. The temperature is then reduced to 16˚C before initiating protein expression by the addition of 0.1-0.5 mM isopropyl-β-D-thiogalactopyranoside (IPTG).

3. Cells are grown for an additional 20 hours at 16˚C. Cells are then harvested by centrifugation, and the cell pellet is frozen at –80˚C.

4. The frozen cell pellet is thawed at 37˚C and resuspended in cell breakage buffer containing 40 mM $NaHPO_4$ [pH 7.5], 600 mM KCl, 5% glycerol, 10 mM imidazole [pH 7.8], 0.1 mM Tris(2-caroxyethyl)phosphine hydrochloride (TCEP), 0.05% Tween-20, 10 µM E-64, 100 µM 4-(2-Aminoethyl)benzenesulfonyl fluoride hydrochloride (AEBSF), 1 mM Benzamindine and 1 mM Phenylmethanesulfonyl fluoride (PMSF). The cells are then lysed by sonication on ice, and the lysate was clarified by ultracentrifugation.

5. The clarified lysate is then incubated for 30 min with a Talon metal affinity resin equilibrated with Nickel Buffer A (40 mM NaHPO4 [pH 7.5], 300 mM KCl, 5% glycerol, 15 mM imidazole, 0.02% Tween-20, 1 mM Benzamidine, 1 mM PMSF, 0.125% myo-inositol). Before elution, the column is washed extensively with Buffer Nickel A.

6. Proteins are eluted from the Talon metal affinity column with a step of Buffer Nickel A containing 400 mM imidazole [pH 7.8]. Immediately after elution, the sample is adjusted to 5 mM EDTA [pH 8] and 1 mM TCEP.

7. The eluate is then dialyzed against Heparin Buffer (20 mM NaHPO4 [pH 7.5], 100 mM KCl, 5% glycerol, 0.01% Tween-20, 1 mM TCEP, 2 mM EDTA, 0.125% myo-inositol) for 1.5 hours, with 1 L buffer changes every 30 min.

8. The dialyzed eluate is then loaded onto a 5 ml HiTrap Heparin column equilibrated with Heparin Buffer, and proteins are eluted with a single step of Heparin Buffer containing 500 mM KCl.

9. The HiTrap Heparin purified fraction (~ 4 ml) is then dialyzed against Storage buffer (40 mM NaHPO4 [pH 7.5], 300 mM KCl, 10% glycerol, 0.01% Tween-20, 1 mM TCEP, 0.5 mM EDTA, 0.125% myo-inositol) for 2 hours at 4˚C.

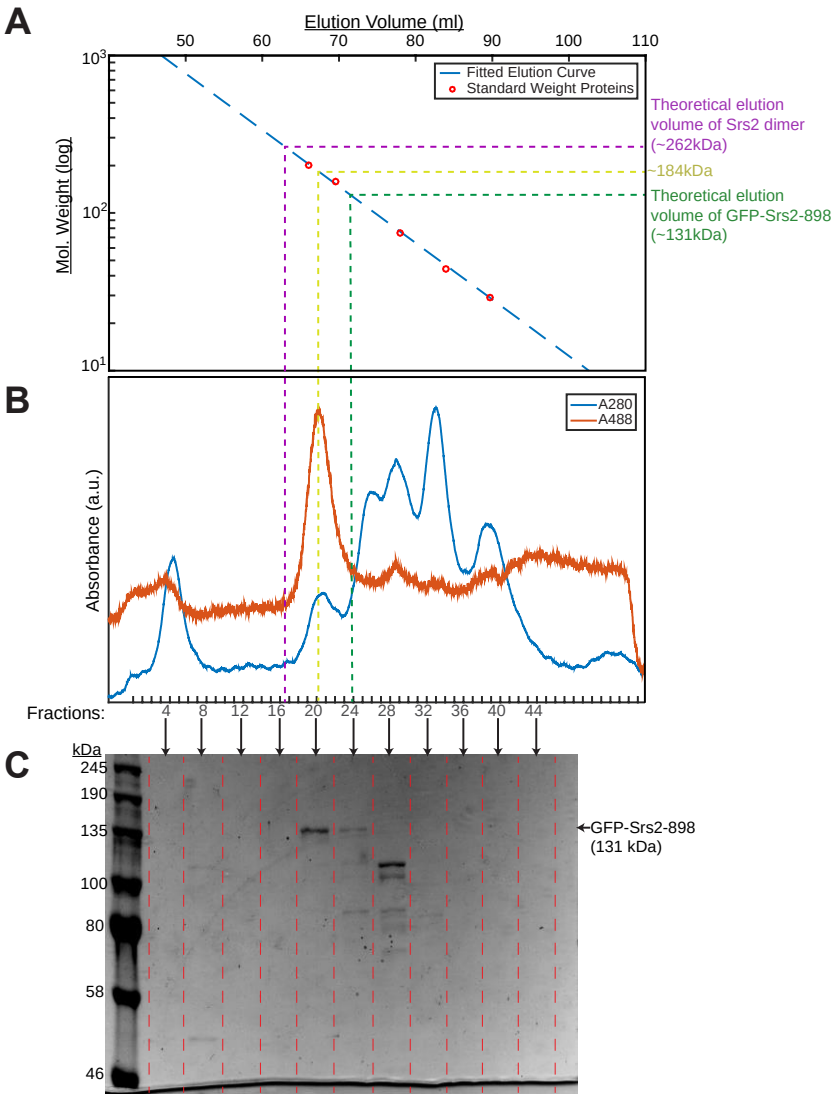


**Figure 2-1. Multimeric state of purified GFP-Srs2.** (A) A semilog plot of elution volumes versus molecular weight (log) was generated using a set of globular protein standards to determine the multimeric status of the purified Srs2. The yellow dotted line indicates the predicted size of the peak containing Srs2 as determined by SDS-PAGE in (C). The green dotted line indicates the predicted elution volume of monomeric Srs2. (B) Elution profile of GFP-Srs2-898 from a Superdex200 16/600 size exclusion column with absorbance traces at 280 & 488nm to determine protein and GFP elution locations respectively. The elution volume aligns with the numbers displayed at the top x-axis of (A). Numbers at the bottom indicate fractions collected with arrows pointing down to their corresponding lane. (C) An SDS-PAGE analysis of several fractions taken at regular intervals from the elution profile in (B). A protein ladder is included on the left with appropriate sizes, and the location of GFP-Srs2-898 is denoted by an arrow on the right.

10. The sample is then applied to a Superdex 200 size exclusion column previously equilibrated with Storage Buffer.

11. Peak fractions from the Superdex 200 corresponding to monomeric Srs2 are then pooled, flash frozen in liquid nitrogen, and stored in single-use aliquots at -80˚C (Figure 2-1, see below).

Note with Figure 2-1 that while the GFP-Srs2 protein elutes at a size that is ~50kDa heavier than predicted, we attribute this to the non-globular shape of the tagged protein that would increase its apparent size relative to the standard curve generated using globular proteins. This apparent increase in molecular weight was seen for all Srs2 variants. We conclude that the Srs2 protein within this narrow peak is monomeric, as dimeric Srs2 molecules are predicted to elute at ≥260kDa (≤63ml).

*2.2.3 Purification of fluorescently tagged RPA*

We use RPA to remove secondary structure from the ssDNA so that the molecules can be easily extended by buffer flow, and the fluorescent proteins also allow us to visualize the ssDNA with no need for any addition DNA-labeling dyes[169]. In addition, RPA-ssDNA is the physiological substrate for the early stages of HR in eukaryotes[170,171]. We used both wtRPA (Rfa1-6xHis) and fluorescent RPA (N-Rfa1-7A-XFP-6xHis) which bears the GFP or mCherry fusion on the C-terminus of the Rfa1 separated by a 7-alanine linker; note, that this GFP-tagged version of RPA retains biological function *in vivo*[43].

1. *S. cerevisiae* RPA variants were encoded in a pET11d plasmid and expressed in *E. coli*.

2. Cells are harvested by centrifugation, and the cell pellet is frozen at -80˚C.

3. The cell pellet is then thawed and resuspended in cell lysis buffer (50 mM $NaHPO_4$, 250 mM KCl, 5 mM imidazole [pH 7.9], 5% glycerol, 0.1mM TCEP, 0.02% Tween-20, 10 µM E-64, 100 µM AEBSF, 1 mM Benzamindine, 1mM PMSF and myo-Inositol 0.25%), and lysed by sonication.

4. The lysate is clarified by ultracentrifugation and applied in batch to a Talon metal affinity resin previously washed with Buffer A (30 mM NaHPO4 [pH 7.5], 250 mM KCl, 5% glycerol, 10 mM imidazole, 0.02% Tween-20, 0.1 mM TCEP, 1mM Benzamidine, 1 mM PMSF, 0.125% myo-inositol), and incubated with rotation for 30 min at 4˚C.

5. The column is extensively washed with Buffer A, and the bound RPA is then eluted with Buffer A containing 400 mM imidazole [pH 7.8].

6. The eluted protein is then dialyzed against Superdex buffer (30 mM NaHPO4 [pH 7.5], 250 mM KCl, 10% glycerol, 0.02% Tween-20, 1 mM TCEP, 0.5 mM EDTA, 0.25% myo-inositol).

7. The dialyzed fraction is injected onto a Superdex 200 16/600 column. The peak containing trimeric RPA is pooled, concentrated and flash frozen for -80˚C storage.

*2.2.4 Preparation of single-stranded DNA*

An important benefit of ssDNA curtain assays is that they allow of the use of long ssDNA substrates, on the order of ≥40,000 nucleotides in length. Use of this long ssDNA is important because TIRFM imaging allows one to visualize along the entire contour lengths of the molecules and thus obtain spatial and temporal information from many different regions at once. These ssDNA substrates are prepared by rolling circle replication using a circular ssDNA template and a biotinylated primer (Figure 2-2)[165,169], as described below.

1. The biotinylated primer is annealed to a circular M13 DNA template by slow cooling.
2. Rolling circle reaction was set up by mixing annealed M13 template, dNTPs and purified $\phi$29 polymerase and incubating at 30C for 20 minutes[169]

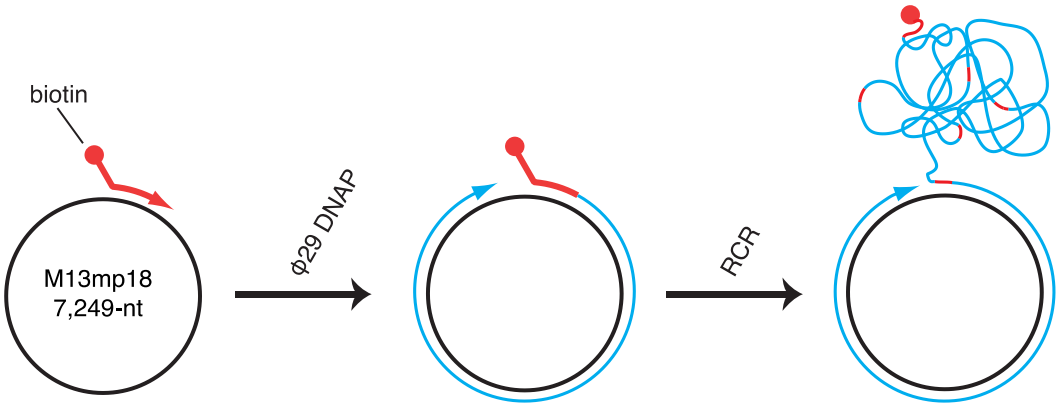


**Figure 2-2. Generation of long ssDNA substrates**. Outline of procedure for preparation of 5' biotinylated ssDNA substrate by rolling circle replication of a circular M13mp18 ssDNA template. See section 2.2.4 for details.

## 2.3 PROCEDURES FOR SSDNA CURTAIN ASSEMBLY

An important aspect of DNA curtain experiments is the requirement for a supported lipid bilayer, which is deposited onto the nano-patterned surface of the sample chamber; detailed descriptions of nanofabrication and flow cell assembly procedures have been described elsewhere[164,165]. The bilayer passivates the surface to minimize nonspecific adsorption of proteins, as well as serving as a mobile anchor point for tethering the 5′ ends of the ssDNA substrates. Tethering is achieved by spiking the bilayer with a small fraction of biotinylated lipids to which the biotinylated ssDNA molecules are anchored through a biotin-streptavidin linkage (Figure 2-3).

### *2.3.1 Liposome stock solutions*

A liposome stock solution is required to deposit the lipid bilayer onto the sample surface, and here we describe basic procedures for preparation of the liposome stock.

1. Lipid stocks are prepared by dissolving 1g DOPC, 100mg PEG-2000 DOPE, and 5mg biotinylated DOPE in 10ml chloroform.

2. Transfer 200 µl of the lipid stock to a 2-ml glass vial and apply a gentle stream of nitrogen gas to slowly evaporate the chloroform from the lipid stock; this step should take several minutes. When complete, the lipid stock should appear as a solid residue visible on the side of the glass vial.

3. The vial is further placed in a vacuum desiccator overnight to eliminate any traces of chloroform.

4. 2 ml of lipid buffer (10 mM Tris-HCl [pH 8.0], 100 mM NaCl) is then added to the dried lipid residue. The dry lipids are resuspended into the buffer with the help of an automatic pipet. The sample should be incubated at room temperature for approximately 1 hour to help hydrate the lipids. Following this incubation, the sample is then vortexed until all the dried lipids are suspended into solution as judged by visual inspection.

5. The dissolved lipid mixture is then sonicated in an ice bath in 5-10 second bursts, with 1-minute intervals between bursts. Sonicate until the turbid lipid solution becomes clear – this typically takes ~3-5 minutes of total sonication time.

6. After sonication, the resulting liposomes are syringe filtered and is ready for use or 4C storage.

*2.3.2 Lipid bilayers and ssDNA substrate attachment*

Here, we describe how the bilayer is deposited onto the flow cell surface and how the ssDNA is attached to the bilayer. Note, that if air bubbles pass through the sample chambers they will destroy the lipid bilayer; in our experience, disruption of the bilayer due to passage of an air bubble through the

sample chamber is a common failure point. Drop-to-drop connections and degassing buffers prior to use can help minimize bubble accumulation and is highly recommended.

1. Connect two syringes to the inlet and outlet flow cell ports and flush with MilliQ water, followed by lipid buffer (10 mM Tris-HCl [pH 8], 100 mM NaCl)[164,165].

2. Mix 40 µl of the liposome stock solution with 960 µl of lipid buffer and inject ~200 µl of the mixture into the flow cell, and then repeat this process every 5-8 minutes until all of the liposome mixture is used. After the final injection, wash the flow cell with 3 ml of lipid buffer and incubate for ~20 minutes at room temperature to allow formation of the bilayer.

3. Any areas of the flow cell surface that remain exposed after bilayer deposition are then blocked by gently flushing 3 ml of HR buffer (30 mM Tris-Ac [pH 7.5], 50 mM KCl, 5 mM MgAc, 1 mM DTT, 0.3 mg/ml BSA) through the chamber and the flow cell is incubated for an addition ~5 minutes at room temperature.

4. Slowly flush a solution of ~10 ng/ml streptavidin in HR buffer to saturate the biotinylated lipids with streptavidin to provide anchor points for the biotinylated ssDNA.

5. Flush the sample chamber with HR buffer to remove all traces of free streptavidin.

6. Dilute 200µl of the rolling circle reaction stock from section 2.2.4 in 800 µl HR buffer and inject into the sample chamber to tether the ssDNA to the lipid bilayer.

7. Once complete, the flow cell can be mounted onto the microscope stage and connected to a sample injection system; our group uses a simple injection system comprised of a syringe pump and a high-pressure switch valve, which can be used for sample injections[164,165].

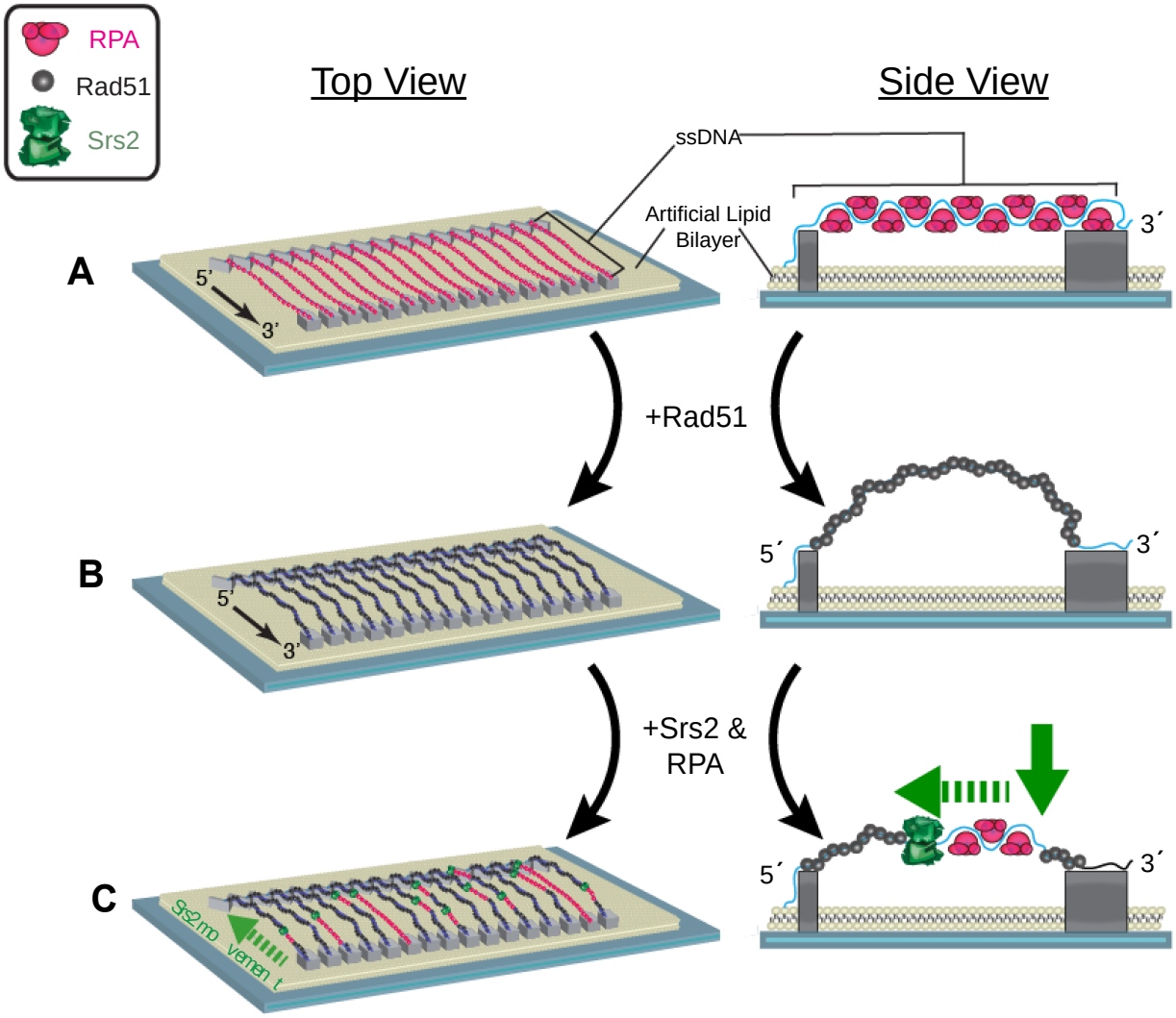


**Figure 2-3. ssDNA curtains to observe single molecule Srs2 activity.** (A-C) Schematic depiction of the ssDNA curtain assay with a top view on the left showing the array of tethered ssDNA molecules, and a side view on the right of a single ssDNA molecule. In (A), ssDNA has already been tethered to the artificial lipid bilayer and RPA has bound the length of the DNA. (B) Unbound RPA in solution has been flushed out and Rad51 is injected. Because RPA has a fluorescent tag, the Rad51 exchange is visualized by the rapid loss of fluorescence along with a length-ening of ssDNA as Rad51-ssDNA has a persistence length that is 1.5 times longer than RPA-ssDNA. (C) Adding catalytic amounts of Srs2 along with RPA shows a rapid reappearance of fluorescent RPA signal as the Srs2 clears a ssDNA-Rad51 filament in the expected 3' to 5' direction.

*2.3.3 Using RPA-GFP to visualize ssDNA*

We use GFP- or mCherry-tagged RPA to both fluorescently label the tethered ssDNA molecules and to help remove the ssDNA secondary structure prior to testing the activities of other HR proteins (Figure 2-3A)[169]. The use of GFP-RPA offers the additional benefit that RPA-ssDNA is the physiological relevant substrate for early steps in HR[170,172]. Here, we outline a typical procedure for labeling and extending double-tethered ssDNA curtains with RPA-GFP or RPA-mCherry. It should be noted that the same procedures can be used with unlabeled RPA, but the ssDNA will not be visible by TIRFM until another fluorescently-tagged molecule, such as GFP-Rad52 (Chapter 3) or dsDNA (Figure 4-6), is injected into the sample chamber[173].

Note that for experiments using the combination of GFP and mCherry, we use a two-color prism-type TIRFM system equipped with a 488-nm laser for detecting GFP, and a 561-nm laser for detecting mCherry. To avoid the bleed through from the green into the red channel during image acquisition, we use a custom-built shuttering system in which the image from the green (GFP) and the red (mCherry) channels are recorded independently, and the green and red images are offset by 100 milliseconds. With this shutter system, when one camera records the red channel image, the green laser is shuttered off, and vice versa.

1. At the start, HR buffer containing 100pM RPA variant is passing through the sample chamber containing prepared ssDNA curtain from the previous section.

2. A 500 µl sample loop is opened to deliver a 6 M urea pulse through the sample chamber at a flow rate of 0.8 ml/min. This pulse of 6 M urea does not affect the lipid bilayer or disrupt the biotin-streptavidin linkages, and is used to help remove any residual ssDNA secondary structure, $\phi$29 DNA polymerase, or M13 circular ssDNA template.

3. The urea is flushed with HR buffer containing 100pM RPA variant for approximately 5-10 minutes (Figure 2-4,B,C; time point *i*).

4. The location and the quality of the RPA-bound ssDNA curtains can now be verified by visual inspection using TIRFM (Figure 2-4A). The RPA-ssDNA molecules are ready to directly proceed to either section 2.4.1 or 2.4.2.

## 2.4 VISUALIZING SRS2 TRANSLOCATION ACTIVITY USING SSDNA CURTAINS

Here, we provide detailed examples of experimental methods for visualizing the behavior of either unlabeled (Figure 2-4B) or XFP-Srs2 (Figure 2-4C) as it acts upon Rad51- or RPA-bound ssDNA.

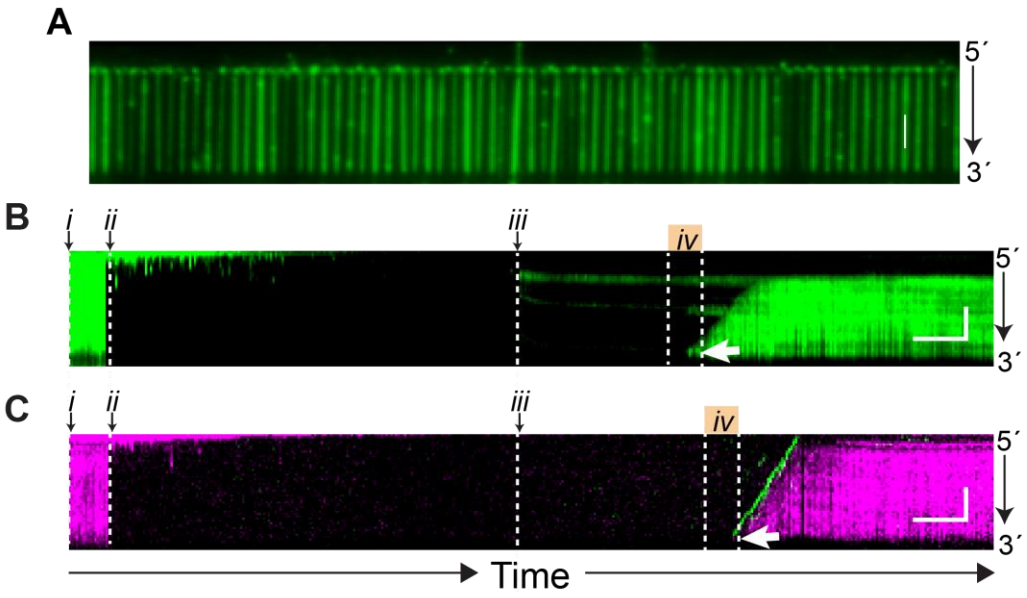


**Figure 2-4. A typical Srs2 experimental timecourse on a Rad51 filament**. (A) A representative image of an array of ssDNA bound by RPA-GFP at the experiement outset. Each DNA molecule is oriented with the 5' end at the top. This would correspond to the top view of Figure 2-3A. White scale bar is 3μm. (B,C) Kymograms of individual ssDNA molecules analogous to the side view schematics in Figure 2-3 with time on the x-axis. These examples are of single-tether molecules without the downstream anchor. At the start of the experiment (i), the ssDNA is coated with fluorescent RPA; (ii) indicates when Rad51 is injected and flow is terminated to assemble the Rad51 filaments; (iii) flow is resumed with RPA buffer to flush free Rad51 from the chamber; (iv) a 150 μl pulse of wtSrs2 or GFP-Srs2 is injected into the sample chamber in (B) or (C), respectively. The orange box is the ~45 seconds when Srs2 is predicted to be in solution. The white arrowheads highlight the beginning of Srs2 translocation events. The white scale bars represent 2min x 3um.

*2.4.1 Visualizing Srs2 binding and translocation on RPA-ssDNA*

Srs2 translocating over RPA-bound ssDNA has never been directly visualized. The following procedure describes how to visualize mCherry-Srs2 translocation on ssDNA curtains bound by RPA-GFP (i.e. in the absence of Rad51).

1. At the start, HR buffer containing 100pM GPF-RPA is passing through the sample chamber containing prepared ssDNA curtain from section.

2. To visualize mCherry-Srs2 binding and translocation, inject a 150 µl aliquot of mCherry-Srs2 (typically 100 pM) in HR buffer while maintaining a constant flow rate of 0.2 ml/min. This procedure results in a 45-second injection window during which mCherry-Srs2 can bind to the RPA-ssDNA molecules; after this time period the HR buffer behind the injection loop *does not* contain any Srs2. Therefore, any unbound mCherry-Srs2 will be flushed from the sample chamber. This produce helps minimize the number of mCherry-Srs2 binding events, which makes interpretation of the resulting data much easier

3. As an alternative to the procedure described above, one can also assay the ability of mCherry-Srs2 to remove RPA-GFP from the ssDNA (Figure 3-5). For this, RPA-GFP is simply omitted from the HR buffer that is flushed through the sample chamber following the 150 µl injection of mCherry-Srs2. It should however be noted that the ssDNA can readily break when RPA is absent, making these types measurements more challenging.

*2.4.2 Visualizing Srs2 as it acts upon Rad51-ssDNA*

The following procedure describes how to prepare Rad51 filaments (Figure 2-3B) and visualize Srs2 translocation (Figure 2-3C) beginning with double-tethered ssDNA curtains bound by RPA-GFP. These assays can be used with unlabeled Srs2, and in this case, the movement of Srs2 along the Rad51-

ssDNA can be revealed by the rebinding of fluorescent RPA (Figure 2-4B). Alternatively, fluorescently-tagged Srs2 can be visualized as fluorescent molecules that bind to and translocate along the Rad51-ssDNA, while the tracts of Rad51 that are removed from the DNA can be concurrently visualized by the reappearance of fluorescent RPA (Figure 2-4C).

1. Rad51 filament assembly is initiated by injecting 1-2 µM *S. cerevisiae* Rad51 in HR buffer containing 2 mM ATP in the absence of RPA (Figure 2-4B,C; timepoint *ii*). Rad51 filament formation can proceed in the presence of RPA, but is inhibited with increasing concentrations of RPA in solution.

2. The sample is then incubated in the absence of flow for 10-15 minutes at 32˚C to allow for Rad51 filament assembly. If using fluorescent RPA, the Rad51 assembly reaction can be monitored by visual inspection of the RPA-GFP, which will be displaced from the ssDNA upon Rad51 binding.

3. Buffer flow is then resumed with HR buffer containing 2 mM ATP and 100 pM RPA-GFP to flush away any remaining free Rad51 (Figure 2-4B,C; time point *iii*). The Rad51 filaments will remain stable so long as ATP is present in the buffer, so the RPA-GFP present in the buffer should not bind to the ssDNA, but rather serves to verify that the Rad51 filaments remain intact.

    a. In SM experiments with D-loop structures (Figure 4-8), a step exists here where the Rad51-ssDNA filament is incubated with 5′-ATTO-565-labeled 70mer dsDNA. This dsDNA contains a 15-bp region of homology is flanked by regions of no more that 7-bp homology to the M13ssDNA template. This restricts dsDNA binding to bonafide Rad51-mediated recombination events as demonstrated previously[73].

    b. After a 10-minute incubation without flow or illumination, the laser shutters are opened and the chamber is flushed with HR buffer containing ATP and RPA. The experiments then proceeded to step 4.

4. A 150 µl in-line loop containing Srs2 (typically, at a concentration of 100 pM) diluted in HR buffer containing RPA and ATP is opened, and the ssDNA molecules are observed by TIRFM while continuously flushing with HR buffer. This procedure results in a short pulse of Srs2 in solution (Figure 2-4B,C; time point *iv*), coinciding with the 150 µl injection, while free Srs2 will quickly be flushed from the sample chamber by the continuous buffer flow. This procedure restricts the number of Srs2 molecules that bind to the ssDNA during the initial injection, thus facilitating data analysis by helping to ensure that a relatively small number of translocation trajectories will occur on any given ssDNA molecule.

## 2.5 DATA ANALYSIS

In the following sections, we describe general procedures for analyzing Srs2 data from ssDNA curtain experiments using measurements of GFP-Srs2 translocating on Rad51-ssDNA in the presence of free RPA-mCherry as an example. Similar procedures can be used to analyze the behavior of dark Srs2 on Rad51-ssDNA in the presence of RPA-GFP, or mCherry-Srs2 on RPA-ssDNA, and pertinent details of these procedures are also highlighted below. The general work flow for these analysis procedures is shown in Figure 2-5.

### *2.5.1. Generating kymographs from wide-field images*

All TIRFM data are collected as raw TIFF files using Nikon NIS Elements software, and then these raw TIFF files are converted to kymographs for data analysis (Figure 2-4B,C).

1. First, the raw TIFF files are used to create a tiff stack (*i.e.* movie) showing the entire field of view using Fiji software.

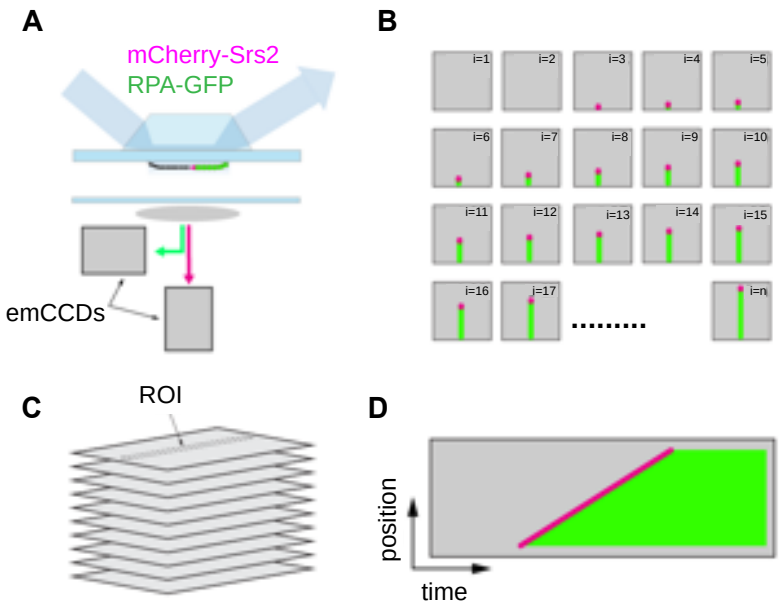


**Figure 2-5. Work flow for data analysis procedures for two-color analysis of Srs2 trajectories**. (A) Schematic illustration of the TIRFM system for analysis of Srs2-mCherry (shown in magenta) translocation on dark Rad51-ssDNA filaments (shown in black) in the presence of RPA-GFP (shown in green); color coding formCherry-Srs2 (magenta) and RPA-GFP (green) is the same throughout the figure. (B) Cartoon illustration of a hypothetic set of raw TIFF files representing the initial binding of Srs2-mCherry to the Rad51-ssDNA (beginning is frame i=1) and following its movement along the ssDNA over the course of an entire experiment (ending in frame i=n). (C) The raw TIFF files are then used to generate a tiff stack (i.e. a movie). (D) Two-color kymographs are then extracted from these movies with NIH ImageJ based upon user-defined ROIs (regions of interest), which represent 1-pixel wide areas encompassing individual ssDNA molecules from within the ssDNA curtain.

2. The resulting tiff stack is then used to generate kymographs that illustrate the events which take place on individual ssDNA molecules during the experimental observation period. Kymographs are generated using the “Reslice” function in Fiji. For this, a 1 pixel wide region of interest (ROI) is superimposed on a selected ssDNA molecule from within the tiff stack, and the corresponding information for every image within the entire tiff stack is compiled as single kymograph. Within each kymograph, the y-axis reflects the spatial information along the length of the ssDNA, and x-axis represents time.

3. The resulting kymographs can then be used to determine the sites at which Srs2 initiates translocation, translocation velocities, and the processivity of each translocating protein.

*2.5.2. Analysis of Srs2 translocation trajectories*

All analysis of Srs2 translocation is performed from the kymographs that are generated as described above.

1. Individual dark Srs2 trajectories were manually analyzed by selecting the starting and ending point of a “wedge” of fluorescent-RPA. These wedges are evaluated as linear traces to estimate velocity, whereas fluorescent Srs2 trajectories are tracked in NIH ImageJ, as described below.

2. To analyze fluorescently-tagged Srs2 trajectories, we use the NIH ImageJ plugin NeuronJ[174]. NeuronJ is a semi-automated algorithm that can be used to define and track contiguous changes in signal intensity, also called “ridges” or “ridge pixels”, in a 2-dimensinal image. In the case of GFP- or mCherry-tagged Srs2, the ridges are the bright fluorescence signals observed for the moving molecules of Srs2.

3. The user defines a starting and end points within the image, and then the program defines and tracks the ridge pixels, and records the x,y coordinates of each trajectory. For our analysis, we define the endpoints as either when the Srs2 signal disappears (*i.e.* dissociation) or when the slope of the Srs2 trajectory reaches a plateau (*i.e.* Srs2 stalls).

4. The x-coordinate values are readily converted from pixel values to units of time. For instance, assuming that data is collected using 5 second shuttering, then a kymograph that started at x = 10 (where “x” corresponds to the x-axis pixel value) and ending when x = 20 would have activity that occurred over a 50-second time period.

5. The y-coordinate pixel values are converted to nucleotides values based upon the estimated lengths of the protein-bound ssDNA substrates. While a single pixel always corresponds to 0.27

μm, the amount of nucleotides within this are will differ based upon the filament composition. For example, naked ssDNA is expected to formextensive secondary structure to efficiently compact DNA, Rad51 extends ssDNA to near B-form, while RPA-ssDNA was measured as 1.5x shorter than Rad51-ssDNA[73,173]. For Rad51-ssDNA, a single pixel corresponds to 0.27 μm or ~725 nt of Rad51-ssDNA per pixel. This calculation was made based upon the observation that dsDNA with homology to a single location within a single repetition of M13mp18 ssDNA displayed peak-to-peak distances of 2.7 μm [73]. A single repetition of M13mp18 ssDNA is 7,249 nt and each pixel within our 60x objective is 0.27 μm. Thus, there are 7,249 nt of Rad51-ssDNA within 10 pixels. For RPA-ssDNA, multiplying the Rad51 value by 1.5 corresponds to ~1,087 nt of ssDNA-RPA filament in a single pixel. Therefore, it must be emphasized that the apparent velocities when converted from pixels/sec to nt/sec values will depend upon these assumed contour lengths of the extended Rad51-ssDNA and RPA-ssDNA complexes within the ssDNA curtains.

6. Once these conversions are completed, translocation velocity (in nt/sec) can be calculated from the kymographs based on the slope of each Srs2 trajectory, which is readily obtained by fitting the tracking data to a linear equation. The resulting data can be presented as distribution histograms to obtain the mean and standard deviation for the Srs2 translocation velocities under any given experimental condition.

7. Srs2 processivity can also be defined from the same analysis of the kymographs. The distance of each translocation event is defined as the total length in nucleotides from each initial Srs2 binding position to the end of the translocation trajectory and defined by the location were Srs2 either dissociated from the ssDNA, photo-bleached, or stopped moving. The resulting values are used to generate survival probability plots, where the apparent processivity values reflect the distance at which 50% of the Srs2 complexes dissociate, photo-bleach or stop moving. Note that the reported error bars for the survival probability correspond to standard deviation calculated by bootstrap analysis using a custom Python script that has been reported elsewhere[166].

## 2.6 BULK BIOCHEMICAL ASSAYS

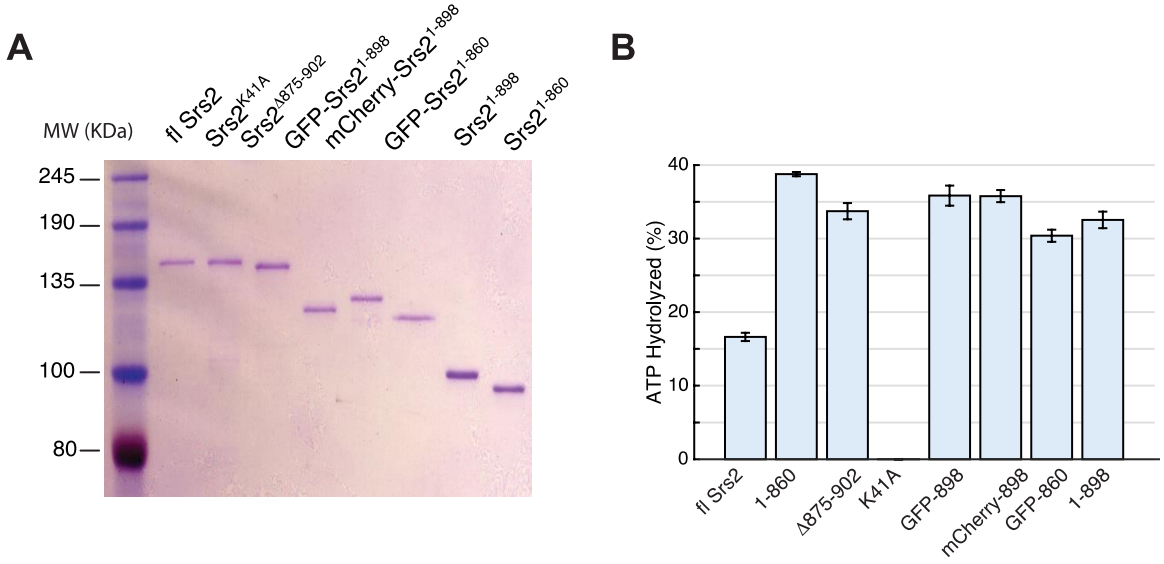


**Figure 2-6. Analysis of Srs2 variants**. (A) SDS/PAGE analysis of various Srs2 protein constructs analyzed in this work. (C) ATP hydrolysis activity assays for the different protein constructs tested in this work. Error bars represent s.d. for three independent experiments.

### *2.6.1 Comparing Srs2 variant activities*

Comparison of each Srs2 variants ATP hydrolysis activity was performed to ensure these proteins behaved as expected (Figure 4-6).

1. Reactions were carried out at 32˚C in HR buffer (30 mM Tris-Ac [pH 7.5], 50 mM KCl, 5 mM MgOAc, 5 µM nucleotides in the form of M13mp18 ssDNA, 1 mM DTT, 0.1 mg/ml BSA, 2 mM ATP and 14 nM [γ-$^{32}$P]ATP).

2. Reactions were initiated by the addition of 10 nM Srs2. Aliquots were removed after 10 minutes and quenched by the addition an equal volume of 500 mM EDTA.

3. The quenched reactions were then spotted onto PEI (polyethyleneimine) TLC plates (Millipore) and resolved in buffer containing 0.5 M LiCl and 0.5 M formic acid. The TLC plates were then exposed to a phosphorous screen and imaged. ATPase activity from minus Srs2 controls was subtracted as background. Values plotted were the mean of triplicate reactions with error bars representing standard deviation (s.d.).

*2.6.2 Analyzing Srs2 ATPase activity on HR intermediates*

By varying the experimental setup, Srs2 ATPase activity could be assessed on various HR intermediates to corroborate SM data. For these purposes, a series of 3 pre-incubation periods was performed prior to Srs2 addition (Figure 2-7A).

1. Reactions were carried out at 32˚C in HR buffer (30 mM Tris-Ac [pH 7.5], 50 mM KCl, 5 mM MgOAc, 5 µM nucleotides in the form of M13mp18 ssDNA, 1 mM DTT, 0.1 mg/ml BSA, 2 mM ATP and 14 nM [γ-$^{32}$P]ATP).

2. Reaction buffer or 200nM wtRPA was added and incubated for 5 minutes before adding a concentration series of 0-100nM SNAP-Rad52(orf3) followed by another 5-minute incubation. Buffer or 2µM Rad51 was next added followed by a final 5-minute incubation before adding 10nM Srs21-898 and starting a timer.

3. Alliquots were removed at the indicated time points and quenched with an equal volume of 500mM EDTA.

4. The quenched reactions were analyzed by TLC the same as in section 2.6.1 and results are plotted in Figure 2-7. Discussion of the results is found in Chapters 3 and 5.

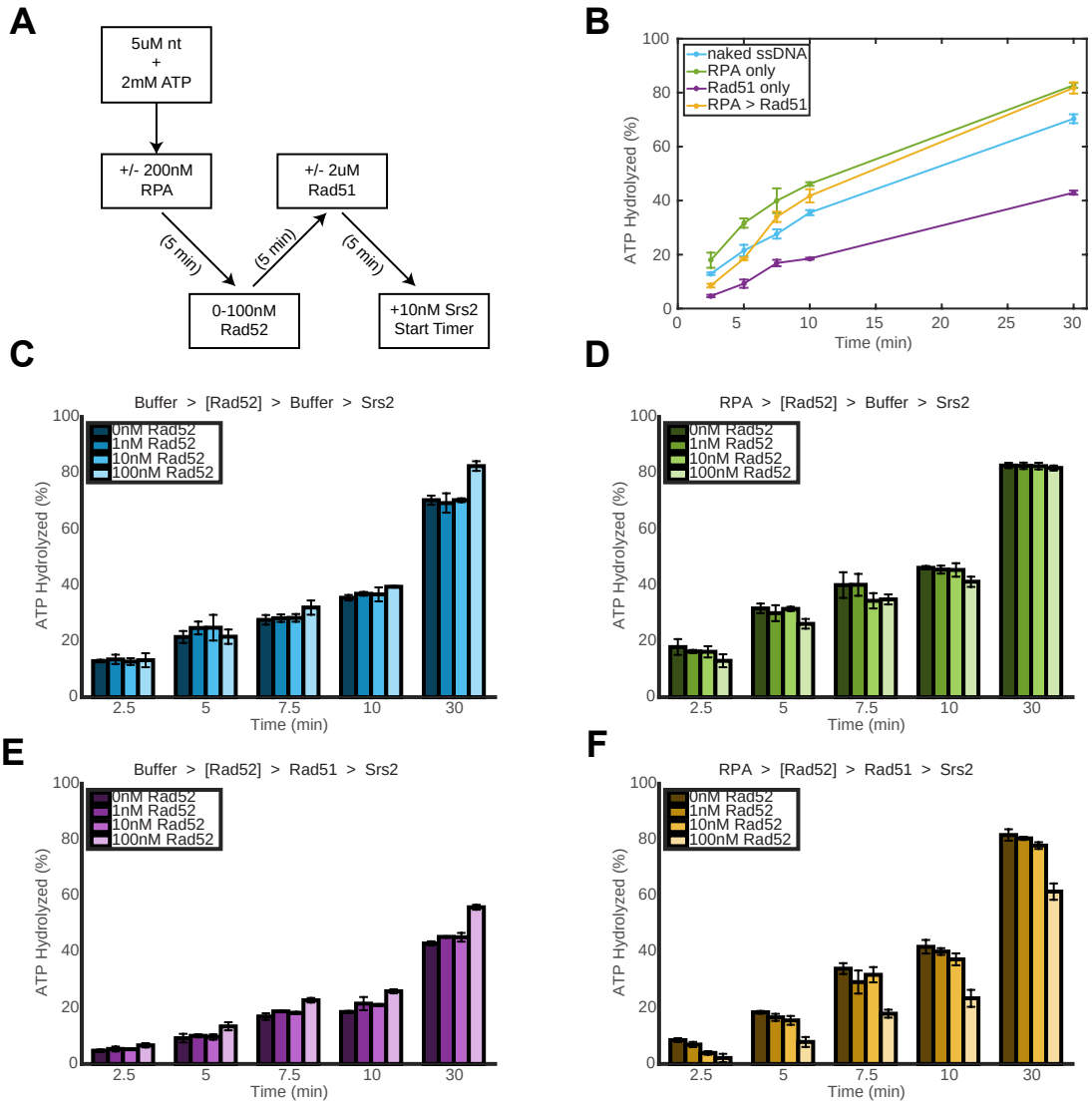


**Figure 2-7. Srs2 ATPase activity in the presence of HR proteins.** (A) Schematic of reaction setup. (B) Plot of ATPase activity with or without RPA and/or Rad51, but in all cases lacking Rad52. RPA and Rad51 both slightly inhibit Srs2 ATPase activity compared to Srs2 on naked ssDNA. (C-F) Bar graphs of the effect of increasing concentrations of Rad52 on Srs2 ATPase activity. The additions and their order are listed above each plot, with the ">" symbol representing a 5-minute incubation. For each plot, the [0nM] Rad52 corresponds to those values plotted in (B). In all cases, Rad52 had no effect on the ATPase activity of Srs2 beyond that attributed by RPA and/or Rad51. Values plotted were the mean of triplicate reactions with error bars representing standard deviation.

## 2.7 CONCLUSIONS AND FUTURE DIRECTIONS

Helicases play crucial roles in all aspects of nucleic acid metabolism, and mutations in these important motor proteins can give rise to severe genetic disorders and cancer-prone syndromes[105,175,176]. Here, we have described assays that can be used to visualize the behaviors of the *S. cerevisiae* helicase and anti-recombinase Srs2 as it acts upon long ssDNA substrates bound by either Rad51 or RPA. We anticipate that relatively simple modifications of the procedures described here will allow these protocols to be applied to many other types of helicases and motor proteins that act upon single-stranded DNA. We can also envision some technical improvements that may increase the utility of this approach. In particular, the long ssDNA molecules used in these assays are inherently more challenging to work with than dsDNA, which is a relatively stiff molecule that is well behaved in flow. Therefore, although we can directly measure distances in micron or pixels, we can only estimate the lengths (in nucleotides) of the ssDNA molecules under observation. One way to overcome this problem may be to include fluorescent fiduciary markers at known locations along the ssDNA, which would allow for more accurately measure the lengths of Rad51-ssDNA and RPA-ssDNA rather than relying upon length estimates. In addition, the methodologies described here for tracking Srs2 movement rely upon relatively simple tracking procedure found in the NIH ImageJ plugin NeuronJ. This approach is fast and relatively simple, so it is very suitable for many types of investigations. However, it cannot be used to decipher high-resolution features of the trajectories – for instance, we can clearly see examples of pauses and changes in velocity in the Srs2 kymographs. Analysis of these detailed features would require implementation of a more intensive particle tracking algorithm that could be utilized for tracking the progress of GFP- or mCherry-tagged Srs2.

SM studies are technology driven, and advances in these technologies offer the potential for greater spatial and temporal resolution, which in turn will lead to more detailed biophysical insights. Examples of such advances could include faster cameras with greater spatial resolution and higher sensitivity, as well as brighter, more stable fluorophores that can be imaged for longer periods of time without photo-bleaching. It is also important that existing SM methods be used to tackle questions that are perhaps more reflective of recombination as it takes place within the living cell. These types of questions do not necessarily require any new technology development, but instead require continued

study and development of the biochemical systems already under investigation. As with any reductionist biochemical approach, many of the SM studies of recombination have focused on trying to understand the detailed properties of one or two proteins in order to infer their particular contributions to the overall recombination pathway. Therefore, a major challenge faced by researchers in the SM field will be to gradually increase the complexity of the systems under investigation as they strive to further define the biophysical basis for biological processes. For instance, most of the SM studies of recombinase filaments have been confined to analysis of only the recombinases (*e.g.* RecA or Rad51), and therefore reflect only the basal properties of these proteins. It is clear from many years of genetic, cell biology and biochemical studies that the presynaptic complex contains many other proteins in addition to the recombinases, although the precise protein composition and spatial organization of these proteins within the presynaptic complex remain ill–defined. Moving forward, it will be essential to begin trying to understand whether and how the presence of these additional recombination accessory proteins influence filament assembly and dynamics, the homology search, and strand invasion. Similarly, it will also be important to determine how these processes take place within the context of chromatin, how chromatin–remodeling factors work together with recombination machinery, and how recombination is coordinated with DNA replication.

As these studies continue to mature, they are likely to provide further insights into recombination mechanisms. In the groundbreaking paper describing the DSBR model, the authors conclude that while genetic studies have been invaluable in the elucidation of recombination pathways, *"…we suggest that biochemical experiments will be necessary to determine the actual mechanism of initiation of … recombination"*[3]. We extend this sentiment by indicating that the biochemical information must span a range of spatial and temporal scales, and this information must also be integrated with an in–depth understanding of the biology of recombination and the consequences of its outcomes. The new optical microscopy tools available for single molecule investigations of homologous recombination can help make this a reality, and the coming years should prove extremely fruitful for those investigating recombination mechanisms.

# CHAPTER 3: YEAST SRS2 HELICASE PROMOTES REDISTRIBUTION OF SINGLE-STRANDED DNA-BOUND RPA AND RAD52 IN HOMOLOGOUS RECOMBINATION REGULATION

---

This work was originally published as: De Tullio L, Kaniecki K, Kwon Y, Crickard JB, Sung P, Greene EC. Yeast Srs2 Helicase Promotes Redistribution of Single-Stranded DNA-Bound RPA and Rad52 in Homologous Recombination Regulation. *Cell Rep*. 2017 Oct 17;21(3):570-577.

Author contributions: L.D.T. designed and conducted the single molecule experiments and data analysis with assistance from K.K. L.D.T. and K.K. cloned, purified and characterized Srs2 constructs. Y.K. expressed and purified Rad51, and J.B.C. assisted with bulk biochemical analysis of Srs2. E.C.G. supervised the project and wrote the manuscript with input from L.D.T., K.K. Y.K., J.B.C., and P.S.

---

## 3.1 SUMMARY

Srs2 is a Super-Family 1 helicase that promotes genome stability by dismantling toxic DNA recombination intermediates. However, the mechanisms by which Srs2 remodels or resolves recombination intermediates remain poorly understood. In this chapter, single molecule imaging is used to visualize Srs2 in real time as it acts on single-stranded DNA (ssDNA) bound by protein factors that function in recombination. For the first time, we directly observe that Srs2 is capable of rapid translocation (~170 nucleotides per second) over RPA-bound ssDNA in a processive and 3′→5′ directional bias. RPA is evicted from DNA during the passage of Srs2. Remarkably, Srs2 also readily removes the recombination mediator Rad52 from RPA-ssDNA, and in doing so promotes rapid redistribution of both Rad52 and RPA. Interestingly, $Srs2^{1-860}$ that lacks the Rad51 interaction domain also has difficulty initiating this RPA eviction activity and suggests this domain may be generally required for loading onto protein-coated ssDNA. These findings have important mechanistic implications for understanding how Srs2 and related nucleic acid motor proteins resolve potentially pathogenic nucleoprotein intermediates.

## 3.2 RESULTS

### *3.2.1 Visualizing the behaviors of Srs2 on RPA-coated ssDNA*

Srs2 has a robust ssDNA-dependent ATPase activity, and ATP hydrolysis is observed even in the presence of RPA, raising the possibility that Srs2 can translocate along ssDNA substrates bound by RPA[177]. Analysis of Srs2 bound to RPA-ssDNA by electron microscopy also suggests that Srs2 translocates along RPA-bound ssDNA[178]. However, RPA binds to ssDNA with affinities on the order of ~$10^{-9}$-$10^{-10}$M[170,172], and we detect no turnover of ssDNA-bound RPA for ≥2 hours in ssDNA curtain assays when free RPA is absent[173,179]. These findings raise the question of how RPA might impact Srs2. To address this question, we visualized mCherry-tagged Srs2 molecules as they interacted with ssDNA bound by GFP-RPA, specifically aiming to characterize binding and translocation events (Figure 3-1A & B). GFP-tagged Srs2 supports DNA replication and recombination *in vivo*[128] and mCherry-Srs2 retained near wild-type levels of ATP hydrolysis activity *in vitro* (Figure 2-7B). Full-length Srs2 has a tendency to aggregate, so unless stated otherwise, the single-molecule experiments were conducted with a C-terminally truncated version of Srs2 comprised of amino acids 1 to 898 ($Srs2^{898}$). The truncated Srs2 retains wild-type levels of ATPase, DNA helicase, and Rad51 filament disruption activities[65,125] and is referred to as Srs2 within this chapter (Figure 2-7B). Experiments were performed at 32˚C and all buffers contained 100 pM RPA and 2 mM ATP, unless otherwise stated. Fluorescent Srs2 (150 µl at 100 pM) was injected into the sample chamber, and we then observed its interactions with the RPA-coated ssDNA under constant buffer flow (0.2 ml/min). These reaction conditions, allowed us to observe only those Srs2 molecules that associated with the RPA-ssDNA substrate during the ~45 second incubation time window. This strategy helps minimize overlapping Srs2 binding and translocation events.

The mCherry-Srs2 was able to interact with RPA-ssDNA and translocated rapidly over surprisingly long distances (Figures 3-1B & 3-2A). Srs2 translocation occurred in the 3′→5′ direction, as expected[117]. Similar findings were made for mCherry-Srs2 on ssDNA bound by either GFP-tagged or unlabeled RPA, confirming that the properties of RPA are not altered by either the GFP or mCherry tag (Figure 3-2). The combined data sets for mCherry- and GFP-tagged Srs2 revealed that Srs2 translocated at an apparent velocity of 170 ± 80 nucleotides per second (nt/sec) (mean ± s.d.) (N=396)

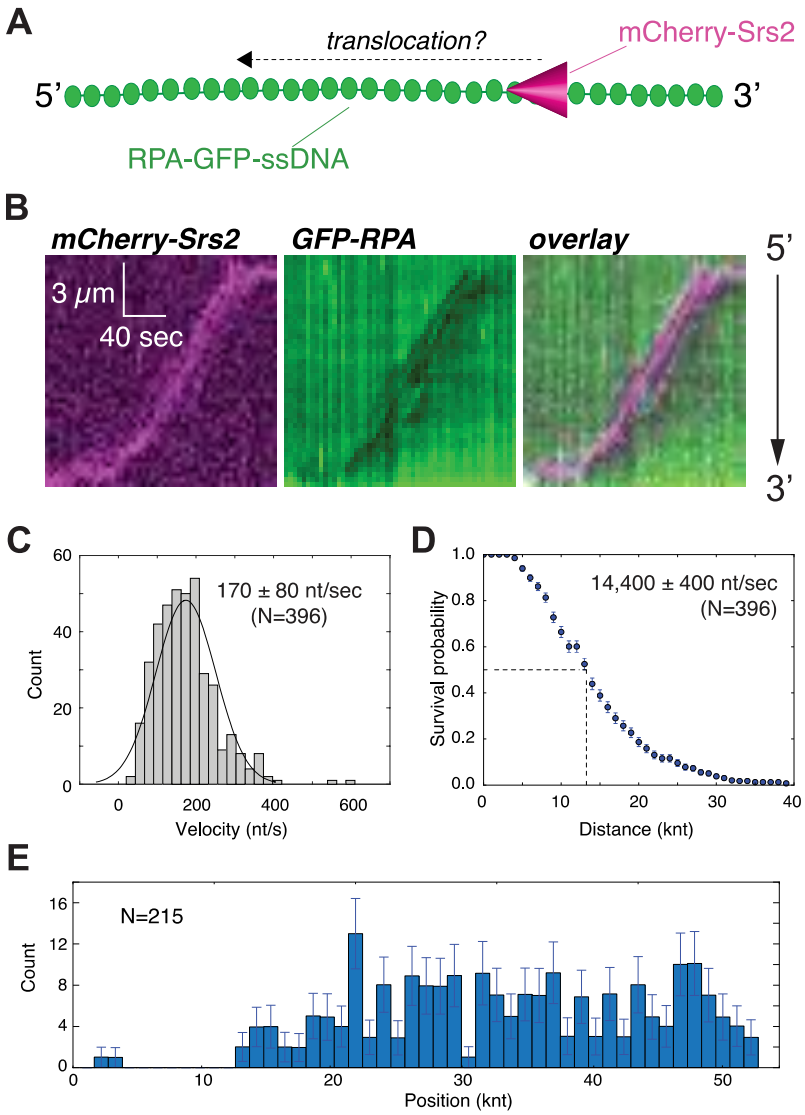


**Figure 3-1. Srs2 translocation on ssDNA molecules bound by S. cerevisiae GFP-RPA.** (A) Schematic depiction of the assay used to visualize mCherry-Srs2 translocation on GFP-RPA-coated ssDNA. (B) Kymographs demonstrating the movement of mCherry-Srs2 (magenta) along GFP-RPA bound ssDNA (green). The orientation of the ssDNA is indicated, and the images show the mCherry-Srs2 fluorescence signal, the GFP-RPA fluorescence signal, and the overlaid fluorescence signals, as indicated. (C) Velocity distribution and (D) survival probability measurement for mCherry-Srs2 translocating on RPA bound ssDNA; error bars represent s.d. calculated from bootstrapping analysis. The dashed line in (D) highlights the distance at which 50% of the Srs2 complex stop translocating, which we report as processivity values in the text. (E) Distribution of initial Srs2 binding sites; error bars represent s.d. calculated from bootstrapping analysis. The data in (C-E) represent the combined data sets for GFP-Srs2 and mCherry-Srs2.

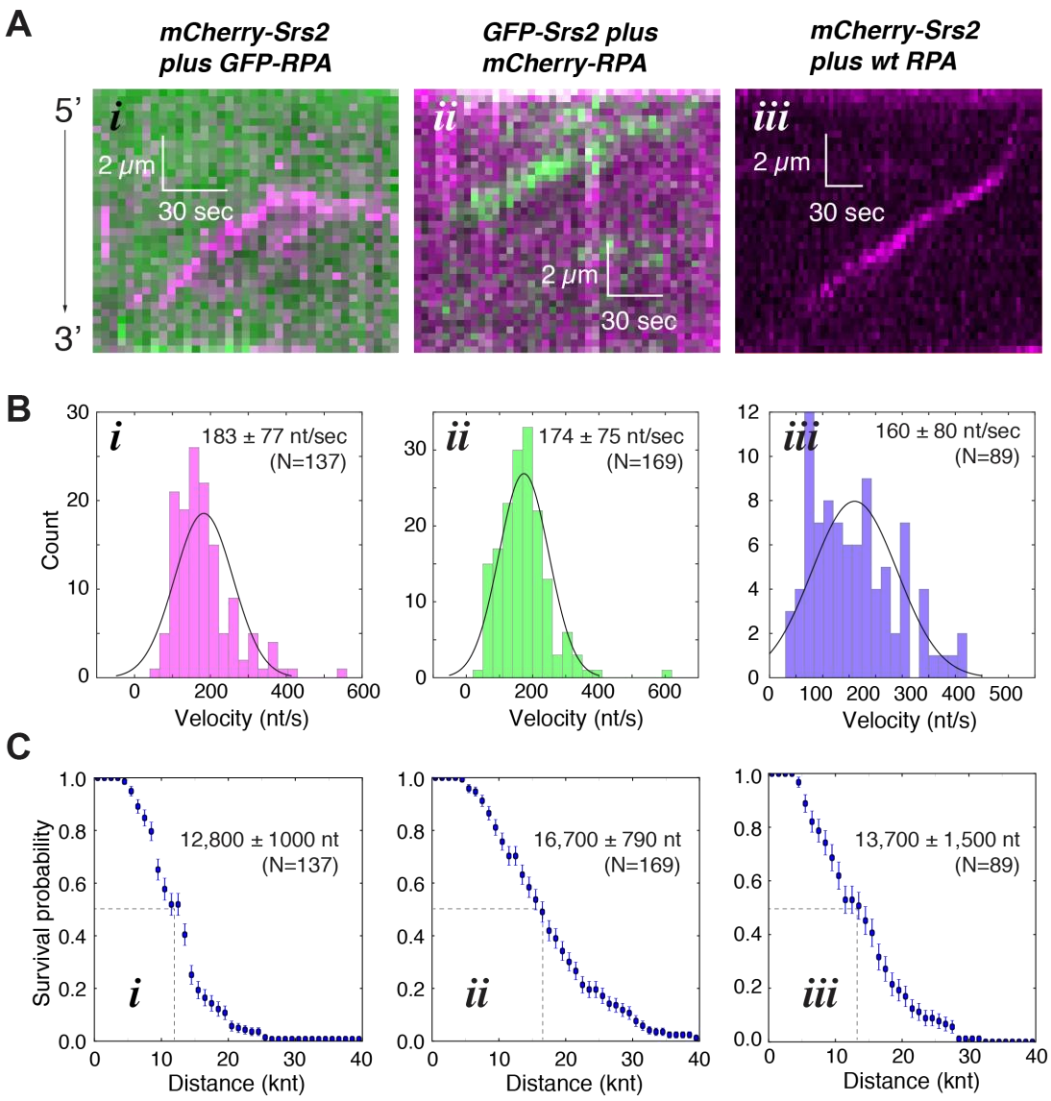


**Figure 3-2. Translocation data for the different Srs2 and RPA constructs.** Related to Figure 4-1. (A) Typical kymographs showing the behavior of (i) mCherry-Srs2 with GFP-RPA, (ii) GFP-Srs2 with mCherry-RPA, and (iii) mCherry-Srs2 with wild-type (unlabeled) RPA. (B) Velocity distributions and (C) survival probability data for each of the three different Srs2 and RPA combinations, as indicated; error bars represent s.d. calculated from bootstrapping analysis. Note that the data presented in Figures 3-1C & D of the main text represents the combination off all three of these independent data sets for Srs2 velocity and processivity.

(Figure 3-1C) and exhibited an average processivity of 14,400 ± 370 nucleotides (Figure 3-1D). Srs2 translocation initiated at seemingly random positions along the RPA-ssDNA, indicating that there was no preferred site for initial Srs2 binding (Figure 3-1E). Experiments using the ATPase deficient Srs2-K41A mutant protein (100 pM), which bears a lysine to arginine mutation in the Walker A box[123] showed that ATP hydrolysis is indispensable for translocation (Figure 3-3A,B).

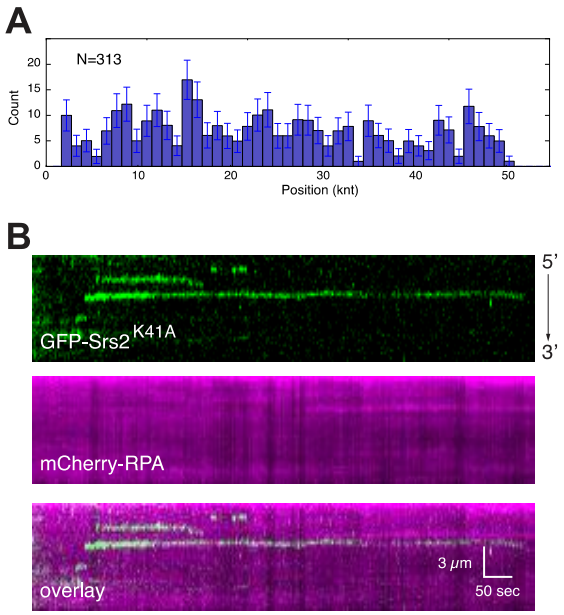


**Figure 3-3. ATPase deficient mutant Srs2 $^{K41A}$ cannot translocate on RPA-ssDNA.** Related to Figure 3-1. (A) Binding site distribution histogram of GFP-Srs2 K41A on mCherry-RPA-ssDNA. (B) Kymograph showing GFP-Srs2 K41A (green) bound to ssDNA coated with mCherry-RPA (magenta).

### *3.2.2 Deletion of the Rad51-interaction domain reduces Srs2 association with RPA-ssDNA*

Srs2 possesses a domain that allows for interaction with Rad51[125] (Figure 1-6A) and the truncation mutant Srs2$^{860}$ lacking this domain has ATPase and helicase activities that are comparable to wild-type Srs2 (Figure 2-7). However, cells expressing Srs2$^{860}$ exhibit a hyper-recombination phenotype[125], and the truncated mutant is unable to efficiently disrupt Rad51 filaments[65,125]. It remains unclear whether the deficiencies ascribed this mutant stem from impaired Rad51 interaction, or that the mutant protein harbors other functional deficiencies. To our surprise, we were unable to detect significant association of mCherry-Srs2$^{860}$ with RPA-ssDNA at the same concentration (100 pM) of Srs2$^{898}$ described above. Specifically, we observed a total of only nine Srs2$^{860}$ translocation events, revealing an average velocity of 160 ± 70 nt/sec (N=9) and a processivity of 12,700 ± 2,750 nucleotides. These results suggested that Srs2$^{860}$ is compromised for initial association with the RPA-ssDNA complex, but once bound, the Srs2 mutant is nonetheless proficient in translocation through the RPA-coated DNA. In agreement with this conclusion, we detected many more translocation events when the concentration of

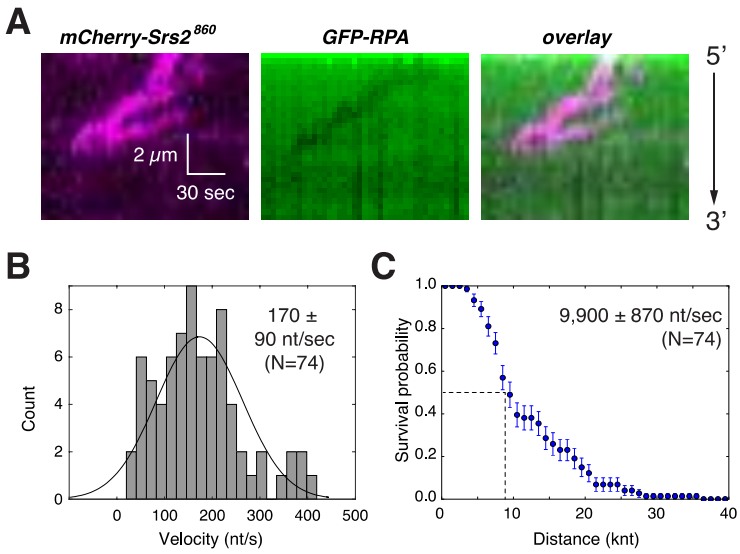


**Figure 3-4. Srs2$^{860}$ is impaired in association with the RPA-ssDNA complex.** (A) Kymograph showing mCherry-Srs2$^{860}$ translocation on an GFP-RPA-ssDNA molecule for data collected at 1 nM mCherry-Srs2$^{860}$. (B) Velocity distribution and (C) Survival probability plot for mCherry-Srs2$^{860}$; error bars represent s.d. calculated from bootstrapping analysis.

mCherry-Srs2$^{860}$ was increased to 1 nM (Figure 3-4A), revealing an average apparent velocity of 170 ± 90 nt/sec and an average processivity of 9,900 ± 870 nucleotides (Figure 3-4B,C). Together, these observations suggest that the C-terminal domain of Srs2 is necessary for efficient association with RPA-ssDNA.

### *3.2.3 Srs2 evicts RPA from ssDNA*

Inspection of the GFP-RPA signal in the kymographs suggested that Srs2 might be stripping RPA from the ssDNA during translocation (*e.g.* Figure 3-1B). Specifically, short tracts of dark ssDNA that were transiently devoid of GFP-RPA were observed, and these tracts always coincided with the passage of mCherry-Srs2. However, in the experiments described above, free GFP-RPA (100 pM) was always present, and this available protein pool could easily replenish any GFP-RPA that might have been displaced by Srs2. As a consequence, the transient tracts of naked ssDNA did not persist for more than a few seconds after the passage of Srs2 (Figure 3-1B).

We sought to more definitely determine whether Srs2 removes RPA during translocation using mCherry-Srs2 and GFP-RPA (Figure 3-5A). Free GFP-RPA was omitted from the buffer to minimize the

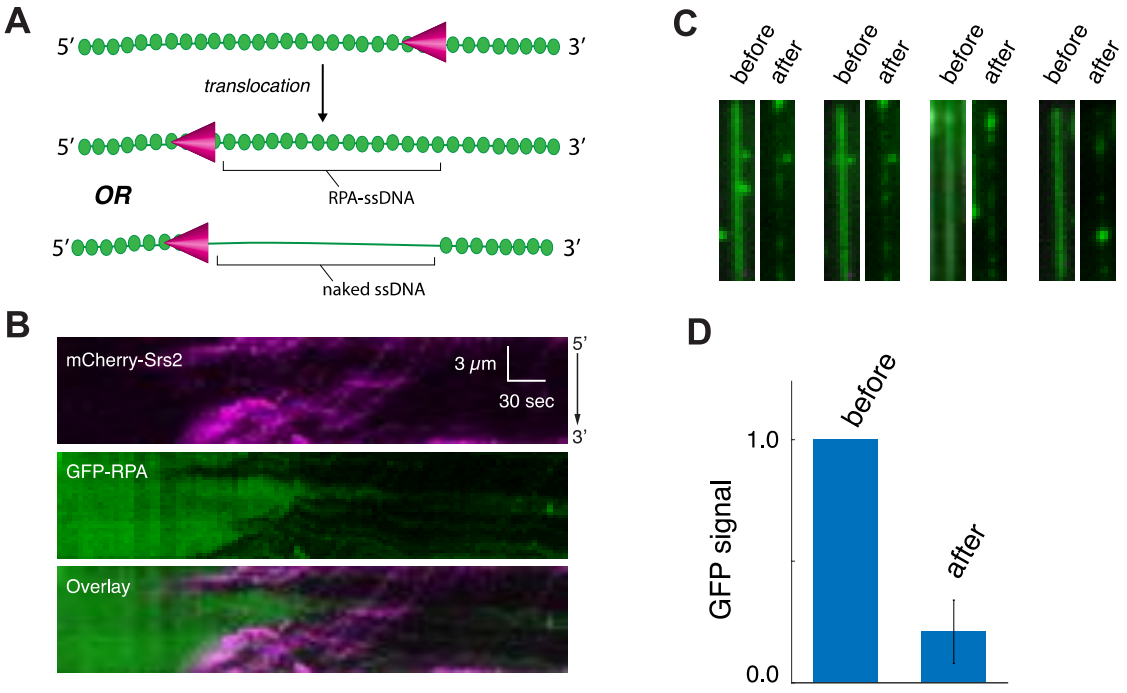


**Figure 3-5. Srs2 strips RPA from ssDNA during translocation.** (A) Schematic showing Srs2 translocation without concomitant removal of RPA (top) and Srs2 translocation coinciding with the removal of Srs2 (bottom). (B) mCherry-Srs2 translocation on GFP-RPA bound ssDNA when free GFP-RPA is absent from solution. The three kymographs show the mCherry-Srs2 fluorescence signal (top), the GFP-RPA signal (middle), and the overlaid images (bottom), as indicated. (C) Images of GFP-RPA bound ssDNA before and after injection of mCherry-Srs2. (D) Fractional loss of normalized GFP-RPA signal (integrated over entire ssDNA molecules; N=20) due to the action of Srs2.

possibility that free RPA would occupy ssDNA after the passage of Srs2. These experiments demonstrated that mCherry-Srs2 clears GFP-RPA from ssDNA during translocation, such that ~80% of the GFP-RPA becomes dislodged (Figure 3-5B,D). Given the high binding affinity of RPA for ssDNA[170,172], the residual GFP-RPA that remained after passage of Srs2 may have been due to rebinding of free GFP-RPA that had been displaced by Srs2 elsewhere.

### *3.2.4 Srs2 translocation on near naked versus RPA-bound ssDNA*

Inspection of the Srs2 kymographs revealed additional features reflecting the interactions between Srs2 and RPA-ssDNA. Under the conditions of our experiments, the initial Srs2 binding events

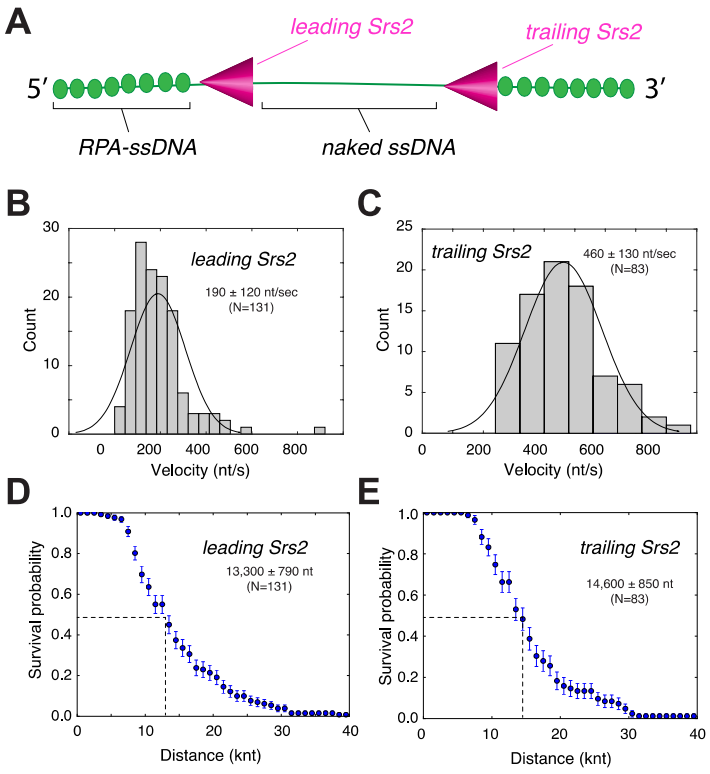


**Figure 3-6. Translocation properties of the leading and trailing Srs2.** (A) Schematic designating the identity of the leading and trailing Srs2. Velocity distributions for the leading (B) and trailing (C) mCherry-Srs2. Survival probability of the (D) leading and (E) trailing mCherry-Srs2; error bars represent s.d. calculated from bootstrapping analysis.

were relatively rare; we typically observed no more than two to three initiation events per ssDNA molecule (*e.g.* Figure 3-1B & 3-5B). However, once Srs2 began translocating, many new Srs2 binding events occurred in its wake, and these latter events were especially prevalent in experiments in which free RPA was absent (*i.e.* Figure 3-5B). Indeed, upon stripping GFP-RPA from the ssDNA, subsequent Srs2 binding events appeared to occur more frequently on the newly created near naked ssDNA (Figure 3-5B). We will refer to Srs2 molecules that became associated with the RPA-ssDNA substrate initially as the "lead" Srs2 molecules, and the Srs2 molecules that bound the newly created near naked ssDNA as "trailing" Srs2 molecules (Figure 3-6A). We use to the term "near naked DNA" to indicate that there is a small amount of GFP-RPA still present (as indicated above; Figure 3-5D). At the concentration of mCherry-Srs2 required to efficiently nucleate the initial translocation events (100 pM), subsequent loading of Srs2 onto the near naked ssDNA became so prevalent that we were unable to accurately document its

frequency. However, we were able to quantitate the translocation characteristics of the leading and trailing Srs2 molecules. This analysis revealed that the lead Srs2 had an apparent velocity of 190 ± 120 nts/sec and processivity of 13,300 ± 790 nts (N=131)(Figure 3-6B,D), slightly faster, but otherwise comparable to reactions in which free RPA was present (Figure 3-1C,D). Remarkably, the trailing Srs2 translocated ~2.5-fold faster, displaying an apparent velocity of 460 ± 130 nts/sec and processivity of 14,600 ± 850 nts (N=83)(Figure 3-6C,E).

*3.2.5 Srs2 evicts Rad52 from ssDNA*

Rad52 is one of the first recombination proteins to arrive at RPA-coated ssDNA present at the ends of processed DSBs[19]. Interestingly, Rad52 is thought to counteract the anti-recombinase activity of Srs2[127,128], although the molecular basis for these observations remains unknown. We have shown that Rad52 is readily recruited to RPA-ssDNA and remains tightly bound to these complexes with lifetimes ≥ 2 hours[173]. This remarkable stability raises the question of whether Rad52 might regulate Srs2 by restricting its translocation on ssDNA. To address this issue, we determined how Srs2 would behave in the presence of Rad52 (Figure 3-7A). For these experiments, RPA-ssDNA complex was prepared with unlabeled RPA. Then, GFP-tagged Rad52 (5 nM, 150 µl) was injected into the sample chamber at a constant flow rate of 0.2 ml/min, and any unbound GFP-Rad52 was flushed from the sample chamber. As reported before[173], Rad52 associated with the RPA-ssDNA complex avidly. Next, mCherry-Srs2 (100 pM) was injected in buffer containing 100 pM unlabeled RPA and 2 mM ATP. Remarkably, Srs2 was able to translocate on the ssDNA complexes, with Rad52 being rapidly stripped from the ssDNA during Srs2 translocation (Figure 3-7B). Inspection of the GFP-Rad52 kymographs revealed that Srs2 was able to push at least some of the Rad52 along the ssDNA, although there was not a pronounced accumulation of GFP-Rad52 towards the 5′ ends of the ssDNA, indicating that Rad52 was being evicted from the ssDNA (Figure 3-7B).

Analysis of the translocation velocities revealed that the leading Srs2 molecules displayed an apparent translocation velocity of 200 ± 80 nt/sec (Figure 3-7C) and a processivity of 14,000 ± 1,500 nt on

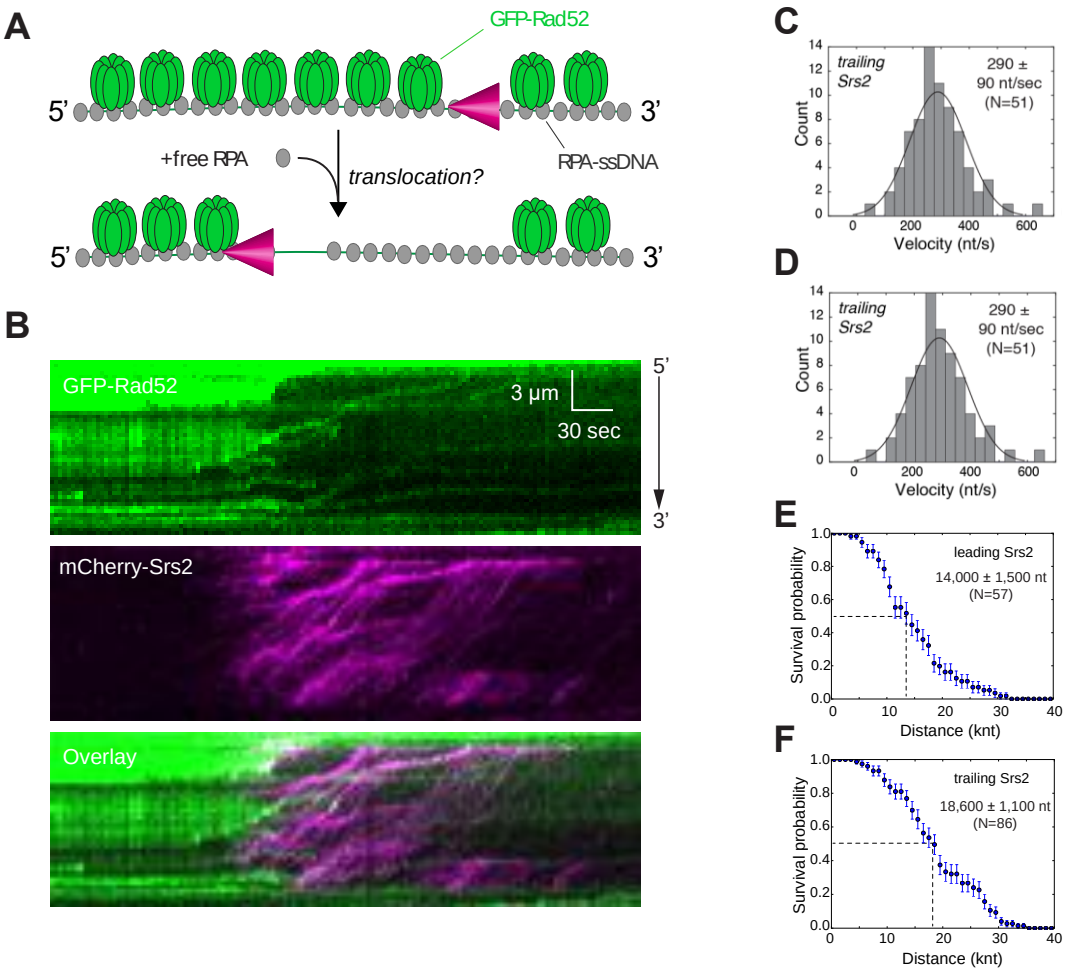


**Figure 3-7. Srs2 can strip Rad52 from the RPA-ssDNA complex.** (A) Schematic for experiment to determine whether Srs2 can remove GFP-Rad52 from the RPA-ssDNA complex. (B) Kymographs depicting examples of what takes place when mCherry-Srs2 acts upon unlabeled RPA-ssDNA in the presence of bound GFP-Rad52. During data collection, the reaction buffer contained 100 pM free RPA (unlabeled), but did not contain free GFP-Rad52. Velocity distribution histograms for the (C) leading and (D) trailing mCherry-Srs2 complexes taken from data collected in the presence of bound GFP-Rad52. Survival probability plots for the (E) leading and (F) trailing mCherry-Srs2 for experiments conducted with GFP-Rad52 bound to unlabeled RPA-ssDNA complexes; error bars represent s.d. calculated from bootstrapping analysis. There was no free Rad52 present in solution when Srs2 was injected.

the Rad52-RPA-ssDNA complexes (Figure 3-7E,F), indicating that the presence of Rad52 has no inhibitory effect on Srs2 translocation. Interestingly, the trailing Srs2 molecules translocated more rapidly than the leading ones, displaying an apparent translocation velocity of 290 ± 90 nt/sec and a processivity of 18,600 ± 1,100 nt (Figure 3-7D). Moreover, we found that the apparent velocity of Srs2 increases from 170 ± 80 nt/sec in the absence of Rad52 (Figure 3-1C) to 200 ± 80 nt/sec in the presence of Rad52

(Figure 3-7C). However, Rad52 has little or no effect on the rate of ATP hydrolysis by Srs2, which would seem to argue against a stimulatory effect of Rad52 on Srs2 translocation velocity (Figure 2-7). We speculate that the faster translocation rate of Srs2 stems from an alteration in the tension on the tethered ssDNA by Rad52.

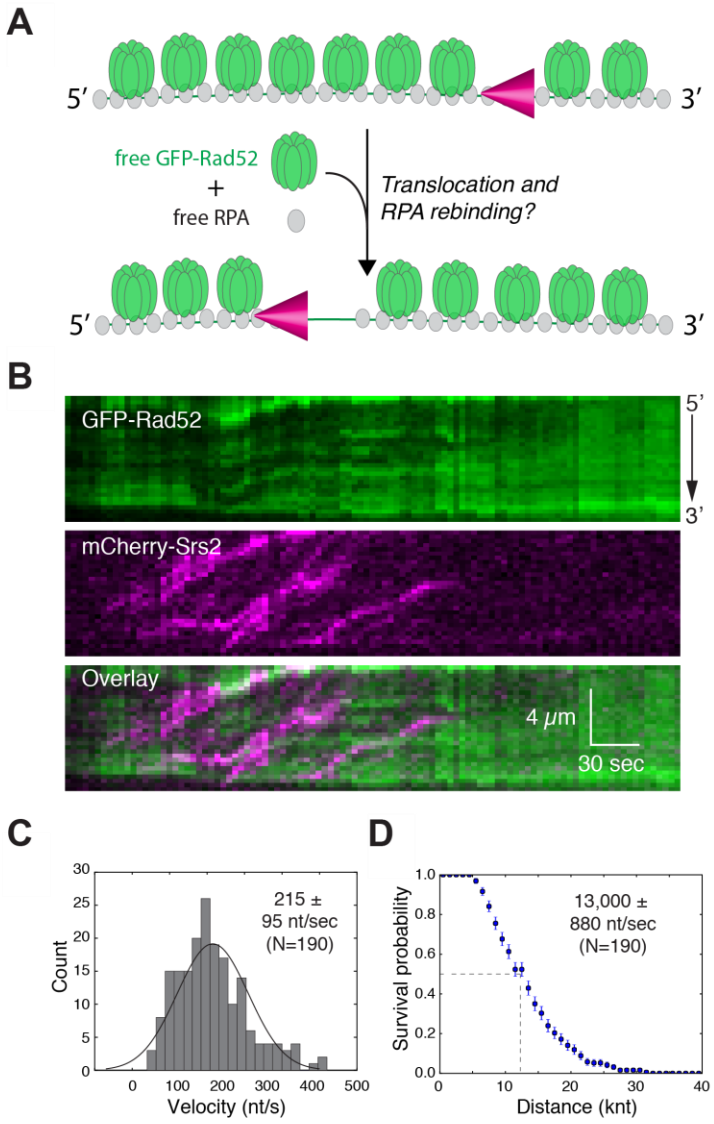


**Figure 3-8. Srs2 promotes recycling of bound Rad52.** Related to Figure 3-7. (A) Schematic for experiment to determine whether new GFP-Rad52 can rebind to the RPA-ssDNA complexes after passage of mCherry-Srs2. (B) Kymographs depicting examples of what takes place when mCherry-Srs2 acts upon unlabeled RPA-ssDNA in the presence of free and bound GFP-Rad52. During data collection, the reaction buffer contained 100 pM free RPA (unlabeled), and also contained 5 nM free GFP-Rad52. (C) Velocity distribution histograms and (D) survival probability graphs for Srs2 complexes taken from data collected in the presence of 5 nM GFP-Rad52.

*3.2.6 Srs2 promotes redistribution of both RPA and Rad52*

We next sought to determine whether Srs2 could promote Rad52 recycling. To address this issue, we conducted experiments where GFP-Rad52 (5 nM) and unlabeled RPA (100 pM) were present in the reaction buffer together with Srs2 (Figure 3-8A). The results demonstrated that GFP-Rad52 re-

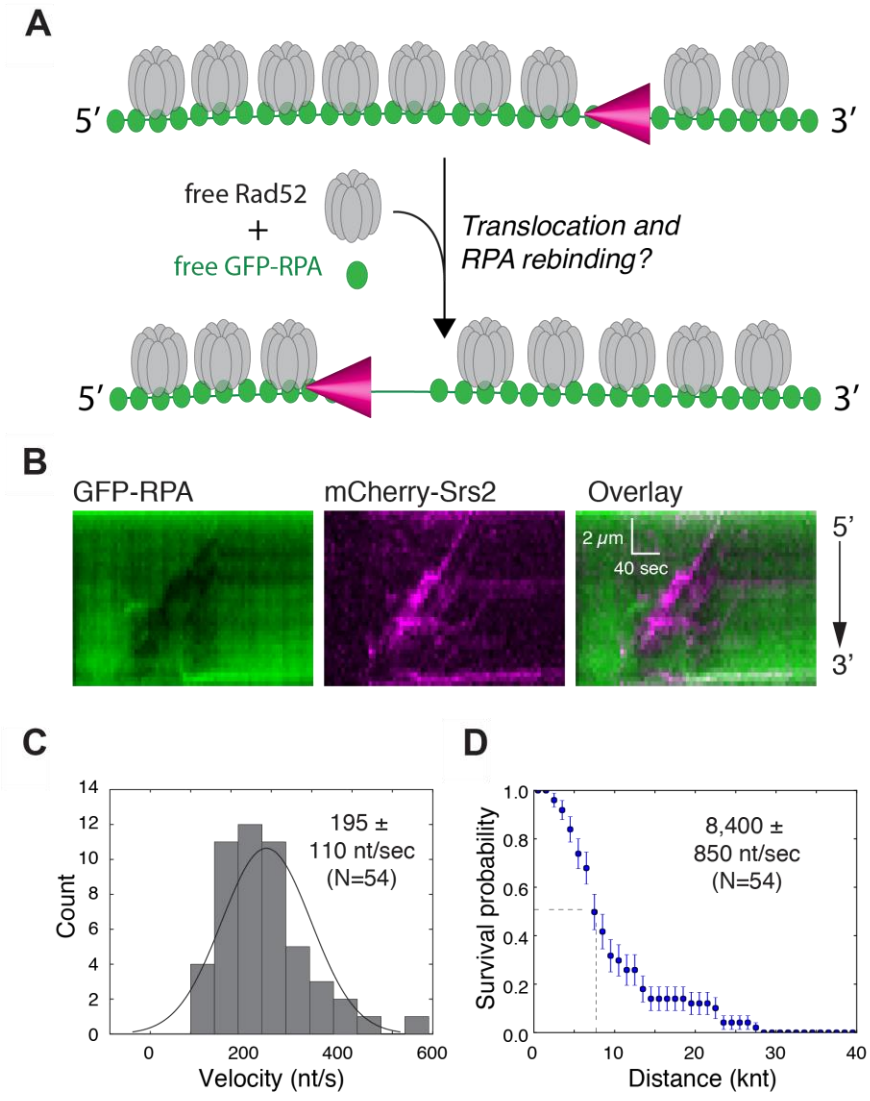


**Figure 3-9. Srs2 promotes RPA recycling in the presence of free Rad52.** Related to Figure 3-7. (A) Schematic for experiment to determine whether new GFP-RPA can rebind to the Rad52-RPA-ssDNA complexes after the passage of mCherry-Srs2. (B) Kymographs depicting examples of what takes place when mCherry-Srs2 acts upon Rad52-RPA-ssDNA in the presence of free and bound Rad52 (unlabeled). During data collection, the reaction buffer contained 100 pM free GFP-RPA, and also contained 5 nM free Rad52 (unlabeled). (C) Velocity distribution histograms and (D) survival probability graphs for mCherry-Srs2 complexes taken from data collected in the presence of 5 nM Rad52 present in solution.

associates with ssDNA after the passage of Srs2 (Figure 3-8B). Under these conditions, Srs2 traveled at an apparent velocity of 215 ± 95 nt/sec (Figure 3-8C) and exhibited an average processivity of 13,000 ± 880 nts (Figure 3-8D). In addition, experiments using unlabeled Rad52 (5 nM) and GFP-RPA (100 pM) confirmed that GFP-RPA is also able to rebind ssDNA after passage of the translocating Srs2 when Rad52 was present (Figure 3-9). Note that these data were not ascribed to lead and trailing Srs2 molecules as they would experience a similar environment when free Rad52 and RPA were present and both proteins would rapidly re-associate with the ssDNA. This treatment of the Srs2 translocation data is supported by the observation of a single well-defined peak for the translocation velocity when free RPA and Rad52 were present (Figure 3-8C & Figure 3-9C). We conclude that Srs2 can remove both RPA and Rad52 from ssDNA, and as a consequence promotes the redistribution of both proteins.

# CHAPTER 4: DISSOCIATION OF RAD51 PRESYNAPTIC COMPLEXES AND HETERODUPLEX DNA JOINTS BY TANDEM ASSEMBLIES OF SRS2

---

This work was originally published as: Kyle Kaniecki, Luisina De Tullio, Bryan Gibb, Youngho Kwon, Patrick Sung, & Eric C. Greene. Dissociation of Rad51 presynaptic complexes and heteroduplex DNA joints by tandem assemblies of Srs2. *Cell Rep*. 2017 Dec 12;21(11):3166-3177.

Author contributions: K.K. designed and conducted the single molecule experiments and data analysis with assistance from L.D.T. B.G. established the initial ssDNA curtain assays for Srs2. Y.K. expressed and purified Rad51 and Dmc1. E.C.G. supervised the project and wrote the manuscript with input from K.K., L.D.T., B.G., Y.K., and P.S.

---

## 4.1 SUMMARY

In chapter 1, Srs2 was presented as a SF1 member helicase/translocase and an efficient anti-recominase that acts to disrupt Rad51-ssDNA filaments. In order to better understand the mechanisms that regulate Srs2, we directly visualized purified Srs2 as it acts upon single-stranded DNA (ssDNA) molecules bound by the Rad51 recombinase. We demonstrated that Srs2 is a highly processive translocase capable of stripping thousands of Rad51 molecules from ssDNA at a rate of ~50 monomers per second. We showed that Srs2 is recruited to RPA clusters embedded with the Rad51 filaments, and that multimeric arrays of Srs2 assemble during translocation on ssDNA through a mechanism involving iterative Srs2 loading events at sites that have been cleared of Rad51. We also demonstrate that Srs2 acts on heteroduplex DNA joints through two alternative pathways, both of which result in rapid disruption of the heteroduplex intermediate. Based upon these findings, we present a model describing the recruitment and regulation of Srs2 as it acts upon homologous recombination intermediates.

## 4.2 RESULTS

### *4.2.1 Disruption of Rad51-ssDNA filaments by Srs2*

*S. cerevisiae* Srs2 contains a core SF1 helicase domain that is homologous to the bacterial helicase UvrD, a C-terminal region responsible for interactions with Rad51, and a second C-terminal domain that mediates protein-protein interactions and is a target for post-translational modifications (Figure 1-6A)[122,180]. For our experiments, we used Srs2 preparations that were either unlabeled, or tagged at the N-terminus with either GFP or mCherry, as indicated. This labeling strategy was selected because N-terminal GFP-Srs2 fusion constructs are functional *in vivo*[128]. Full-length Srs2 is prone to aggregation, so unless stated otherwise, all constructs were truncated at amino acid 898, yielding $Srs2^{898}$. Previous studies have shown that $Srs2^{898}$ is proficient in ATP hydrolysis and in the disruption of Rad51-ssDNA filaments[65,125,149]. We also prepared $Srs2^{K41A}$, which is defective in ATP hydrolysis[123], and the truncation mutants $Srs2^{860}$ and $Srs2^{\Delta 875\text{-}902}$, which lack the Rad51 interaction domain[65,125]. The different purified forms of Srs2 were all tested for ATP hydrolysis activity (Figure 2-6A,B).

We have previously used double-tethered ssDNA curtains and total internal reflection fluorescence microscopy (TIRFM) to visualize the behaviors of Srs2 on RPA-coated ssDNA in the presence and absence of Rad52[181]. Here, we use single- and double-tethered ssDNA curtains to visualize the movement of Srs2 on Rad51-coated ssDNA (Figure 2-3). Presynaptic complexes were prepared using wild-type *S. cerevisiae* Rad51, as described [66,73]. Rad51 was not fluorescently labeled, instead the assembly and disassembly of the presynaptic complex was assessed by monitoring the binding of GFP-tagged RPA. Once assembled, the Rad51 filaments remain intact for hours in the presence of ATP [73].

To determine whether Srs2 could remove Rad51 from the ssDNA, we injected unlabeled $Srs2^{898}$ in 150 µl of buffer containing 2 mM ATP and 100 pM GFP-RPA. Reactions were observed under constant buffer flow (0.2 ml/min), and Srs2 that did not bind during the initial sample injection was flushed away by buffer flow, so the resulting observations only report the behaviors of Srs2 proteins that bind to the RPA-

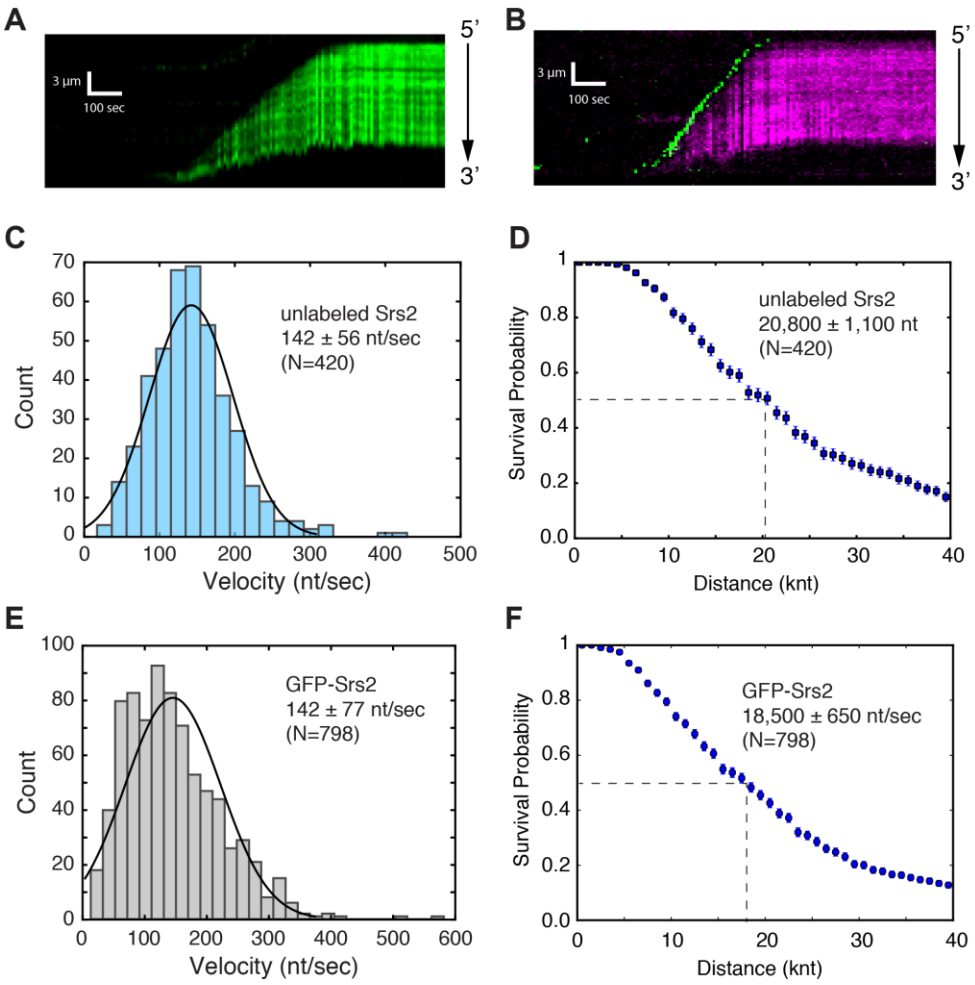


**Figure 4-1. ssDNA curtain assays for Srs2 translocation.** (A) Kymograph showing unlabeled Srs2$^{898}$ removing unlabeled Rad51 from a single-tethered ssDNA molecule; Srs2-mediated Rad51 displacement is revealed by the binding of GFP-RPA (green). (B) Kymograph showing GFP-Srs2$^{898}$ (green) removing unlabeled Rad51 from a single-tethered ssDNA molecule; Rad51 displacement is revealed by the binding of mCherry-RPA (magenta). (C) Velocity distribution and (D) survival probability of unlabeled Srs2$^{898}$ acting on Rad51-ssDNA. (E) Velocity distribution and (F) survival probability of GFP-Srs2$^{898}$ acting on Rad51-ssDNA. Dashed lines in (D) and (F) highlight the values at which half of the complexes stop translocating. Error bars in the survival probability plots represent s.d. calculated from bootstrap analysis.

ssDNA during a ~45 second time window. This strategy was necessary to help minimize overlapping Srs2 binding and translocation events. Under these conditions, we observed extensive Srs2-dependent removal of Rad51 from the ssDNA, as evidenced by the reappearance of GFP-RPA (Figure 4-1A & Figure 2-4B). Rad51 removal did not occur when the ATPase defective Srs2$^{K41A}$ mutant protein was tested, confirming that the observed activity required ATP hydrolysis by Srs2 (Figure 4-2). Moreover, inspection of the kymographs revealed that GFP-RPA reappeared in distinctive wedge-shaped patterns (Figure 4-1A, Figure2-4B & Figure 4-2). These patterns suggested that Rad51 removal stemmed from the

3′→5′ motor activity of Srs2, with each track of GFP-RPA resulting from the processive translocation of Srs2 along the ssDNA.

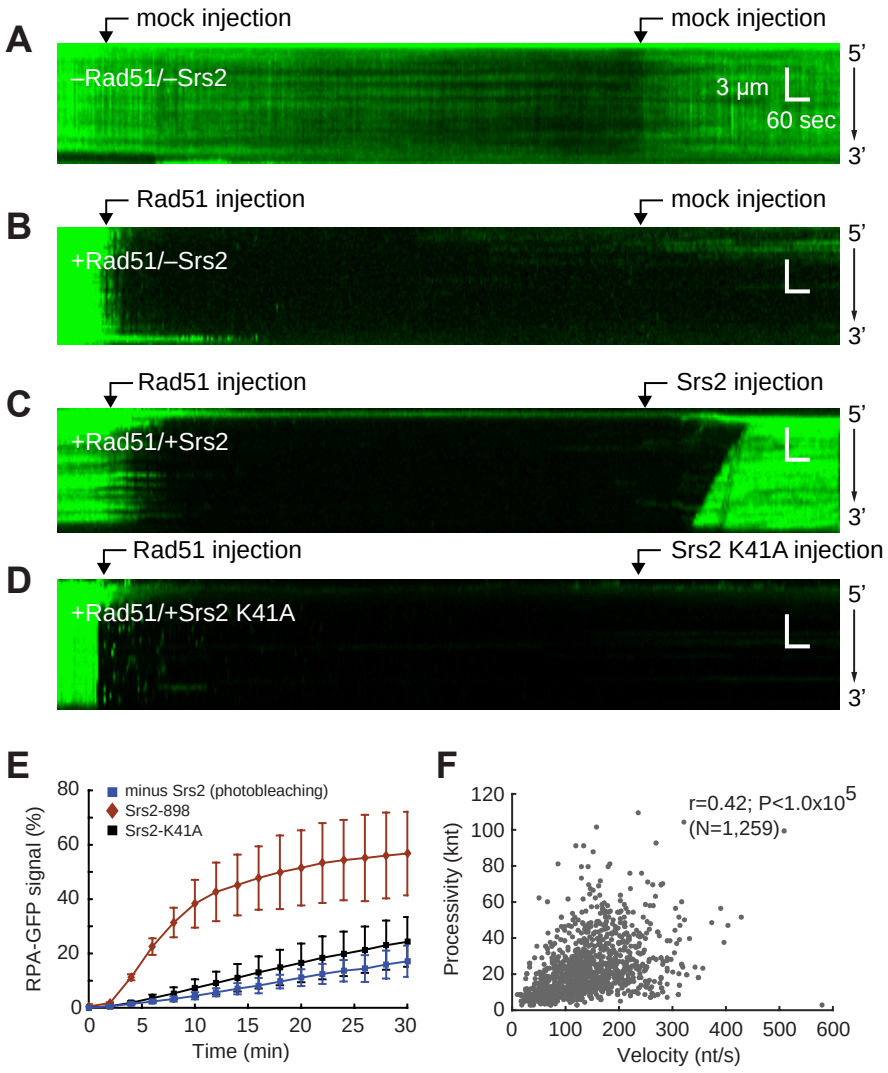


**Figure 4-2. Control experiments for Srs2-dependent disruption of the Rad51 filaments.** (A) Kymograph showing that RPA remains bound to the ssDNA when no Rad51 is injected into the sample chamber. In this case, the gradual time-dependent loss of GFP-RPA signal is due to photo-bleaching, and the photo-bleached RPA molecules are exchanged for fresh GFP-RPA with the mock Srs2 injection. (B) Kymograph showing Rad51 filament assembly. Filament assembly is revealed as the rapid loss of GFP-RPA signal upon injection of Rad51, and Rad51 remains bound to the ssDNA during and after the mock Srs2 injection. (C) Kymograph illustrating the rapid displacement of Rad51 from the ssDNA upon injection of $Srs2^{898}$. (D) Kymograph showing that $Srs2^{K41A}$ does not resulting in Rad51 filament disassembly. (E) Quantitation of the rate for Rad51 removal based upon the re-binding of GFP-RPA to the ssDNA. In these examples, the GFP-RPA signal (%) reflects the integrated signal intensity averaged over the entire lengths of at least 10 double-tethered ssDNA molecules. (F) Scatter plot illustrating that there is a moderate correlation between Srs2 velocity and processivity for data collected at 100 pM Srs2.

We conducted two-color experiments using GFP-Srs2 and mCherry-RPA to validate the expectation that Srs2 was positioned at the leading 5′ edge of each growing tract of GFP-RPA. As predicted, GFP-Srs2 could be seen translocating in the 3′→5′ direction along the presynaptic complexes leaving behind extended tracks of mCherry-RPA on the ssDNA (Figure 4-1B & Figure 2-4C) . Similar results were obtained in two-color experiments using mCherry-Srs2 and GFP-RPA (see below). Experiments using GFP-Srs2$^{K41A}$ revealed that GFP-Srs2$^{K41A}$ bound to the Rad51-ssDNA filaments, but was unable to initiate translocation. These findings provide further evidence that Srs2 movement dependent upon ATP hydrolysis.

Analysis of the GFP-RPA tracks yielded an apparent velocity for unlabeled Srs2 on Rad51 filaments of 142 ± 56 nucleotides per second (nt/sec). Moreover, Srs2 was remarkably processive, with the observed complexes traveling an average distance of 20,800 ± 1,100 nt (N=420) before stopping (Figure 4-1C & 4-1D). The apparent velocity and processivity values for GFP-Srs2 were 142 ± 77 nt/sec and 18,500 ± 650 nt (N=798), respectively (Figure 4-1E,F & Table 4-1). In all cases, the movement of Srs2 occurred in the 3′→5′ direction. We conclude that *S. cerevisiae* Srs2 is a highly processive ssDNA translocase capable of rapidly stripping Rad51 from the presynaptic complex.

*4.2.2 Srs2 is recruited to RPA clusters within the presynaptic complex*

It has remained unknown how Srs2 is recruited to recombination intermediates. To address this question, we next mapped the locations at which Srs2 bound to the presynaptic complexes. The initial Srs2 binding positions appeared randomly distributed along the ssDNA, with a moderate preference for regions closer to the 3′ end of the ssDNA (Figure 4-3A). The Rad51 filaments in our assays are not contiguous, but instead contain short clusters of RPA that were also randomly distributed along the length of the presynaptic complex (Figure 4-3B,C)[173]. Based on measurements of the cumulative GFP-RPA signal before and after presynaptic complex assembly, the remaining RPA clusters constitute ~2–5% of the total RPA that was present on the ssDNA prior to Rad51 binding, and the majority of the ssDNA (~95-98%) is bound by Rad51[173]. Comparison of all Srs2 initiation sites with the entire population of RPA cluster distributions revealed no obvious correlation (c.f. Figure 4-3A,B). However, when examined

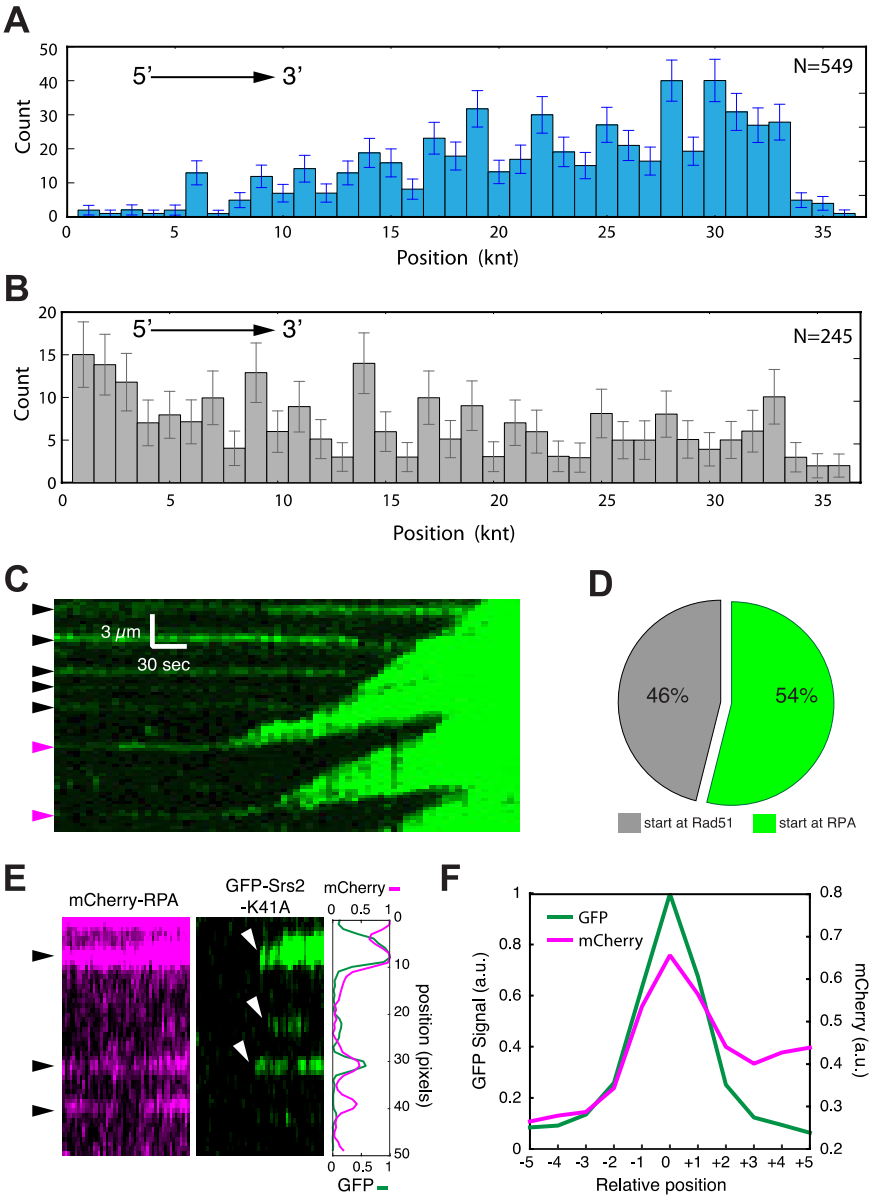


**Figure 4-3. Srs2 is preferentially targeted to RPA clusters embedded within the Rad51 presynaptic complex.** (A) Distribution of initial Srs2 binding sites and (B) distribution of RPA clusters embedded within the Rad51 presynaptic complex; error bars represent s.d. calculated by bootstrap analysis. Kymographs showing (C) unlabeled Srs2$^{898}$ translocation beginning from GFP-RPA clusters, and (D) Pie chart displaying the fraction of Srs2 initiation events that coincided with visible RPA clusters. (E) kymographs and line plot showing the association of GFP-Srs2$^{K41A}$ with mCherry-RPA. (F) Plot showing the relative GFP-Srs2$^{K41A}$ and mCherry-RPA signal distributions (N=67).

on an individual basis, Srs2 had a marked preference for initiating translocation at sites that coincided with RPA (Figure 4-3C). We observed that 54% of the Srs2 recruitment events occurred at these RPA clusters, even though these RPA clusters only make up a very small fraction (~2–5%) of the total ssDNA

present (Figure 4-3D). These values suggest a ~20- to ~60-fold greater likelihood for Srs2 to initiate translocation at an RPA cluster relative to locations at which we detect no RPA. Importantly, the remaining Srs2 recruitment events may also be occurring at RPA clusters that are either too small to detect or may have been photo-bleached over the time scales of our measurements. These results were further validated by examining the binding locations of GFP-Srs2$^{K41A}$ on presynaptic complexes prepared with mCherry-RPA and dark Rad51, which revealed that GFP-Srs2$^{K41A}$ had a strong preference for binding to mCherry-RPA (Figure 4-3E,F). Taken together, these findings support a model in which Srs2 is recruited to small clusters of RPA embedded within the Rad51 presynaptic complex.

### *4.2.3 Tandem assemblies of Srs2 promote efficient Rad51 disruption*

Interestingly, our data hinted at the possibility that the processive disruption of Rad51 filaments observed in our assays may involve more than just one Srs2 molecule. Specifically, in experiments using 100 pM Srs2, we observed highly processive translocation activity (Figure 4-4A). However, at lower Srs2 concentrations (10 pM) we observed mostly short patches of Rad51 removed from the ssDNA (Figure 4-4A), and the apparent velocity also increased with Srs2 concentration (Figure 4-4B). These results suggested that at low concentrations Srs2 was less able to catalyze the highly processive filament disruption.

We often observed fluorescent Srs2 molecules colliding with one another while stripping Rad51 from ssDNA, or larger Srs2 complexes separating into smaller independent units, suggesting that assemblies of Srs2 might be traveling along the same ssDNA molecules. Moreover, we also often observed multiple Srs2 binding and translocation events on the same ssDNA molecule, especially over regions of the ssDNA that had already been cleared of Rad51 (Figure 4-4C), consistent with the notion that Srs2 binds preferentially to RPA-ssDNA relative to Rad51-ssDNA. Interestingly, the trailing Srs2 complexes traveling along RPA-ssDNA often caught up to and merged with the leading Srs2 complexes that are at the 3′ edge of the Rad51 filament. Examples of these mergers were especially evident in cases where the leading Srs2 displayed fortuitous reduction in velocity (Figure 4-4C).

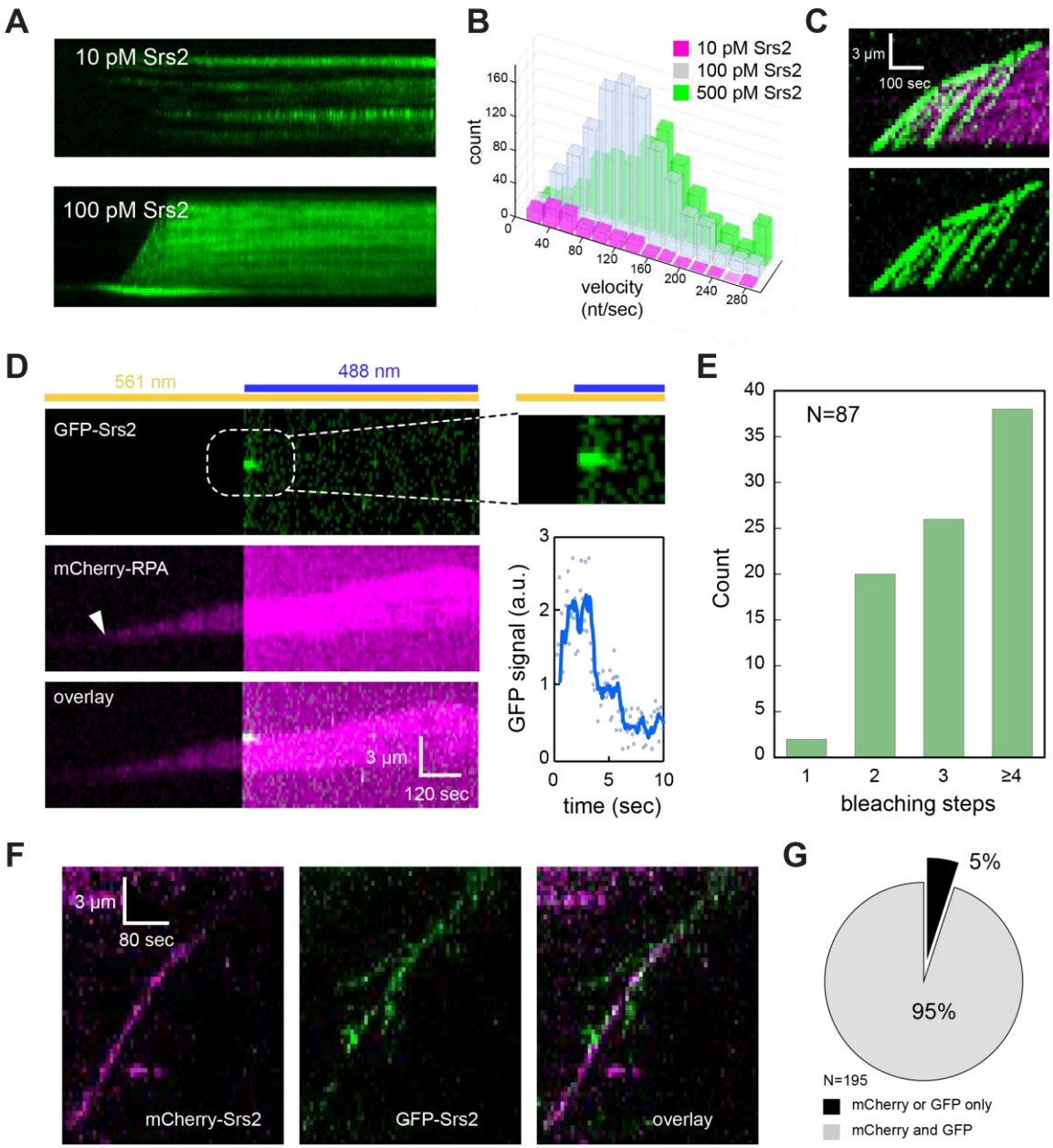


**Figure 4-4. Srs2 forms multimeric complexes during processive translocation.** (A) Kymographs showing the typical behavior of Srs2898 at 10 pM and 100 pM, as indicated. (B) Velocity distribution898 profiles for experiments conducted at 10, 100, or 500 pM Srs2898. (C) Kymograph highlighting an example of numerous Srs2 merging events. (D) Kymographs and graph showing photobleaching step measurements used to confirm that GFP-Srs2898 was not acting as a monomer during processive translocation. Orange and blue lines indicate when the sample was being illuminated with the 561-nm and 488-nm lasers, respectively. (E) Distribution of different bleaching steps measured for translocating GFP-Srs2898 complexes. (F) Example of kymograph showing a two-color mixing experiment with GFP-Srs2898 and mCherry-Srs2898, and (G) fraction of complexes that contained overlapping GFP and mCherry fluorescence.

Visual inspection of the GFP-Srs2 trajectories also suggested that these complexes were much brighter than might be expected for a single GFP molecule. To validate this interpretation, we used 561-nm laser illumination to first identify tracts of Rad51 that were being dismantled by GFP-Srs2 (100 pM) based upon the appearance of mCherry-RPA (Figure 4-4D). We then quickly viewed the sample with high-intensity 488-nm laser illumination while continuously imaging the GFP-Srs2 signal (Figure 4-4D). As expected, GFP-Srs2 was located at the leading edges of the growing tracts of mCherry-RPA, and the GFP signal quickly photo-bleached under these conditions, allowing us to estimate the number of GFP molecules present in the Srs2 complexes based upon the number of photo-bleaching steps (Figure 4-4D). These experiments confirmed that the majority of the GFP-Srs2 complexes displayed multiple photo-bleaching steps, with ~97% of the Srs2 complexes exhibiting two or more bleaching steps (N=84/97), and ~44% exhibiting at least four bleaching steps (N=38/97)(Figure 4-4E).

Finally, we performed two-color mixing experiments using a combination of GFP-Srs2 and mCherry-Srs2. If Srs2 acted as monomeric units while disrupting the Rad51 filaments, then GFP- and mCherry-Srs2 should appear as separate entities on the ssDNA. However, if Srs2 multimers were responsible for disrupting the Rad51 filaments, then the fluorescence signals from GFP- and mCherry-Srs2 should overlap on the ssDNA. Consistent with this latter interpretation, when GFP-Srs2 (50 pM) and mCherry-Srs2 (50 pM) were pre-mixed and injected into the sample chamber, only ~5% of the observed signals could be ascribed to only one color (N=10/195), whereas ~95% of the observed complexes (N=185/195) contained overlapping GFP and mCherry signals (Figure 4-4F,G). These observations all support the conclusion that the highly processive Srs2 complexes observed in our assays were comprised of multiple Srs2 molecules traveling together along the ssDNA.

### *4.2.4 The Rad51 interaction domain is required for Srs2 loading*

Efficient removal of Rad51 from ssDNA requires a direct contact between Rad51 and Srs2 (Figure 1-6A)[65,125]. *In vitro* studies have shown that an srs2 mutant ($Srs2^{860}$) lacking these amino acids cannot interact with Rad51 and also showed greatly diminished ability to disrupt Rad51 filaments[65]. However, these *in vitro* studies have shown that the interaction defective $Srs2^{860}$ mutant protein has

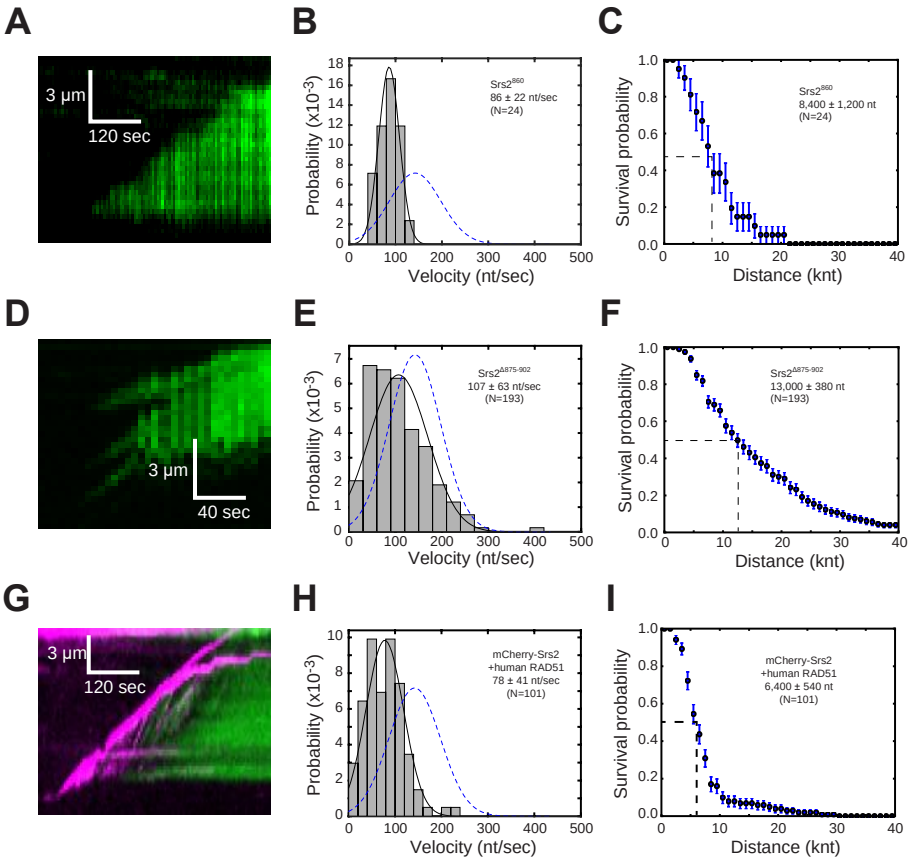


**Figure 4-5. Srs2 mutants that affect Rad51 clearance.** (A) Kymograph, (B) velocity distribution and (C) survival probability for Srs2$^{860}$. (D) Kymograph, (E) velocity distribution and (F) survival probability for Srs2$^{\Delta 875\text{-}902}$. (G) Kymograph, (H) velocity distribution and (I) survival probability for *S. cerevisiae* mCherry-Srs2$^{898}$ acting on ssDNA bound by human RAD51. Error bars for the survival probability plots represent s.d. calculated by bootstrap analysis. The velocity distributions in (B), (E) and (H) are superimposed on the Gaussian fit (blue dashed line) for the velocity distribution of unlabeled Srs2 taken from Figure 4-1C.

residual activity in Rad51-ssDNA filament disruption, and overexpression of this Srs2$^{860}$ mutant can provide some biological activity[65,125]. We considered two possibilities for the reduced displacement of Rad51 from ssDNA upon deletion of the Rad51 interaction domain from Srs2: (*i*) it could attenuate initial association of Srs2 with the Rad51-ssDNA filament; or (*ii*) it might reduce Srs2 processivity, velocity or both. To distinguish between these models, we assessed the ability of the C-terminally truncated GFP-Srs2$^{860}$ to dismantle Rad51 filaments. These assays revealed that most of the Rad51 filaments (~98%) remained fully intact upon injection of Srs2$^{860}$, confirming that truncation of the Srs2 C-terminus greatly diminishes its ability to disrupt the Rad51 filaments. Remarkably, there were a few examples (24 total) of Rad51 filaments being dismantled by Srs2$^{860}$ (Figure 4-5A). These rare Srs2$^{860}$ translocation events were

~40% slower than reactions with $Srs2^{898}$, exhibiting a rate of 86 ± 22 nt/sec (N=24) (Figure 4-5B & Table 4-1). Although $Srs2^{860}$ was not as processive as $Srs2^{898}$, the mutant protein still traveled an average distance of 8,400 ± 1,200 nucleotides before stopping (Figure 4-5C). We next tested $Srs2^{\Delta 875-902}$, which lacks the Rad51 interaction domain, but retains all of the remaining C-terminal amino acids[125]. Interestingly, we were able to observe more translocation events for $Srs2^{\Delta 875-902}$ compared to $Srs2^{860}$, revealing translocation and processivity values of 107 ± 63 nt/sec and 13,000 ± 380 nt (N=193), respectively (Figure 4-5D,F & Table 4-1). Together, these findings suggest that truncating the Srs2 C-terminal domain markedly reduces the number of initial binding events, but once bound, the core SF1 helicase domain of Srs2 retains the ability to disrupt Rad51 filaments, albeit at a reduced velocity relative to $Srs2^{898}$. Taken together, these results indicate that the Rad51 interaction domain in Srs2 is not necessary for Rad51 filament disruption. These findings also imply that amino acids located within the C-terminal region of Srs2 help promote its association with the presynaptic complex.

*4.2.5 Disruption of human Rad51 by yeast Srs2*

We next asked whether *S. cerevisiae* Srs2 could clear human RAD51 from ssDNA. If species-specific contacts were necessary for Rad51 clearance from DNA, then yeast Srs2 should not be able to dismantle filaments of human RAD51. We found no evidence for disruption of the human RAD51 filaments under the same conditions (*i.e.* 100 pM Srs2) where *S. cerevisiae* Rad51 was efficiently removed from the ssDNA. However, *S. cerevisiae* Srs2 is capable of removing human RAD51 from ssDNA at a Srs2 concentration (1 nM) that is 10-times greater than used in experiments with *S. cerevisiae* Rad51 (Figure 4-5G). When clearance of human RAD51 was evident, Srs2 exhibited a translocation velocity of 80 ± 40 nt/sec and an average processivity of 6,400 ± 540 nt (N=101) while clearing human RAD51 (Figure 4-5H,I & Table 4-1). In addition, these Srs2 complexes were much brighter than observed in experiments with *S. cerevisiae* Rad51, and it was evident that this increase in signal intensity was the consequence of multiple trailing Srs2 complexes moving rapidly along the RPA-ssDNA and then merging with the slower Srs2 ensembles positioned at the receding 3′ edge of the human RAD51 filaments (Figure 4-5G). We conclude that species-specific protein-protein contacts help

promote efficient Srs2-mediated removal of Rad51 from ssDNA, but are not an absolute requirement in this regard.

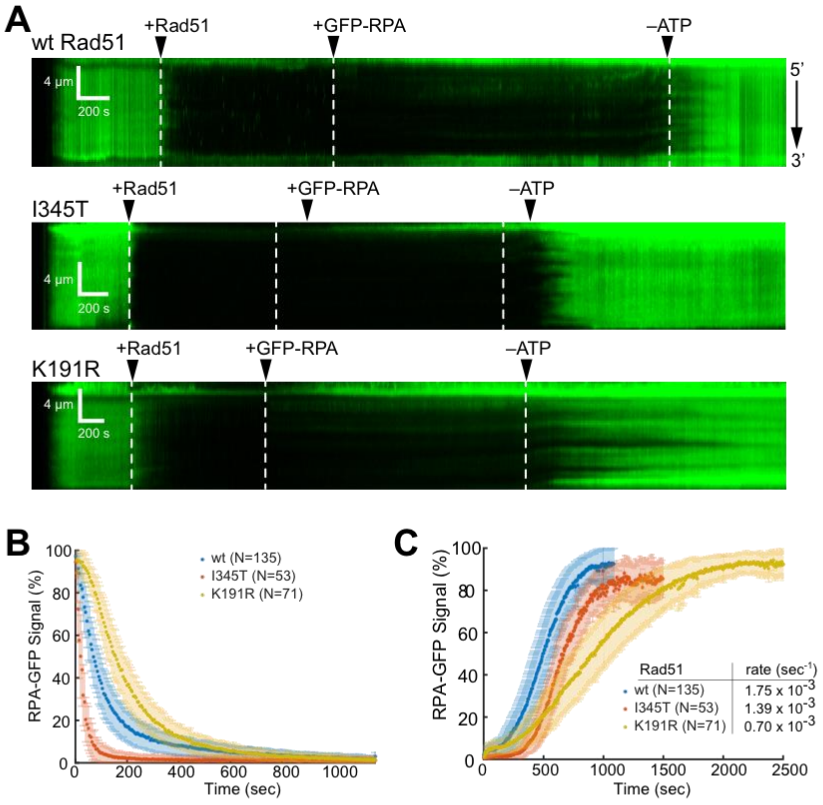


**Figure 4-6. Assembly and disassembly properties of Rad51$^{K191R}$ and Rad51$^{I345T}$.** (A) Kymograph showing the assembly of wild-type Rad51 (1 μM) on a double-tethered ssDNA molecule in the presence of 2 mM ATP. Disassembly of the Rad51 filament was initiated by removing ATP from the injection buffer. In both cases, the presence or absence of Rad51 on the ssDNA is assessed based upon the fluorescence signal of GFP-RPA. (B) Kymograph showing assembly and disassembly of Rad51$^{I345T}$ (1 μM) on a double-tethered ssDNA molecule in the presence of 2 mM ATP. (C) Kymograph showing assembly and disassembly of Rad51$^{K191R}$ (7 μM) on a double-tethered ssDNA molecule in the presence of 2 mM ATP. Note that assembly of Rad51$^{K191R}$ was significantly compromised relative to wild-type Rad51, which is why these reactions required a higher protein concentration to achieve good coverage of the ssDNA. Note that the time scale bars are different for (A-C). Quantitation of the (D) assembly and (E) disassembly characteristics for wild-type Rad51, Rad51$^{K191R}$ and Rad51$^{I345T}$. In these examples, the GFP-RPA signal (%) reflects the integrated signal intensity averaged over the entire lengths of at least 10 double-tethered ssDNA molecules.

*4.2.6 Rad51 ATP hydrolysis is required for efficient Srs2 activity*

The mutation of the lysine residue in the Walker A box of yeast Rad51 (Rad51$^{K191R}$) ablates DNA-dependent ATP hydrolysis activity and engenders sensitivity to certain DNA damaging agents[63,67-69]. However, the Rad51$^{K191R}$ mutant protein still binds to ssDNA and promotes DNA strand exchange[67-69]. Previous bulk biochemical analysis has suggested that Srs2 is not as capable of removing Rad51$^{K191R}$ from ssDNA[65]. Interestingly, Rad51$^{K191R}$ is not efficiently recruited to DNA breaks, but this deficiency is suppressed by the srs2Δ mutation, suggesting that Srs2 may remove Rad51$^{K191R}$ from ssDNA *in vivo*[67]. We asked whether Srs2 could remove Rad51$^{K191R}$ from ssDNA in our assays. We approached this problem by first assessing the assembly and disassembly properties of Rad51$^{K191R}$. These results showed that while Rad51$^{K191R}$ is compromised for filament assembly, it also dissociated from the ssDNA ~2.5-fold more slowly than wt Rad51 (Figure 4-6). Importantly, Srs2 was able to remove Rad51$^{K191R}$ from ssDNA (Figure 4-7A), but translocated at just 36 ± 20 nt/sec and exhibited a processivity of 7,700 ± 590 nt (N=120) while moving along the Rad51$^{K191R}$-ssDNA filaments (Figure 4-7B,C & Table 4-1). This ~75% reduction of the translocation velocity is quite striking and provides clear evidence for enhanced resistance of the Rad51$^{K191R}$ filament to Srs2.

*3.2.7 Rad51 suppressor mutations of Rad55-Rad57 are resistant to Srs2 disruption*

The stability of the Rad51 presynaptic filament is modulated by a balance between the stabilizing function of Rad55-Rad57 and the destabilizing function of Srs2[92]. Interestingly, Rad51$^{I345T}$ was isolated as a suppressor mutation that partially bypasses the requirement for Rad55-Rad57, suggesting that the Rad51$^{I345T}$ presynaptic complex might be more resistant to Srs2[75]. We therefore examined the ability of Srs2 to disrupt presynaptic complexes prepared with Rad51$^{I345T}$. These experiments revealed that Srs2 is able to remove Rad51$^{I345T}$ from ssDNA (Figure 4-7D), albeit more slowly than observed with wild-type Rad51, revealing velocity and processivity values of 85 ± 48 nt/sec and 11,300 ± 920 nt (N=239)(Figure 4-7E,F & Table 4-1). In agreement with previous findings[182], Rad51$^{I345T}$ assembled more rapidly into filaments on ssDNA compared to wt Rad51, and also displayed a delay in filament disassembly when

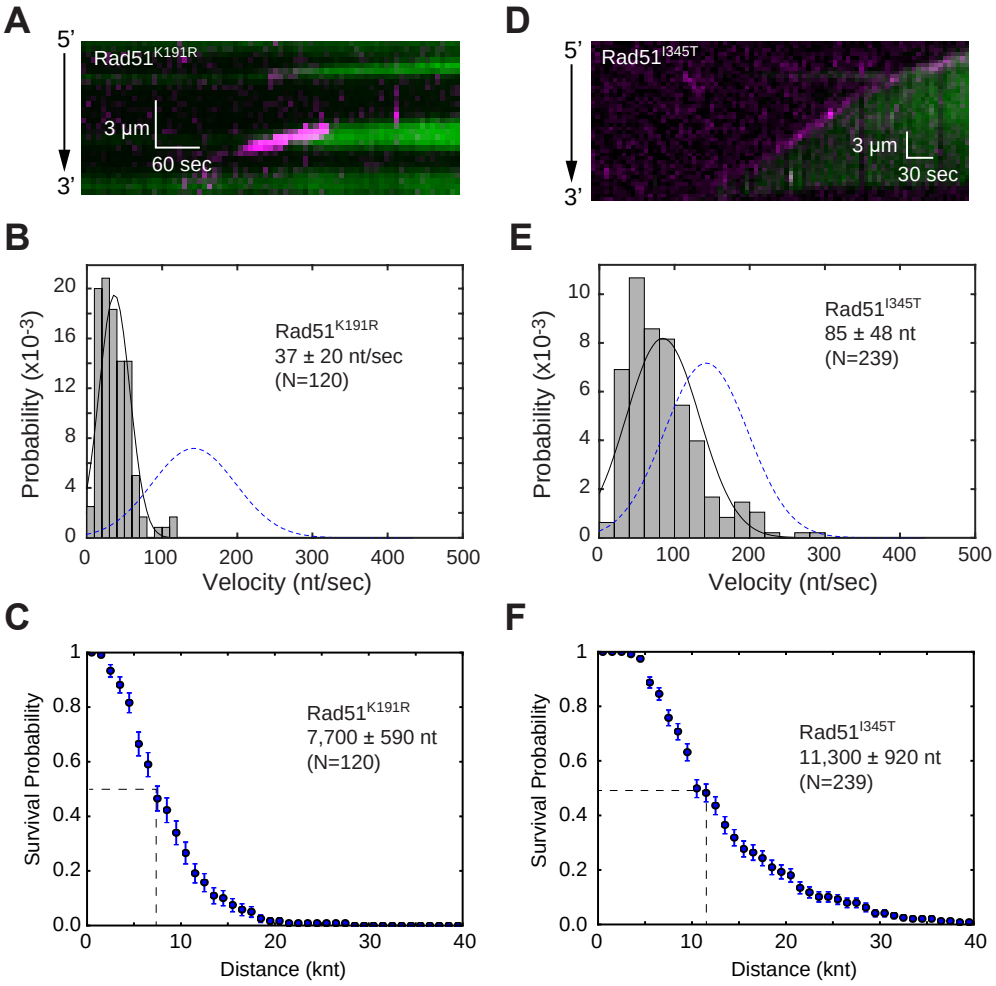


**Figure 4-7. Rad51 mutations that restrict clearance by Srs2.** (A) kymograph, (B) velocity distribution, and (C) survival probability analysis for mCherry-Srs2$^{898}$ translocation on presynaptic complexes prepared with Rad51$^{K191R}$. (D) kymograph, (E) velocity distribution, and (F) survival probability analysis for mCherry-Srs2$^{898}$ translocation on presynaptic complexes prepared with Rad51$^{I345T}$. Error bars for the survival probability plots represent s.d. calculated by bootstrap analysis. The velocity distributions in (B) and (E) are superimposed on the Gaussian fit (blue dashed line) for the velocity distribution of unlabeled Srs2 taken from Figure 4-1C.

chased with buffer lacking ATP (Figure 4-6). Together, these findings suggest that Rad51$^{I345T}$ may overcome the genetic requirement for Rad55-Rad57 due to an increased affinity for ssDNA, which in turn lowers Srs2 velocity and processivity.

*4.2.8 Srs2-mediated disruption of heteroduplex DNA joints*

We have previously established assays for observing interactions between the Rad51 presynaptic complexes and short (70-bp) dsDNA substrates[66,73]. We next asked whether Srs2 could process nucleoprotein intermediates that harbor ATTO 565-labeled dsDNA substrates bearing 15-nt of homology to the ssDNA that is bound by Rad51[66,73]. The fluorescently-tagged dsDNA substrates were pre-incubated with the Rad51 filaments, and then GFP-Srs2 was injected into the sample chamber to determine its impact upon the fluorescent dsDNA molecules. Under these conditions, the dsDNA substrates undergo homologous pairing to form a paranemic joint that resembles a D-loop (Figure 4-8A,B).

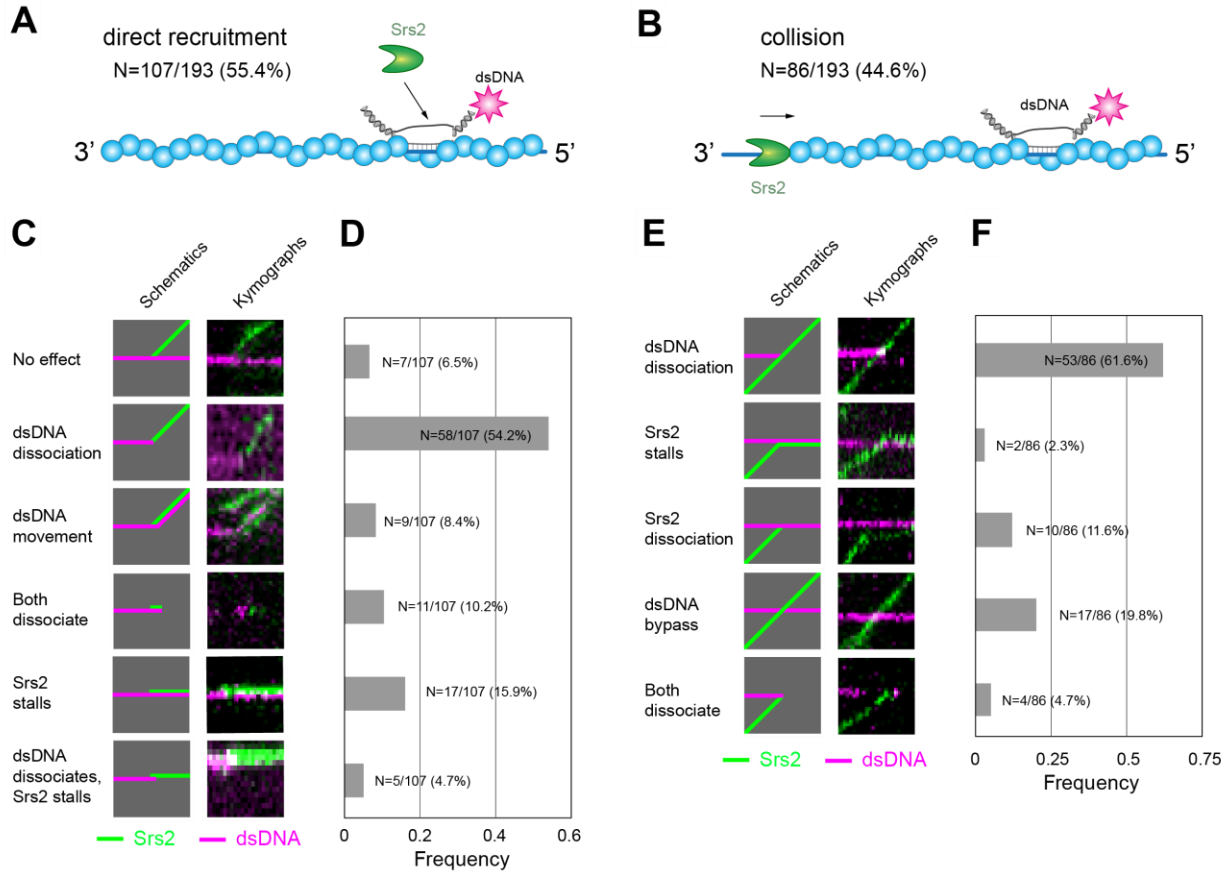


**Figure 4-8. Srs2 disruption of heteroduplex DNA joints.** Illustration showing two pathways for Srs2 interactions with the bound dsDNA fragments through either (A) direct recruitment or (B) collision events. (C) Schematic illustrations and kymographs depicting the observed outcomes of Srs2 interactions involving direct binding to the dsDNA fragments. (D) Relative frequency of each direct binding outcome. (E) Schematic illustrations and kymographs depicting the observed outcomes of Srs2 interactions involving collisions with the dsDNA fragments. (F) Relative frequency of each collision outcome.

Srs2 interactions with these short dsDNA substrates could be segregated into two classes: (*i*) direct recruitment events where Srs2 appeared to bind directly to the DNA joint (Figure 4-8A); and (*ii*) collision events involving translocation of Srs2 along the Rad51-ssDNA presynaptic complex until the DNA joints were encountered (Figure 4-8B). Direct recruitment was the most common outcome for both substrates, accounting for ~55% of all interactions between Srs2 and the bound dsDNA substrates (Figure 4-8A). The most common outcomes for the direct recruitment events were the rapid dissociation of the dsDNA substrates followed by continued Srs2 translocation along the presynaptic complex (54.2%, N=58/107)(Figure 4-8C,D). We also observed other types of less common events when Srs2 was directly recruited to the D-loops, including Srs2 stalling with concomitant displacement of the dsDNA (15.9%, N=17/107), dissociation of both Srs2 and the dsDNA (10.2%, N=11/107), and examples where the dsDNA appeared to move with Srs2 (8.4%, N=9/107)(Figure 4-8C,D). Finally, a small fraction of the events assigned as direct recruitment had no effect on the dsDNA, and Srs2 continued translocation towards the 5′ ends of the ssDNA (6.5%, N=7/107)(Figure 4-8C,D). One possible explanation in these later cases was that Srs2 was unable to unwind the DNA joint sufficiently to allow it to dissociate from the presynaptic complexes, and these events may be mechanistically related to what takes place when Srs2 bypasses a bound dsDNA. Alternatively, Srs2 may have been recruited near the dsDNA, but did not actually interact with the dsDNA itself.

Collison events accounted for ~45% of all observed interactions between Srs2 and the dsDNA bound to the Rad51-ssDNA presynaptic complexes. The most common outcome for these collision events was rapid displacement of the dsDNA from the presynaptic complex followed by continued movement of Srs2 along the presynaptic complex (61.6%, N=53/86)(Figure 4-8E,F). In addition to dsDNA dissociation, we also observed instances where Srs2 stalled or dissociated upon encountering the dsDNA (2.3%, N=2/86 and 11.6%, N=10/86, respectively), (Figure 4-8E,F). In addition, a significant fraction of the collisions resulted in Srs2 bypassing the dsDNA (19.8%, N=17/86)(Figure 4-8E,F). Because the ssDNA itself is not labeled, one explanation for these apparent bypass events may be that Srs2 was bound one of two overlapping ssDNA molecules. If this is the case, then our reported value (61.6%) for dsDNA dissociation during the collision events would represent a lower bound for the Srs2-mediated disruption of the dsDNA during the collisions events. Taken together, we conclude that Srs2 can readily remove short

dsDNA fragments that are bound to the Rad51-ssDNA presynaptic complex and can do so through either direct recruitment to the heteroduplex DNA joint or by colliding with the heteroduplex DNA after approaching from the 3′→5′.

| **Srs2 variant** | **Srs2 conc.** | **Rad51 variant** | **mean velocity (nt/sec)** | **stand. dev.** | **N** | **p-value** (relative to Srs2 plus Rad51) | **Figure panel** |
|---|---|---|---|---|---|---|---|
| Srs2 | 100 pM | wt Rad51 | 142 | ±56 | 420 | NA | 4-1C |
| GFP-Srs2 | 100 pM | wt Rad51 | 142 | ±77 | 798 | 0.924 | 4-1E |
| $Srs2^{860}$ | 100 pM | wt Rad51 | 86 | ±22 | 24 | $1.04 \times 10^{-11}$ | 4-5B |
| $Srs2^{\Delta 875\text{-}902}$ | 100 pM | wt Rad51 | 107 | ±63 | 193 | $8.71 \times 10^{-11}$ | 4-5E |
| mCherry-Srs2 | 1 nM | human RAD51 | 78 | ±41 | 101 | $3.65 \times 10^{-29}$ | 4-5H |
| mCherry-Srs2 | 100 pM | Rad51 K191R | 37 | ±20 | 120 | $7.08 \times 10^{-124}$ | 4-7B |
| mCherry-Srs2 | 100 pM | Rad51 I345T | 85 | ±48 | 239 | $1.26 \times 10^{-37}$ | 4-7E |

**Table 4-1. Comparison of translocation velocities from Chapter 4 experiments.** Summarized are the translocation velociteis for each combination of Srs2 and Rad51. Significantly difference velocities from $Srs2^{898}$ were measured using Student's paired t-test. Only the GFP-$Srs2^{898}$ was not different from $Srs2^{898}$

# CHAPTER 5: DISCUSSION

## 5.1 OVERVIEW

This work has examined some of the key ways Srs2 can moderate genetic recombination through the disassembly and redistribution of some of the molecular players of this pathway. Chapter 1 explored some of the key ways life employs genetic recombination, the dynamic nature of the molecular players involved, and examined how helicases function with a particular emphasis on Srs2. Chapter 2 outlined the advantages of SM approaches and detailed ssDNA curtains as a new tool to study helicase and translocase activity within the context of recombination proteins. Chapters 3 and 4 presented the results of employing our helicase assay on nucleoprotein filaments that would include various combinations of RPA, Rad51, Rad52 and donor dsDNA. The results are undergirded by conforming to many of the previously ascribed activities of these molecules (e.g., Srs2 stripes Rad51 from ssDNA in a 3′→5′ biased direction), while also adding new features not previously described (e.g., Srs2 dissociating RPA-Rad52 complexes).

As is often the case with the development of a new tool, there is much work left to be done on this system. New members in the Greene lab along with our collaborators will be ideally placed to take advantage of this foundation and build upon the complexity by adding recombination mediators (ex. Rad55-Rad57, Shu complex, etc.), examining various dsDNA donor templates, and mutational studies to gain an unprecedented depth of knowledge about these complex and elusive molecules. Furthermore, a similar approach could be used to investigate different helicases that are known to interact with the recombination machinery (ex. Mph1, Rad54, HsRECQ5, etc.).

## 5.2 MECHANISM OF SRS2 RECRUITMENT

While it is established that Srs2 dismantles Rad51 filaments, it has remained unclear how Srs2 is recruited to the presynaptic complex and other HR intermediates[65,120-122,149,180,183,184]. C-terminal truncation mutants, $Srs2^{898}$ and $Srs2^{860}$, have equivalent ATPase activity on naked ssDNA in bulk assays (Figure 2-6). However, in chapters 3 and 4, we provided evidence that $Srs2^{860}$ is compromised in its ability to initiate translocation on both RPA (Figure 3-4) and Rad51 (Figure 4-5) filaments. In chapter 4, we provided evidence that $Srs2^{898}$ is preferentially recruited to small clusters of RPA that remain embedded within the Rad51 presynaptic complex (Figure 4-3, Figure 5-1). These results indicate residues 861-898 are likely important for initiating processive translocation on RPA-ssDNA.

As an alternative explanation, we should consider the possibility that the RPA puncta that remain after Rad51 exchange are hairpin structures and that Srs2 is recruited to the 5′ flap structure. It is worth note that the Shu complex has been demonstrated to preferentially bind forked and flapped ss/dsDNA junctions *in vitro* and antagonizes Srs2 recruitment to sites of DSBs *in vivo*. Indeed, $UvrD^{D402P}$ has been shown to have a 6-fold increase for binding to 5′ flaps and the corresponding residue in Srs2 is already a proline[110]. If this were the case, ssDNA curtain experiments employing Rad51 and fluorescent Shu protein complexes would likely co-localize with these mediators to RPA puncta and potentially prevent Srs2 initiation from these locations. Our lab recently obtained purified Csm2-Psy3 heterodimer bearing a SNAP tag for fluorescent labeling and will be testing this hypothesis in the near future.

Experiments with 1nM $Srs2^{860}$ on RPA filaments resulted in more processive translocation events with a similar velocity and processivity to 100pM $Srs2^{898}$ activities. While the equivalent 1nM $Srs2^{860}$ experiment was not performed on a Rad51 filament, the velocity and processivity measures for the rare processive events have significantly reduced velocities when compared with $Srs2^{898}$ (Table 4-1). These results suggest residues 861-898 may be involved in two separate activities; generally initiating translocation at RPA-bound ssDNA and specifically in disrupting Rad51 filaments during translocation. Challenging Rad51 filaments with 1nM $Srs2^{860}$ could provide additional support for this hypothesis.

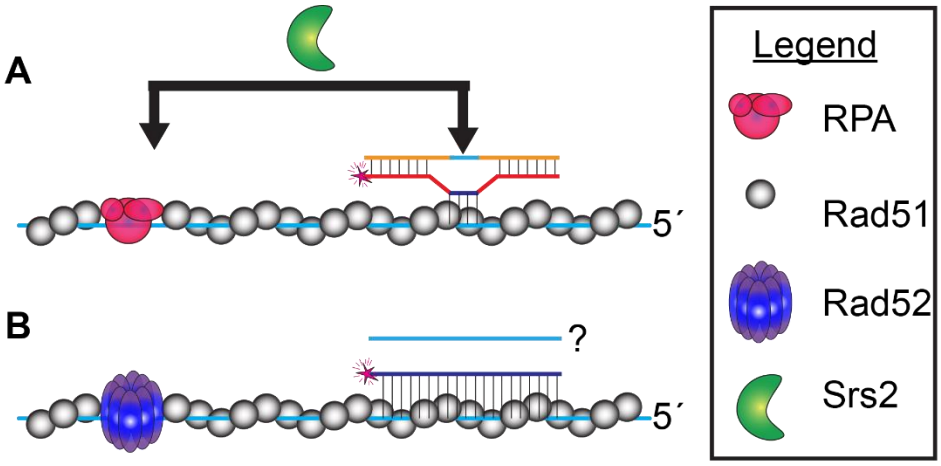


**Figure 5-1. Srs2 is recruited to breaks in the Rad51-ssDNA filament.** (A) Srs2 will preferentially begin Rad51 filament disruption from locations of RPA or dsDNA binding. Blue regions within the dsDNA represent sequence homology to the ssDNA filament. (B) It is not yet known whether similar recruitment would occur from locations of Rad52 or a fully homologous dsDNA template and represent key experiments readily attainable.

Chapter 3 demonstrated that Srs2 can strip RPA from the ssDNA and observed that new Srs2 recruitment events take place even more readily on the newly cleared naked ssDNA. Analyzing Srs2 trajectories over the newly cleared ssDNA demonstrated an apparent 2.5-fold and 3.25-fold increase in translocation velocities when compared to densely packed RPA or Rad51 filaments, respectively[181]. An important implication of this finding is that as Srs2 begins stripping Rad51 from ssDNA, the newly created near-naked ssDNA that forms behind the leading Srs2 complex becomes available for the recruitment of additional Srs2 molecules that quickly catch up to the leading molecule.

Thus, the recruitment mechanism may consist of interactions with RPA, ssDNA, or both. To further explore these possibilities, Y2H experiments, far westerns, or ssDNA curtains employing SSB in place of RPA could be used to test for interaction between Srs2 and RPA. Additionally, electro-mobility shift assays (EMSA) testing the binding preference for Srs2$^{898}$ and Srs2$^{860}$ for various DNA structures, including flaps, overhangs, and hairpins, could indicate whether these residues are involved in loading Srs2 to various nucleic acid substrates.

In summary, the findings presented here suggest that Srs2 may preferentially associates with RPA clusters between Rad51 filaments. Furthermore, Srs2 also preferentially initiates Rad51 clearance from the location of a paired 15bp D-loop intermediate, representing a different structure Srs2 is likely recruited to (Figure 4-8). Given that Srs2 translocates in the 3′→5′ direction, and the Rad51$^{Y388H}$ and

Rad51$^{G393D}$ mutants are impaired for their interaction with Srs2, we propose that the access of Srs2 is restricted to the 3′ end of the Rad51 filament. Within this context, the purported negative regulators of Srs2 anti-recombinase activity, which include the Rad55-Rad57 heterodimer, the SHU complex, and Rad52, may act by limiting access of the 3′ end of the Rad51 presynaptic complex.

### 5.3 ROLE OF TANDEM SRS2 ASSEMBLIES IN PROCESSIVE TRANSLOCATION

The functional oligomeric states of DNA helicases have proven remarkably difficult to determine[185]. In many cases, there is evidence that helicases can behave as tandem assemblies while acting upon nucleic acids, and that the changes in their oligomeric state regulate their activities[185]. Specific examples of tandem helicase assemblies include the bacteriophage T4 SF1 helicase DdaA[186], the hepatitis C virus SF2 helicase NS3[187], and *E. coli* RecQ[188]. In addition, recent studies have shown that *E. coli* UvrD translocates either as a monomer or as two tandem monomers, and that the tandem monomers are more processive than a single monomer[147,189]. Similarly, recent biochemical results have suggested that more than one Srs2 monomer is required for efficient DNA unwinding[190].

Our work now demonstrates that processive disruption of Rad51 filaments involves multiple Srs2 molecules acting upon the same filament end. This conclusion is also consistent with electron microscopy images of Srs2 on Rad51-ssDNA, which revealed Srs2 species that are oligomeric in appearance[178]. We propose that Srs2-dependent removal of Rad51 from the ssDNA lead to new tracts of RPA-ssDNA or near naked ssDNA, which can then function as loading sites for additional Srs2 molecules (Figure 5-2A,B). Separate measurements presented in chapter 3 indicate that Srs2 translocates on RPA-ssDNA at a rate that is ~20% faster than that on Rad51-ssDNA and travels even faster on naked ssDNA[181]. The ability of Srs2 to translocate more rapidly on RPA-ssDNA would allow any newly loaded Srs2 molecules to quickly catch up to and merge with the leading Srs2 ensemble already present at the receding 3′ edge of the Rad51 filament. It should be noted that although our work shows that tandem assemblies of Srs2 are involved in processive disruption of Rad51 filaments *in vitro*, we do not know the oligomeric state of Srs2 *in vivo*. The observation that fluorescent Srs2 foci are observed in SC experiments indicates Srs2 may be in high enough concentration to build such arrays of Srs2 at sites of DSBs *in vivo*. Similarly, the

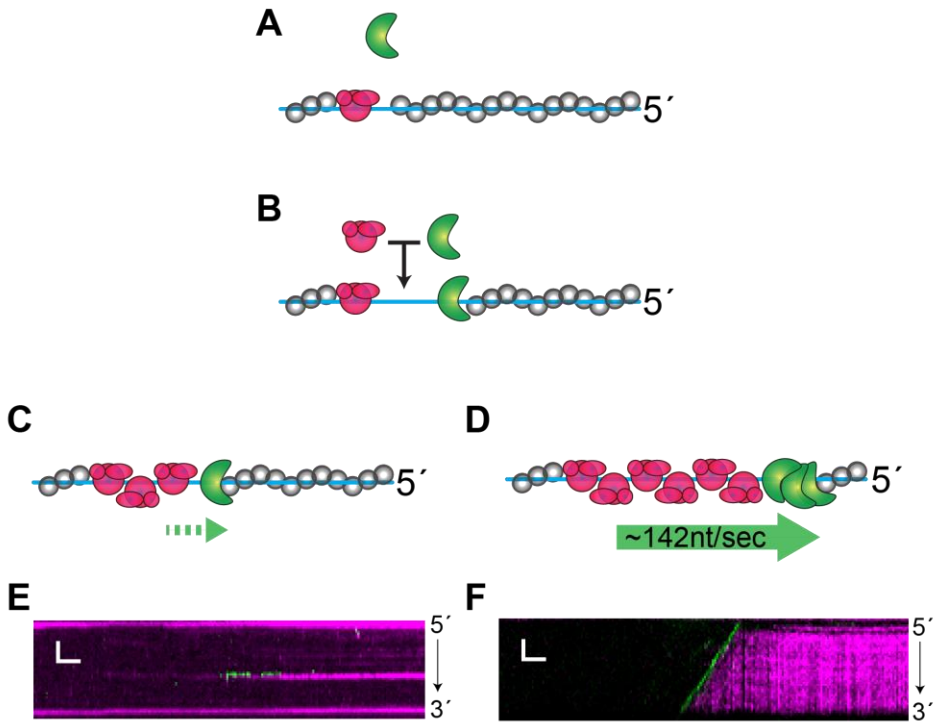


**Figure 5-2. Models for the recruitment and formation of tandem Srs2 ensembles.** (A) Initial recruitment of Srs2 occurs at locations of persistent RPA after Rad51 exchange. (B) The initial translocation of monomeric Srs2 clears a small portion of ssDNA behind it that can recruit additional monomers. (C,E) At low concentrations of Srs2 (10pM in E), translocation is slow and prone to stalling after short distances below the resolution of our system. (D,F) Higher concentrations of Srs2 (100 pM in F) enable the formation of multi-protein "arrays" and impart significantly increased velocity and processiviity rates. See also Figure 4-4A.

oligomeric state of Srs2 when tethered to a PCNA is unknown and may modulate the response of a replisome to certain replication stressors.

Srs2 translocation has been examined by bulk biochemical and single molecule FRET assays[65,149]. Results from these studies have suggested that Srs2 remains monomeric while acting on its substrates, translocating at ~300 nt/sec over an estimated distance of ~1,500 nucleotides on naked ssDNA, and removing Rad51 at a rate of ~12 monomers per second, corresponding to ~36 nt/sec[65]. In contrast, our results suggest that arrays of Srs2 can translocate over remarkably long distances (~18,000 nt) on Rad51-ssDNA while traveling at an apparent velocity of ~140 nt/sec, corresponding to the disruption of ~6,000 Rad51 monomers at a rate of ~50 monomers per second. We attribute the differences between our findings and the published results to the use of much longer ssDNA substrates and the inclusion of free RPA in our study, thus enhancing assembly of the tandem Srs2 ensembles that possess greater processivity and velocity.

### 5.4 SRS2 TRANSLOCATION ON RPA-COATED SSDNA

For the first time, we have directly observed rapid Srs2 translocation on ssDNA that is saturated with RPA and can travel over distances spanning thousands of nucleotides, giving no indication that RPA offers a serious impediment despite it's extremely high affinity for ssDNA[170,172]. Assuming that RPA has a maximum binding site size of ~30 nucleotides under the buffer conditions used for our measurements[193], and that the ssDNA was saturated with RPA, then an apparent translocation rate of ~170 nt/sec and processivity of ~15,000 nt would correspond to the removal of ~6 molecules of RPA per second and ~500 molecules of RPA removed from the ssDNA per Srs2 translocation event.

Recent studies have shown that *S. cerevisiae* Pif1, and the *E. coli* UvrD and Rep helicases can push isolated *E. coli* SSB tetramers along ssDNA[150]. However, it remained unclear how helicases might behave when the ssDNA is fully coated by single strand binding proteins. Our results point to an alternative scenario for Srs2 acting on ssDNA substrates densely populated by RPA, namely, highly efficient eviction of RPA from the ssDNA. Interestingly, RPA-ssDNA complexes act as conserved signal to help trigger the DNA damage checkpoint by activating the ATR (ataxia telangiectasia mutated- and Rad3-related; Mec1 in *S. cerevisiae*)-ATRIP (ATR-interacting protein; Ddc2 in *S. cerevisiae*) protein kinase complex[17]. However, *srs2*Δ strains fail to recover from the DNA damage checkpoint-mediated growth arrest even after DNA repair has taken place, and these recovery defects are alleviated by *mec1*Δ[131]. Consistent with our findings, one possible explanation for these genetic results is that checkpoint recovery requires a clean-up process involving Srs2-mediated removal of persistent RPA from repaired intermediates.

### 5.5 SRS2 DISRUPTION OF RAD52-CONTAINING RECOMBINATION INTERMEDIATES

Although the best characterized role of Srs2 is to dismantle recombination intermediates containing Rad51, we have little understanding of how this activity is regulated. The clearest evidence for Srs2 regulatory control have come from experiments showing that the Rad55-Rad57 heterodimer may inhibit Rad51 filament disruption by limiting Srs2 translocation. However, the authors also noted that

Rad55-Rad57 does not impair Srs2 ATPase activity in bulk. Similarly, while Rad52 is a proposed negative regulator of Srs2 anti-recombinase activity, we found Srs2 ATPase activity was largely unperturbed using various combinations of RPA, Rad52, and Rad51 (Figure 2-7).

Preliminary SM experiments challenging mixed GFP-Rad52/Rad51 filaments show results that are difficult to interpret and thus were not published. Srs2 appears to be able to bypass Rad52 on Rad51-ssDNA, although this requires some molecular gymnastics whereby Rad52 generally appeared dynamic upon bypass. It could be that Srs2 is capable of dismantling Rad52, while the multiple RPA, Rad51 and DNA binding sites present on Rad52 allow it to quickly rebind after passage of an Srs2. Future studies will be necessary to explore the impact of Rad51 mediators on Srs2 translocation. However, our results argue against a direct action of Rad52 as an antagonist of Srs2 binding or translocation on RPA-ssDNA filaments. Instead, our findings suggest that, by releasing Rad52 from ssDNA, Srs2 helps redirect Rad52-dependent Rad51 presynaptic filament assembly to alternative locations[128].

Chapter 1 detailed the mechanisms of SSA as an alternative NHEJ pathway that is reliant upon both RPA and Rad52. The finding that Srs2 removes Rad52 from RPA-ssDNA suggests the possibility that Srs2 could antagonize this error-prone pathway. In contrast to this idea, *srs2* deletion resulted in a decrease of SSA[194]. The double *rad51* mutation suppressed the decreased frequency of SSA in the *srs2* mutant, indicating that while Srs2 might inhibit both HR and SSA, the kinetics of building Rad51 filaments in *srs2* deletion outpaces those of SSA by Rad52.

### 5.6 SRS2 IS DIRECTLY RECRUITED TO HETERODUPLEX DNA JOINTS

Genetic and biochemical studies have implicated Srs2 in disrupting strand invasion intermediates such as D-loops and extended D-loops[27,130,191]. The ability of Srs2 to disrupt these structures is thought to play two important roles during homologous recombination. First, Srs2 dismantles inappropriate intermediates, some proportion of which may be comprised of D-loops. Second, Srs2-mediated heteroduplex DNA disruption promotes synthesis-dependent strand annealing (SDSA), and in doing so suppresses the formation of crossover recombination products, which is important to prevent loss of heterozygosity and chromosomal rearrangements. These studies raise the question of how Srs2 is

targeted to strand invasion intermediates. Our findings show that Srs2 can engage dsDNA paired with the Rad51-ssDNA presynaptic complex by either translocating along the Rad51-ssDNA until encountering the DNA joint, or by binding to the heteroduplex DNA joint directly. Indeed, our finding that over half of all observed Srs2 recruitment at sites of Rad51-filament bound dsDNA is especially notable given that there were only ~3-5 dsDNA fragments bound per ~35,000 nt of presynaptic ssDNA, and would correspond to ≤2% of the total available DNA present[66,73]. These considerations highlight the strong enrichment for Srs2 binding interactions with the bound dsDNA molecules compared to the remaining portions of the presynaptic complex and support a model in which Srs2 is directly recruited to Rad51-generated heteroduplex DNA joints.

It should be noted that the DNA structures created by our SM experiments do not contain a 3′-ssDNA end that is invading a dsDNA template as would be expected for a properly paired D-loop. Instead, the structures we generate are likely to be recognized as improperly paired intermediates. While fully homologous 70mer dsDNAs would also not represent a proper D-loop, measuring Srs2 activity on these structures would add to our knowledge of how Srs2 potentially mediates HR (Figure 5-1B).

### 5.7 CONCLUDING REMARKS

Here, we have established methods for examining anti-recombinases in real time as they act on long ssDNA substrates mimicking early homologous recombination intermediates, and these experiments have provided insights into the action of Srs2 on HR intermediates. Other helicases, such as yeast Mph1 and mammalian FBH1, RECQ5, and RTEL1, have been implicated in the regulation of homologous recombination either via disruption of the Rad51 presynaptic filament or strand invasion intermediates[175,176,195]. Preliminary experiments with RECQ5 on HsRAD51 filaments indicate this helicase functions similar to Srs2 in presynaptic filament disruption and underscore the general utility of the assay to study helicase-mediated regulation of HR (Figure 5-3).

However, we have only a rudimentary understanding of how Srs2 and other regulators of homologous recombination act to prevent the formation of aberrant recombination intermediates. Moreover, Rad52, Rad55-Rad57, and the SHU complex, have all been implicated in the negative

regulation of Srs2 activity[87,92,128]. Future studies using our single molecule assays will likely shed light on the mechanisms of anti-recombinases and how the activities of these DNA motor proteins are regulated by the aforementioned factors and their orthologs in other eukaryotes.

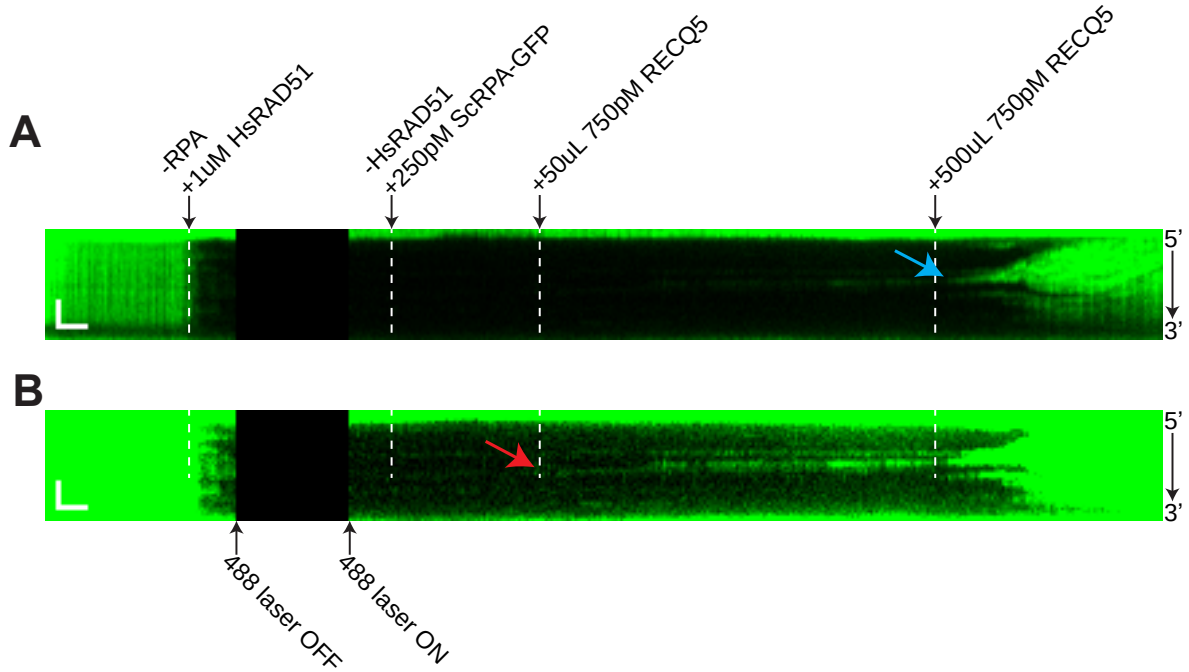


**Figure 5-3. RECQ5 antagonizes HsRAD51 filaments.** Panels (A) and (B) are the same kymogram. (B) has a higher saturation to show mild GFP increase with the first, 50ul injection of RECQ5 (red arrow). The second injection of RECQ5 was the same concentration, but 500ul were delivered. The second injection begins (blue arrow) a highly processive Rad51 antagonism event in the anticipated 3' to 5' direction, clearing HsRAD51 from the filament and allowing RPA-GFP to rebind the ssDNA.These results demonstrate RECQ5 has very similar activity to Srs2 clearance of ScRad51 filaments. White scale bars = 3 micron x 1 minute.

## REFERENCES


1 Holliday, R. A mechanism for gene conversion in fungi (Reprinted). *Genet Res* **89**, 285-307, doi:10.1017/S0016672308009476 (2007).

2 Meselson, M. S. & Radding, C. M. A general model for genetic recombination. *Proc Natl Acad Sci U S A* **72**, 358-361 (1975).

3 Szostak, J. W., Orr-Weaver, T. L., Rothstein, R. J. & Stahl, F. W. The double-strand-break repair model for recombination. *Cell* **33**, 25-35 (1983).

4 Aboussekhra, A., Chanet, R., Adjiri, A. & Fabre, F. Semidominant suppressors of Srs2 helicase mutations of Saccharomyces cerevisiae map in the RAD51 gene, whose sequence predicts a protein with similarities to procaryotic RecA proteins. *Mol Cell Biol* **12**, 3224-3234 (1992).

5 Chapman, J. R., Taylor, M. R. & Boulton, S. J. Playing the end game: DNA double-strand break repair pathway choice. *Mol Cell* **47**, 497-510, doi:10.1016/j.molcel.2012.07.029 (2012).

6 Jackson, S. P. & Bartek, J. The DNA-damage response in human biology and disease. *Nature* **461**, 1071-1078, doi:10.1038/nature08467 (2009).

7 McKinnon, P. J. DNA repair deficiency and neurological disease. *Nat Rev Neurosci* **10**, 100-112, doi:10.1038/nrn2559 (2009).

8 Mazouzi, A., Velimezi, G. & Loizou, J. I. DNA replication stress: causes, resolution and disease. *Exp Cell Res* **329**, 85-93, doi:10.1016/j.yexcr.2014.09.030 (2014).

9 Sfeir, A. & Symington, L. S. Microhomology-Mediated End Joining: A Back-up Survival Mechanism or Dedicated Pathway? *Trends Biochem Sci* **40**, 701-714, doi:10.1016/j.tibs.2015.08.006 (2015).

10 Chiruvella, K. K., Liang, Z. & Wilson, T. E. Repair of double-strand breaks by end joining. *Cold Spring Harb Perspect Biol* **5**, a012757, doi:10.1101/cshperspect.a012757 (2013).

11 Lengsfeld, B. M., Rattray, A. J., Bhaskara, V., Ghirlando, R. & Paull, T. T. Sae2 is an endonuclease that processes hairpin DNA cooperatively with the Mre11/Rad50/Xrs2 complex. *Mol Cell* **28**, 638-651, doi:10.1016/j.molcel.2007.11.001 (2007).

12 Cannavo, E. & Cejka, P. Sae2 promotes dsDNA endonuclease activity within Mre11-Rad50-Xrs2 to resect DNA breaks. *Nature* **514**, 122-125, doi:10.1038/nature13771 (2014).

13 Zhu, Z., Chung, W. H., Shim, E. Y., Lee, S. E. & Ira, G. Sgs1 helicase and two nucleases Dna2 and Exo1 resect DNA double-strand break ends. *Cell* **134**, 981-994, doi:10.1016/j.cell.2008.08.037 (2008).

14 Symington, L. S. & Gautier, J. Double-strand break end resection and repair pathway choice. *Annu Rev Genet* **45**, 247-271, doi:10.1146/annurev-genet-110410-132435 (2011).

15 Paciotti, V., Clerici, M., Lucchini, G. & Longhese, M. P. The checkpoint protein Ddc2, functionally related to S. pombe Rad26, interacts with Mec1 and is regulated by Mec1-dependent phosphorylation in budding yeast. *Genes Dev* **14**, 2046-2059 (2000).

16 Refolio, E., Cavero, S., Marcon, E., Freire, R. & San-Segundo, P. A. The Ddc2/ATRIP checkpoint protein monitors meiotic recombination intermediates. *J Cell Sci* **124**, 2488-2500, doi:10.1242/jcs.081711 (2011).

17 Zou, L. & Elledge, S. J. Sensing DNA damage through ATRIP recognition of RPA-ssDNA complexes. *Science* **300**, 1542-1548, doi:10.1126/science.1083430 (2003).

18 Sweeney, F. D. *et al.* Saccharomyces cerevisiae Rad9 acts as a Mec1 adaptor to allow Rad53 activation. *Curr Biol* **15**, 1364-1375, doi:10.1016/j.cub.2005.06.063 (2005).
19 Symington, L. S., Rothstein, R. & Lisby, M. Mechanisms and regulation of mitotic recombination in Saccharomyces cerevisiae. *Genetics* **198**, 795-835, doi:10.1534/genetics.114.166140 (2014).
20 Sebesta, M. *et al.* Role of PCNA and TLS polymerases in D-loop extension during homologous recombination in humans. *DNA Repair (Amst)* **12**, 691-698, doi:10.1016/j.dnarep.2013.05.001 (2013).
21 Heyer, W. D., Li, X., Rolfsmeier, M. & Zhang, X. P. Rad54: the Swiss Army knife of homologous recombination? *Nucleic Acids Res* **34**, 4115-4125, doi:10.1093/nar/gkl481 (2006).
22 McVey, M., Khodaverdian, V. Y., Meyer, D., Cerqueira, P. G. & Heyer, W. D. Eukaryotic DNA Polymerases in Homologous Recombination. *Annu Rev Genet* **50**, 393-421, doi:10.1146/annurev-genet-120215-035243 (2016).
23 Sakofsky, C. J., Ayyar, S. & Malkova, A. Break-induced replication and genome stability. *Biomolecules* **2**, 483-504, doi:10.3390/biom2040483 (2012).
24 Malkova, A., Ivanov, E. L. & Haber, J. E. Double-strand break repair in the absence of RAD51 in yeast: a possible role for break-induced DNA replication. *Proc Natl Acad Sci U S A* **93**, 7131-7136 (1996).
25 Dilley, R. L. *et al.* Break-induced telomere synthesis underlies alternative telomere maintenance. *Nature* **539**, 54-58, doi:10.1038/nature20099 (2016).
26 McEachern, M. J. & Haber, J. E. Break-induced replication and recombinational telomere elongation in yeast. *Annual review of biochemistry* **75**, 111-135, doi:10.1146/annurev.biochem.74.082803.133234 (2006).
27 Liu, J. *et al.* Srs2 promotes synthesis-dependent strand annealing by disrupting DNA polymerase delta-extending D-loops. *Elife* **6**, doi:10.7554/eLife.22195 (2017).
28 Branzei, D. & Foiani, M. Regulation of DNA repair throughout the cell cycle. *Nature reviews. Molecular cell biology* **9**, 297-308, doi:10.1038/nrm2351 (2008).
29 Prakash, S., Johnson, R. E. & Prakash, L. Eukaryotic translesion synthesis DNA polymerases: specificity of structure and function. *Annual review of biochemistry* **74**, 317-353, doi:10.1146/annurev.biochem.74.082803.133250 (2005).
30 Vujanovic, M. *et al.* Replication Fork Slowing and Reversal upon DNA Damage Require PCNA Polyubiquitination and ZRANB3 DNA Translocase Activity. *Mol Cell* **67**, 882-890 e885, doi:10.1016/j.molcel.2017.08.010 (2017).
31 Xue, X. *et al.* Restriction of replication fork regression activities by a conserved SMC complex. *Mol Cell* **56**, 436-445, doi:10.1016/j.molcel.2014.09.013 (2014).
32 Muller, H. J. The Relation of Recombination to Mutational Advance. *Mutat Res* **106**, 2-9 (1964).
33 Soucy, S. M., Huang, J. & Gogarten, J. P. Horizontal gene transfer: building the web of life. *Nat Rev Genet* **16**, 472-482, doi:10.1038/nrg3962 (2015).
34 Hunter, N. Meiotic Recombination: The Essence of Heredity. *Cold Spring Harb Perspect Biol* **7**, doi:10.1101/cshperspect.a016618 (2015).
35 Sun, H., Treco, D., Schultes, N. P. & Szostak, J. W. Double-strand breaks at an initiation site for meiotic gene conversion. *Nature* **338**, 87-90, doi:10.1038/338087a0 (1989).

36 Schultes, N. P. & Szostak, J. W. Decreasing gradients of gene conversion on both sides of the initiation site for meiotic recombination at the ARG4 locus in yeast. *Genetics* **126**, 813-822 (1990).
37 Bergerat, A. *et al.* An atypical topoisomerase II from Archaea with implications for meiotic recombination. *Nature* **386**, 414-417, doi:10.1038/386414a0 (1997).
38 Keeney, S., Giroux, C. N. & Kleckner, N. Meiosis-specific DNA double-strand breaks are catalyzed by Spo11, a member of a widely conserved protein family. *Cell* **88**, 375-384 (1997).
39 Cloud, V., Chan, Y. L., Grubb, J., Budke, B. & Bishop, D. K. Rad51 is an accessory factor for Dmc1-mediated joint molecule formation during meiosis. *Science* **337**, 1222-1225, doi:10.1126/science.1219379 (2012).
40 Bishop, D. K. Rad51, the lead in mitotic recombinational DNA repair, plays a supporting role in budding yeast meiosis. *Cell cycle (Georgetown, Tex.)* **11**, 4105-4106, doi:10.4161/cc.22396 (2012).
41 Bishop, D. K., Park, D., Xu, L. & Kleckner, N. DMC1: a meiosis-specific yeast homolog of E. coli recA required for recombination, synaptonemal complex formation, and cell cycle progression. *Cell* **69**, 439-456 (1992).
42 Schwacha, A. & Kleckner, N. Interhomolog bias during meiotic recombination: meiotic functions promote a highly differentiated interhomolog-only pathway. *Cell* **90**, 1123-1135 (1997).
43 Lisby, M., Barlow, J. H., Burgess, R. C. & Rothstein, R. Choreography of the DNA damage response: spatiotemporal relationships among checkpoint and repair proteins. *Cell* **118**, 699-713, doi:10.1016/j.cell.2004.08.015 (2004).
44 Fan, J. & Pavletich, N. P. Structure and conformational change of a replication protein A heterotrimer bound to ssDNA. *Genes Dev* **26**, 2337-2347, doi:10.1101/gad.194787.112 (2012).
45 Kim, C., Paulus, B. F. & Wold, M. S. Interactions of human replication protein A with oligonucleotides. *Biochemistry* **33**, 14197-14206 (1994).
46 Fanning, E., Klimovich, V. & Nager, A. R. A dynamic model for replication protein A (RPA) function in DNA processing pathways. *Nucleic Acids Res* **34**, 4126-4137, doi:10.1093/nar/gkl550 (2006).
47 Binz, S. K., Sheehan, A. M. & Wold, M. S. Replication protein A phosphorylation and the cellular response to DNA damage. *DNA Repair (Amst)* **3**, 1015-1024, doi:10.1016/j.dnarep.2004.03.028 (2004).
48 Game, J. C. & Mortimer, R. K. A genetic study of x-ray sensitive mutants in yeast. *Mutat Res* **24**, 281-292 (1974).
49 Baumann, P., Benson, F. E. & West, S. C. Human Rad51 protein promotes ATP-dependent homologous pairing and strand transfer reactions in vitro. *Cell* **87**, 757-766 (1996).
50 Tsuzuki, T. *et al.* Targeted disruption of the Rad51 gene leads to lethality in embryonic mice. *Proc Natl Acad Sci U S A* **93**, 6236-6240 (1996).
51 Sonoda, E. *et al.* Rad51-deficient vertebrate cells accumulate chromosomal breaks prior to cell death. *EMBO J* **17**, 598-608, doi:10.1093/emboj/17.2.598 (1998).
52 Muller, B., Koller, T. & Stasiak, A. Characterization of the DNA binding activity of stable RecA-DNA complexes. Interaction between the two DNA binding sites within

RecA helical filaments. *J Mol Biol* **212**, 97-112, doi:10.1016/0022-2836(90)90307-8 (1990).
53 Prevost, C. & Takahashi, M. Geometry of the DNA strands within the RecA nucleofilament: role in homologous recombination. *Q Rev Biophys* **36**, 429-453 (2003).
54 Tombline, G. & Fishel, R. Biochemical characterization of the human RAD51 protein. I. ATP hydrolysis. *J Biol Chem* **277**, 14417-14425, doi:10.1074/jbc.M109915200 (2002).
55 Yu, X., Jacobs, S. A., West, S. C., Ogawa, T. & Egelman, E. H. Domain structure and dynamics in the helical filaments formed by RecA and Rad51 on DNA. *Proc Natl Acad Sci U S A* **98**, 8419-8424, doi:10.1073/pnas.111005398 (2001).
56 Story, R. M., Weber, I. T. & Steitz, T. A. The structure of the E. coli recA protein monomer and polymer. *Nature* **355**, 318-325, doi:10.1038/355318a0 (1992).
57 Conway, A. B. *et al.* Crystal structure of a Rad51 filament. *Nat Struct Mol Biol* **11**, 791-796, doi:10.1038/nsmb795 (2004).
58 Chabbert, M., Cazenave, C. & Helene, C. Kinetic studies of recA protein binding to a fluorescent single-stranded polynucleotide. *Biochemistry* **26**, 2218-2225 (1987).
59 Ma, C. J., Gibb, B., Kwon, Y., Sung, P. & Greene, E. C. Protein dynamics of human RPA and RAD51 on ssDNA during assembly and disassembly of the RAD51 filament. *Nucleic Acids Res* **45**, 749-761, doi:10.1093/nar/gkw1125 (2017).
60 Ma, C. J., Kwon, Y., Sung, P. & Greene, E. C. Human RAD52 interactions with replication protein A and the RAD51 presynaptic complex. *J Biol Chem* **292**, 11702-11713, doi:10.1074/jbc.M117.794545 (2017).
61 Short, J. M. *et al.* High-resolution structure of the presynaptic RAD51 filament on single-stranded DNA by electron cryo-microscopy. *Nucleic Acids Res* **44**, 9017-9030, doi:10.1093/nar/gkw783 (2016).
62 Chen, Z., Yang, H. & Pavletich, N. P. Mechanism of homologous recombination from the RecA-ssDNA/dsDNA structures. *Nature* **453**, 489-484, doi:10.1038/nature06971 (2008).
63 Shinohara, A., Ogawa, H. & Ogawa, T. Rad51 protein involved in repair and recombination in S. cerevisiae is a RecA-like protein. *Cell* **69**, 457-470 (1992).
64 Sung, P. Catalysis of ATP-dependent homologous DNA pairing and strand exchange by yeast RAD51 protein. *Science* **265**, 1241-1243 (1994).
65 Antony, E. *et al.* Srs2 disassembles Rad51 filaments by a protein-protein interaction triggering ATP turnover and dissociation of Rad51 from DNA. *Mol Cell* **35**, 105-115, doi:10.1016/j.molcel.2009.05.026 (2009).
66 Lee, J. Y. *et al.* DNA RECOMBINATION. Base triplet stepping by the Rad51/RecA family of recombinases. *Science* **349**, 977-981, doi:10.1126/science.aab2666 (2015).
67 Fung, C. W., Fortin, G. S., Peterson, S. E. & Symington, L. S. The rad51-K191R ATPase-defective mutant is impaired for presynaptic filament formation. *Molecular and cellular biology* **26**, 9544-9554, doi:10.1128/mcb.00599-06 (2006).
68 Sung, P. & Stratton, S. A. Yeast Rad51 recombinase mediates polar DNA strand exchange in the absence of ATP hydrolysis. *The Journal of biological chemistry* **271**, 27983-27986 (1996).
69 Morrison, C. *et al.* The essential functions of human Rad51 are independent of ATP hydrolysis. *Molecular and cellular biology* **19**, 6891-6897 (1999).
70 van Mameren, J. *et al.* Counting RAD51 proteins disassembling from nucleoprotein filaments under tension. *Nature* **457**, 745-748, doi:10.1038/nature07581 (2009).

71 Amunugama, R. *et al.* RAD51 protein ATP cap regulates nucleoprotein filament stability. *J Biol Chem* **287**, 8724-8736, doi:10.1074/jbc.M111.239426 (2012).
72 Yoshioka, K., Yumoto-Yoshioka, Y., Fleury, F. & Takahashi, M. pH- and salt-dependent self-assembly of human Rad51 protein analyzed as fluorescence resonance energy transfer between labeled proteins. *J Biochem* **133**, 593-597 (2003).
73 Qi, Z. *et al.* DNA sequence alignment by microhomology sampling during homologous recombination. *Cell* **160**, 856-869, doi:10.1016/j.cell.2015.01.029 (2015).
74 Bugreev, D. V. & Mazin, A. V. Ca2+ activates human homologous recombination protein Rad51 by modulating its ATPase activity. *Proc Natl Acad Sci U S A* **101**, 9988-9993, doi:10.1073/pnas.0402105101 (2004).
75 Fortin, G. S. & Symington, L. S. Mutations in yeast Rad51 that partially bypass the requirement for Rad55 and Rad57 in DNA repair by increasing the stability of Rad51-DNA complexes. *EMBO J* **21**, 3160-3170, doi:10.1093/emboj/cdf293 (2002).
76 Gaines, W. A. *et al.* Promotion of presynaptic filament assembly by the ensemble of S. cerevisiae Rad51 paralogues with Rad52. *Nat Commun* **6**, 7834, doi:10.1038/ncomms8834 (2015).
77 Krejci, L., Damborsky, J., Thomsen, B., Duno, M. & Bendixen, C. Molecular dissection of interactions between Rad51 and members of the recombination-repair group. *Mol Cell Biol* **21**, 966-976, doi:10.1128/MCB.21.3.966-976.2001 (2001).
78 Shinohara, A., Shinohara, M., Ohta, T., Matsuda, S. & Ogawa, T. Rad52 forms ring structures and co-operates with RPA in single-strand DNA annealing. *Genes Cells* **3**, 145-156 (1998).
79 Sung, P. Function of yeast Rad52 protein as a mediator between replication protein A and the Rad51 recombinase. *J Biol Chem* **272**, 28194-28197 (1997).
80 Mortensen, U. H., Bendixen, C., Sunjevaric, I. & Rothstein, R. DNA strand annealing is promoted by the yeast Rad52 protein. *Proc Natl Acad Sci U S A* **93**, 10729-10734 (1996).
81 Hays, S. L., Firmenich, A. A., Massey, P., Banerjee, R. & Berg, P. Studies of the interaction between Rad52 protein and the yeast single-stranded DNA binding protein RPA. *Mol Cell Biol* **18**, 4400-4406 (1998).
82 Fujimori, A. *et al.* Rad52 partially substitutes for the Rad51 paralog XRCC3 in maintaining chromosomal integrity in vertebrate cells. *EMBO J* **20**, 5513-5520, doi:10.1093/emboj/20.19.5513 (2001).
83 Feng, Z. *et al.* Rad52 inactivation is synthetically lethal with BRCA2 deficiency. *Proc Natl Acad Sci U S A* **108**, 686-691, doi:10.1073/pnas.1010959107 (2011).
84 Lok, B. H., Carley, A. C., Tchang, B. & Powell, S. N. RAD52 inactivation is synthetically lethal with deficiencies in BRCA1 and PALB2 in addition to BRCA2 through RAD51-mediated homologous recombination. *Oncogene* **32**, 3552-3558, doi:10.1038/onc.2012.391 (2013).
85 Mavaddat, N. *et al.* Cancer risks for BRCA1 and BRCA2 mutation carriers: results from prospective analysis of EMBRACE. *J Natl Cancer Inst* **105**, 812-822, doi:10.1093/jnci/djt095 (2013).
86 Sung, P. Yeast Rad55 and Rad57 proteins form a heterodimer that functions with replication protein A to promote DNA strand exchange by Rad51 recombinase. *Genes Dev* **11**, 1111-1121 (1997).

87 Bernstein, K. A. *et al.* The Shu complex, which contains Rad51 paralogues, promotes DNA repair through inhibition of the Srs2 anti-recombinase. *Mol Biol Cell* **22**, 1599-1607, doi:10.1091/mbc.E10-08-0691 (2011).
88 Albala, J. S. *et al.* Identification of a novel human RAD51 homolog, RAD51B. *Genomics* **46**, 476-479, doi:10.1006/geno.1997.5062 (1997).
89 Cartwright, R., Tambini, C. E., Simpson, P. J. & Thacker, J. The XRCC2 DNA repair gene from human and mouse encodes a novel member of the recA/RAD51 family. *Nucleic Acids Res* **26**, 3084-3089 (1998).
90 Takata, M. *et al.* Chromosome instability and defective recombinational repair in knockout mutants of the five Rad51 paralogs. *Mol Cell Biol* **21**, 2858-2866, doi:10.1128/MCB.21.8.2858-2866.2001 (2001).
91 Johnson, R. D. & Symington, L. S. Functional differences and interactions among the putative RecA homologs Rad51, Rad55, and Rad57. *Mol Cell Biol* **15**, 4843-4850 (1995).
92 Liu, J. *et al.* Rad51 paralogues Rad55-Rad57 balance the antirecombinase Srs2 in Rad51 filament formation. *Nature* **479**, 245-248, doi:10.1038/nature10522 (2011).
93 Shor, E., Weinstein, J. & Rothstein, R. A genetic screen for top3 suppressors in Saccharomyces cerevisiae identifies SHU1, SHU2, PSY3 and CSM2: four genes involved in error-free DNA repair. *Genetics* **169**, 1275-1289, doi:10.1534/genetics.104.036764 (2005).
94 Tao, Y. *et al.* Structural analysis of Shu proteins reveals a DNA binding role essential for resisting damage. *J Biol Chem* **287**, 20231-20239, doi:10.1074/jbc.M111.334698 (2012).
95 Godin, S. *et al.* The Shu complex interacts with Rad51 through the Rad51 paralogues Rad55-Rad57 to mediate error-free recombination. *Nucleic Acids Res* **41**, 4525-4534, doi:10.1093/nar/gkt138 (2013).
96 Zhang, S. *et al.* Structural basis for the functional role of the Shu complex in homologous recombination. *Nucleic Acids Res*, doi:10.1093/nar/gkx992 (2017).
97 Wright, W. D. & Heyer, W. D. Rad54 functions as a heteroduplex DNA pump modulated by its DNA substrates and Rad51 during D loop formation. *Mol Cell* **53**, 420-432, doi:10.1016/j.molcel.2013.12.027 (2014).
98 Li, X. & Heyer, W. D. RAD54 controls access to the invading 3'-OH end after RAD51-mediated DNA strand invasion in homologous recombination in Saccharomyces cerevisiae. *Nucleic Acids Res* **37**, 638-646, doi:10.1093/nar/gkn980 (2009).
99 Kiianitsa, K., Solinger, J. A. & Heyer, W. D. Rad54 protein exerts diverse modes of ATPase activity on duplex DNA partially and fully covered with Rad51 protein. *J Biol Chem* **277**, 46205-46215, doi:10.1074/jbc.M207967200 (2002).
100 Wu, L. & Hickson, I. D. DNA helicases required for homologous recombination and repair of damaged replication forks. *Annu Rev Genet* **40**, 279-306, doi:10.1146/annurev.genet.40.110405.090636 (2006).
101 McGlynn, P. & Lloyd, R. G. Recombinational repair and restart of damaged replication forks. *Nature reviews. Molecular cell biology* **3**, 859-870, doi:10.1038/nrm951 (2002).
102 Michel, B., Grompone, G., Flores, M. J. & Bidnenko, V. Multiple pathways process stalled replication forks. *Proc Natl Acad Sci U S A* **101**, 12783-12788, doi:10.1073/pnas.0401586101 (2004).
103 Mankouri, H. W., Craig, T. J. & Morgan, A. SGS1 is a multicopy suppressor of srs2: functional overlap between DNA helicases. *Nucleic Acids Res* **30**, 1103-1113 (2002).

104 Panico, E. R., Ede, C., Schildmann, M., Schurer, K. A. & Kramer, W. Genetic evidence for a role of Saccharomyces cerevisiae Mph1 in recombinational DNA repair under replicative stress. *Yeast* **27**, 11-27, doi:10.1002/yea.1727 (2010).
105 Bernstein, K. A., Gangloff, S. & Rothstein, R. The RecQ DNA helicases in DNA repair. *Annu Rev Genet* **44**, 393-417, doi:10.1146/annurev-genet-102209-163602 (2010).
106 Watt, P. M., Louis, E. J., Borts, R. H. & Hickson, I. D. Sgs1: a eukaryotic homolog of E. coli RecQ that interacts with topoisomerase II in vivo and is required for faithful chromosome segregation. *Cell* **81**, 253-260 (1995).
107 Prakash, R. *et al.* Yeast Mph1 helicase dissociates Rad51-made D-loops: implications for crossover control in mitotic recombination. *Genes Dev* **23**, 67-79, doi:10.1101/gad.1737809 (2009).
108 Fairman-Williams, M. E., Guenther, U. P. & Jankowsky, E. SF1 and SF2 helicases: family matters. *Curr Opin Struc Biol* **20**, 313-324, doi:10.1016/j.sbi.2010.03.011 (2010).
109 Stelter, M., Acajjaoui, S., McSweeney, S. & Timmins, J. Structural and mechanistic insight into DNA unwinding by Deinococcus radiodurans UvrD. *PLoS One* **8**, e77364, doi:10.1371/journal.pone.0077364 (2013).
110 Tomko, E. J. *et al.* 5'-Single-stranded/duplex DNA junctions are loading sites for E. coli UvrD translocase. *EMBO J* **29**, 3826-3839, doi:10.1038/emboj.2010.242 (2010).
111 Lee, J. Y. & Yang, W. UvrD helicase unwinds DNA one base pair at a time by a two-part power stroke. *Cell* **127**, 1349-1360, doi:10.1016/j.cell.2006.10.049 (2006).
112 Jia, H. *et al.* Rotations of the 2B sub-domain of E. coli UvrD helicase/translocase coupled to nucleotide and DNA binding. *J Mol Biol* **411**, 633-648, doi:10.1016/j.jmb.2011.06.019 (2011).
113 Cheng, W. *et al.* The 2B domain of the Escherichia coli Rep protein is not required for DNA helicase activity. *Proc Natl Acad Sci U S A* **99**, 16006-16011, doi:10.1073/pnas.242479399 (2002).
114 Lawrence, C. W. & Christensen, R. B. Metabolic suppressors of trimethoprim and ultraviolet light sensitivities of Saccharomyces cerevisiae rad6 mutants. *J Bacteriol* **139**, 866-876 (1979).
115 Aboussekhra, A. *et al.* RADH, a gene of Saccharomyces cerevisiae encoding a putative DNA helicase involved in DNA repair. Characteristics of radH mutants and sequence of the gene. *Nucleic Acids Res* **17**, 7211-7219 (1989).
116 Rong, L., Palladino, F., Aguilera, A. & Klein, H. L. The Hyper-Gene Conversion Hpr5-1 Mutation of Saccharomyces-Cerevisiae Is an Allele of the Srs2/Radh Gene. *Genetics* **127**, 75-85 (1991).
117 Rong, L. & Klein, H. L. Purification and characterization of the SRS2 DNA helicase of the yeast Saccharomyces cerevisiae. *The Journal of biological chemistry* **268**, 1252-1259 (1993).
118 Schiestl, R. H., Prakash, S. & Prakash, L. The Srs2 Suppressor of Rad6 Mutations of Saccharomyces-Cerevisiae Acts by Channeling DNA Lesions into the Rad52 DNA-Repair Pathway. *Genetics* **124**, 817-831 (1990).
119 Keyamura, K., Arai, K. & Hishida, T. Srs2 and Mus81-Mms4 Prevent Accumulation of Toxic Inter-Homolog Recombination Intermediates. *PLoS Genet* **12**, e1006136, doi:10.1371/journal.pgen.1006136 (2016).
120 Krejci, L. *et al.* DNA helicase Srs2 disrupts the Rad51 presynaptic filament. *Nature* **423**, 305-309, doi:10.1038/nature01577 (2003).

121 Veaute, X. *et al.* The Srs2 helicase prevents recombination by disrupting Rad51 nucleoprotein filaments. *Nature* **423**, 309-312, doi:10.1038/nature01585 (2003).
122 Sasanuma, H., Furihata, Y., Shinohara, M. & Shinohara, A. Remodeling of the Rad51 DNA strand-exchange protein by the Srs2 helicase. *Genetics* **194**, 859-872, doi:10.1534/genetics.113.150615 (2013).
123 Krejci, L. *et al.* Role of ATP hydrolysis in the antirecombinase function of Saccharomyces cerevisiae Srs2 protein. *J Biol Chem* **279**, 23193-23199, doi:10.1074/jbc.M402586200 (2004).
124 Van Komen, S., Reddy, M. S., Krejci, L., Klein, H. & Sung, P. ATPase and DNA helicase activities of the Saccharomyces cerevisiae anti-recombinase Srs2. *J Biol Chem* **278**, 44331-44337, doi:10.1074/jbc.M307256200 (2003).
125 Colavito, S. *et al.* Functional significance of the Rad51-Srs2 complex in Rad51 presynaptic filament disruption. *Nucleic acids research* **37**, 6754-6764, doi:10.1093/nar/gkp748 (2009).
126 Islam, M. N. *et al.* A variant of the breast cancer type 2 susceptibility protein (BRC) repeat is essential for the RECQL5 helicase to interact with RAD51 recombinase for genome stabilization. *J Biol Chem* **287**, 23808-23818, doi:10.1074/jbc.M112.375014 (2012).
127 Seong, C., Colavito, S., Kwon, Y., Sung, P. & Krejci, L. Regulation of Rad51 recombinase presynaptic filament assembly via interactions with the Rad52 mediator and the Srs2 anti-recombinase. *J Biol Chem* **284**, 24363-24371, doi:10.1074/jbc.M109.032953 (2009).
128 Burgess, R. C. *et al.* Localization of recombination proteins and Srs2 reveals anti-recombinase function in vivo. *J Cell Biol* **185**, 969-981, doi:10.1083/jcb.200810055 (2009).
129 Dupaigne, P. *et al.* The Srs2 helicase activity is stimulated by Rad51 filaments on dsDNA: Implications for crossover incidence during mitotic recombination. *Molecular Cell* **29**, 243-254, doi:10.1016/j.molcel.2007.11.033 (2008).
130 Ira, G., Malkova, A., Liberi, G., Foiani, M. & Haber, J. E. Srs2 and Sgs1-Top3 suppress crossovers during double-strand break repair in yeast. *Cell* **115**, 401-411 (2003).
131 Vaze, M. B. *et al.* Recovery from checkpoint-mediated arrest after repair of a double-strand break requires Srs2 helicase. *Mol Cell* **10**, 373-385 (2002).
132 Yeung, M. & Durocher, D. Srs2 enables checkpoint recovery by promoting disassembly of DNA damage foci from chromatin. *DNA Repair (Amst)* **10**, 1213-1222, doi:10.1016/j.dnarep.2011.09.005 (2011).
133 Heude, M., Chanet, R. & Fabre, F. Regulation of the Saccharomyces cerevisiae Srs2 helicase during the mitotic cell cycle, meiosis and after irradiation. *Mol Gen Genet* **248**, 59-68 (1995).
134 Saponaro, M. *et al.* Cdk1 targets Srs2 to complete synthesis-dependent strand annealing and to promote recombinational repair. *PLoS Genet* **6**, e1000858, doi:10.1371/journal.pgen.1000858 (2010).
135 Armstrong, A. A., Mohideen, F. & Lima, C. D. Recognition of SUMO-modified PCNA requires tandem receptor motifs in Srs2. *Nature* **483**, 59-63, doi:10.1038/nature10883 (2012).

136 Papouli, E. *et al.* Crosstalk between SUMO and ubiquitin on PCNA is mediated by recruitment of the helicase Srs2p. *Mol Cell* **19**, 123-133, doi:10.1016/j.molcel.2005.06.001 (2005).
137 Pfander, B., Moldovan, G. L., Sacher, M., Hoege, C. & Jentsch, S. SUMO-modified PCNA recruits Srs2 to prevent recombination during S phase. *Nature* **436**, 428-433, doi:10.1038/nature03665 (2005).
138 Schwendener, S. *et al.* Physical interaction of RECQ5 helicase with RAD51 facilitates its anti-recombinase activity. *J Biol Chem* **285**, 15739-15745, doi:10.1074/jbc.M110.110478 (2010).
139 Barber, L. J. *et al.* RTEL1 maintains genomic stability by suppressing homologous recombination. *Cell* **135**, 261-271, doi:10.1016/j.cell.2008.08.016 (2008).
140 Simandlova, J. *et al.* FBH1 helicase disrupts RAD51 filaments in vitro and modulates homologous recombination in mammalian cells. *J Biol Chem* **288**, 34168-34180, doi:10.1074/jbc.M113.484493 (2013).
141 Jeong, Y. T., Cermak, L., Guijarro, M. V., Hernando, E. & Pagano, M. FBH1 protects melanocytes from transformation and is deregulated in melanomas. *Cell cycle (Georgetown, Tex.)* **12**, 1128-1132, doi:10.4161/cc.24165 (2013).
142 Moldovan, G. L. *et al.* Inhibition of homologous recombination by the PCNA-interacting protein PARI. *Mol Cell* **45**, 75-86, doi:10.1016/j.molcel.2011.11.010 (2012).
143 Spies, M. *et al.* A molecular throttle: the recombination hotspot chi controls DNA translocation by the RecBCD helicase. *Cell* **114**, 647-654 (2003).
144 Bianco, P. R. *et al.* Processive translocation and DNA unwinding by individual RecBCD enzyme molecules. *Nature* **409**, 374-378, doi:10.1038/35053131 (2001).
145 Myong, S., Rasnik, I., Joo, C., Lohman, T. M. & Ha, T. Repetitive shuttling of a motor protein on DNA. *Nature* **437**, 1321-1325, doi:10.1038/nature04049 (2005).
146 Park, J. *et al.* PcrA helicase dismantles RecA filaments by reeling in DNA in uniform steps. *Cell* **142**, 544-555, doi:10.1016/j.cell.2010.07.016 (2010).
147 Comstock, M. J. *et al.* Protein structure. Direct observation of structure-function relationship in a nucleic acid-processing enzyme. *Science* **348**, 352-354, doi:10.1126/science.aaa0130 (2015).
148 Honda, M., Park, J., Pugh, R. A., Ha, T. & Spies, M. Single-molecule analysis reveals differential effect of ssDNA-binding proteins on DNA translocation by XPD helicase. *Molecular cell* **35**, 694-703, doi:10.1016/j.molcel.2009.07.003 (2009).
149 Qiu, Y. *et al.* Srs2 prevents Rad51 filament formation by repetitive motion on DNA. *Nat Commun* **4**, 2281, doi:10.1038/ncomms3281 (2013).
150 Sokoloski, J. E., Kozlov, A. G., Galletto, R. & Lohman, T. M. Chemo-mechanical pushing of proteins along single-stranded DNA. *Proceedings of the National Academy of Sciences of the United States of America* **113**, 6194-6199, doi:10.1073/pnas.1602878113 (2016).
151 De Tullio, L. *et al.* Yeast Srs2 helicase promotes redistribution of single-stranded DNA-bound RPA and Rad52 in homologous recombination regulation
. *Cell Reports* **In Press** (2017).
152 Kaniecki, K. *et al.* Dissociation of Rad51 presynaptic complexes and heteroduplex DNA joints by tandem assemblies of Srs2
. *Under Review* (2017).

153 Fazio, T., Visnapuu, M. L., Wind, S. & Greene, E. C. DNA curtains and nanoscale curtain rods: high-throughput tools for single molecule imaging. *Langmuir* **24**, 10524-10531, doi:10.1021/la801762h (2008).
154 Gorman, J., Fazio, T., Wang, F., Wind, S. & Greene, E. C. Nanofabricated racks of aligned and anchored DNA substrates for single-molecule imaging. *Langmuir* **26**, 1372-1379, doi:10.1021/la902443e (2010).
155 Graneli, A., Yeykal, C. C., Prasad, T. K. & Greene, E. C. Organized arrays of individual DNA molecules tethered to supported lipid bilayers. *Langmuir : the ACS journal of surfaces and colloids* **22**, 292-299, doi:10.1021/la051944a (2006).
156 Duzdevich, D. *et al.* The dynamics of eukaryotic replication initiation: origin specificity, licensing, and firing at the single-molecule level. *Mol Cell* **58**, 483-494, doi:10.1016/j.molcel.2015.03.017 (2015).
157 Lee, J. Y., Finkelstein, I. J., Arciszewska, L. K., Sherratt, D. J. & Greene, E. C. Single-molecule imaging of FtsK translocation reveals mechanistic features of protein-protein collisions on DNA. *Mol Cell* **54**, 832-843, doi:10.1016/j.molcel.2014.03.033 (2014).
158 Redding, S. *et al.* Surveillance and Processing of Foreign DNA by the Escherichia coli CRISPR-Cas System. *Cell* **163**, 854-865, doi:10.1016/j.cell.2015.10.003 (2015).
159 Sternberg, S. H., Redding, S., Jinek, M., Greene, E. C. & Doudna, J. A. DNA interrogation by the CRISPR RNA-guided endonuclease Cas9. *Nature* **507**, 62-67, doi:10.1038/nature13011 (2014).
160 Wang, F. *et al.* The promoter-search mechanism of Escherichia coli RNA polymerase is dominated by three-dimensional diffusion. *Nat Struct Mol Biol* **20**, 174-181, doi:10.1038/nsmb.2472 (2013).
161 Gorman, J., Plys, A. J., Visnapuu, M. L., Alani, E. & Greene, E. C. Visualizing one-dimensional diffusion of eukaryotic DNA repair factors along a chromatin lattice. *Nat Struct Mol Biol* **17**, 932-938, doi:10.1038/nsmb.1858 (2010).
162 Gorman, J. *et al.* Single-molecule imaging reveals target-search mechanisms during DNA mismatch repair. *Proc Natl Acad Sci U S A* **109**, E3074-3083, doi:10.1073/pnas.1211364109 (2012).
163 Silverstein, T. D., Gibb, B. & Greene, E. C. Visualizing protein movement on DNA at the single-molecule level using DNA curtains. *DNA Repair (Amst)* **20**, 94-109, doi:10.1016/j.dnarep.2014.02.004 (2014).
164 Greene, E. C., Wind, S., Fazio, T., Gorman, J. & Visnapuu, M. L. DNA curtains for high-throughput single-molecule optical imaging. *Methods in enzymology* **472**, 293-315, doi:10.1016/s0076-6879(10)72006-1 (2010).
165 Ma, C. J., Steinfeld, J. B. & Greene, E. C. Single-Stranded DNA Curtains for Studying Homologous Recombination. *Methods Enzymol* **582**, 193-219, doi:10.1016/bs.mie.2016.08.005 (2017).
166 Qi, Z. & Greene, E. C. Visualizing recombination intermediates with single-stranded DNA curtains. *Methods* **105**, 62-74, doi:10.1016/j.ymeth.2016.03.027 (2016).
167 Lisby, M. & Rothstein, R. Cell biology of mitotic recombination. *Cold Spring Harb Perspect Biol* **7**, a016535, doi:10.1101/cshperspect.a016535 (2015).
168 Zacharias, D. A., Violin, J. D., Newton, A. C. & Tsien, R. Y. Partitioning of lipid-modified monomeric GFPs into membrane microdomains of live cells. *Science* **296**, 913-916, doi:10.1126/science.1068539 (2002).

169 Gibb, B., Silverstein, T. D., Finkelstein, I. J. & Greene, E. C. Single-stranded DNA curtains for real-time single-molecule visualization of protein-nucleic acid interactions. *Anal Chem* **84**, 7607-7612, doi:10.1021/ac302117z (2012).
170 Wold, M. S. Replication protein A: a heterotrimeric, single-stranded DNA-binding protein required for eukaryotic DNA metabolism. *Annual review of biochemistry* **66**, 61-92, doi:10.1146/annurev.biochem.66.1.61 (1997).
171 Bianco, P. R., Tracy, R. B. & Kowalczykowski, S. C. DNA strand exchange proteins: a biochemical and physical comparison. *Front Biosci* **3**, D570-603 (1998).
172 Chen, R. & Wold, M. S. Replication protein A: single-stranded DNA's first responder: dynamic DNA-interactions allow replication protein A to direct single-strand DNA intermediates into different pathways for synthesis or repair. *BioEssays : news and reviews in molecular, cellular and developmental biology* **36**, 1156-1161, doi:10.1002/bies.201400107 (2014).
173 Gibb, B. *et al.* Protein dynamics during presynaptic-complex assembly on individual single-stranded DNA molecules. *Nature structural & molecular biology* **21**, 893-900, doi:10.1038/nsmb.2886 (2014).
174 Meijering, E. *et al.* Design and validation of a tool for neurite tracing and analysis in fluorescence microscopy images. *Cytometry A* **58**, 167-176, doi:10.1002/cyto.a.20022 (2004).
175 Brosh, R. M., Jr. DNA helicases involved in DNA repair and their roles in cancer. *Nat Rev Cancer* **13**, 542-558, doi:10.1038/nrc3560 (2013).
176 Branzei, D. & Szakal, B. Building up and breaking down: mechanisms controlling recombination during replication. *Critical reviews in biochemistry and molecular biology*, 1-14, doi:10.1080/10409238.2017.1304355 (2017).
177 Marini, V. & Krejci, L. Unwinding of synthetic replication and recombination substrates by Srs2. *DNA repair* **11**, 789-798, doi:10.1016/j.dnarep.2012.05.007 (2012).
178 Dupaigne, P. *et al.* The Srs2 helicase activity is stimulated by Rad51 filaments on dsDNA: implications for crossover incidence during mitotic recombination. *Molecular cell* **29**, 243-254, doi:10.1016/j.molcel.2007.11.033 (2008).
179 Gibb, B. *et al.* Concentration-dependent exchange of replication protein A on single-stranded DNA revealed by single-molecule imaging. *PLoS One* **9**, e87922, doi:10.1371/journal.pone.0087922 (2014).
180 Niu, H. & Klein, H. L. Multifunctional Roles of Saccharomyces cerevisiae Srs2 protein in Replication, Recombination and Repair. *FEMS Yeast Res*, doi:10.1093/femsyr/fow111 (2016).
181 De Tullio, L. *et al.* Yeast Srs2 Helicase Promotes Redistribution of Single-Stranded DNA-Bound RPA and Rad52 in Homologous Recombination Regulation. *Cell Rep* **21**, 570-577, doi:10.1016/j.celrep.2017.09.073 (2017).
182 Malik, P. S. & Symington, L. S. Rad51 gain-of-function mutants that exhibit high affinity DNA binding cause DNA damage sensitivity in the absence of Srs2. *Nucleic acids research* **36**, 6504-6510, doi:10.1093/nar/gkn720 (2008).
183 Marini, V. & Krejci, L. Srs2: the "Odd-Job Man" in DNA repair. *DNA repair* **9**, 268-275, doi:10.1016/j.dnarep.2010.01.007 (2010).
184 Vasianovich, Y. *et al.* Unloading of homologous recombination factors is required for restoring double-stranded DNA at damage repair loci. *The EMBO journal* **36**, 213-231, doi:10.15252/embj.201694628 (2017).

185 Lohman, T. M., Tomko, E. J. & Wu, C. G. Non-hexameric DNA helicases and translocases: mechanisms and regulation. *Nat Rev Mol Cell Biol* **9**, 391-401, doi:10.1038/nrm2394 (2008).
186 Byrd, A. K. & Raney, K. D. Protein displacement by an assembly of helicase molecules aligned along single-stranded DNA. *Nature structural & molecular biology* **11**, 531-538, doi:10.1038/nsmb774 (2004).
187 Levin, M. K., Wang, Y. H. & Patel, S. S. The functional interaction of the hepatitis C virus helicase molecules is responsible for unwinding processivity. *The Journal of biological chemistry* **279**, 26005-26012, doi:10.1074/jbc.M403257200 (2004).
188 Rad, B., Forget, A. L., Baskin, R. J. & Kowalczykowski, S. C. Single-molecule visualization of RecQ helicase reveals DNA melting, nucleation, and assembly are required for processive DNA unwinding. *Proceedings of the National Academy of Sciences of the United States of America* **112**, E6852-6861, doi:10.1073/pnas.1518028112 (2015).
189 Lee, K. S., Balci, H., Jia, H., Lohman, T. M. & Ha, T. Direct imaging of single UvrD helicase dynamics on long single-stranded DNA. *Nat Commun* **4**, 1878, doi:10.1038/ncomms2882 (2013).
190 Lytle, A. K. *et al.* Context-dependent remodeling of Rad51-DNA complexes by Srs2 is mediated by a specific protein-protein interaction. *Journal of molecular biology* **426**, 1883-1897, doi:10.1016/j.jmb.2014.02.014 (2014).
191 Heyer, W. D., Ehmsen, K. T. & Liu, J. Regulation of homologous recombination in eukaryotes. *Annu Rev Genet* **44**, 113-139, doi:10.1146/annurev-genet-051710-150955 (2010).
192 Kowalczykowski, S. C. An Overview of the Molecular Mechanisms of Recombinational DNA Repair. *Cold Spring Harb Perspect Biol* **7**, doi:10.1101/cshperspect.a016410 (2015).
193 Kumaran, S., Kozlov, A. G. & Lohman, T. M. Saccharomyces cerevisiae replication protein A binds to single-stranded DNA in multiple salt-dependent modes. *Biochemistry* **45**, 11958-11973, doi:10.1021/bi060994r (2006).
194 Carter, S. D., Vigasova, D., Chen, J., Chovanec, M. & Astrom, S. U. Nej1 recruits the Srs2 helicase to DNA double-strand breaks and supports repair by a single-strand annealing-like mechanism. *Proc Natl Acad Sci U S A* **106**, 12037-12042, doi:10.1073/pnas.0903869106 (2009).
195 Symington, L. S. & Heyer, W. D. Some disassembly required: role of DNA translocases in the disruption of recombination intermediates and dead-end complexes. *Genes & development* **20**, 2479-2486, doi:10.1101/gad.1477106 (2006).